YUNIBESITI YA BOKONE-BOPHIRIMA
NORTH WEST UNIVERSITY
NOORDWES UNIVERSITEIT

Thrust load determination for the high pressure turbo unit of the pebble bed micro model

J. Janse van Rensburg B.Eng (Mech)

Dissertation submitted to the School for Mechanical Engineering of the North-West University in partial fulfillment of the requirements for the degree; Master in Engineering.

Supervisor: Mr. J.G. Roberts

November 2006
Potchefstroom





Abstract

Commercial turbochargers used on earth-moving equipment, were used as the turbomachinery for the Pebble Bed Micro Model (PBMM) instead of custom-built turbo units. A premature thrust bearing failure occurred on the High Pressure Turbo Unit (HPTU) of the PBMM during a test. Due to the closed Brayton cycle operation of the PBMM, it might have been possible to exert larger thrust loads on the thrust bearing of the HPTU than normally present in the turbo diesel engine application.

A detailed study was performed on theoretical thrust calculations as applied to turbo machinery. In the literature study, five different thrust calculation methodologies were found. These are the methods of Lobanoff & Ross, Stepanoff, Gülich, Japikse and Liebner. These methodologies were applied to make a theoretical prediction of the thrust of the HPTU.

Experimental thrust measurement were performed on the HPTU, by implementing a metal foil strain gauge thrust measurement system. Thrust load measurements on the HPTU and process parameters, required for the calculation of the thrust, were recorded during a test run of the PBMM. The experimentally measured thrust was compared with the theoretical thrust calculations. It was found that the methodologies of Gülich, Lobanoff & Ross and Stepanoff correlated best with the experimental thrust measurements.

Furthermore, calculations have shown that the thrust exerted on the thrust bearing of the HPTU in the PBMM application, is approximately 1,4 times larger than in a normal turbo diesel engine application.

Uittreksel

Kommersiële turboaanjaers wat in die enjins van grondverskuiwingsmasjinerie gebruik word, is aangewend as turbomasjiene vir die Korrelbed Mikro Model in plaas van spesiaal vervaardigde turbomasjiene. 'n Onverwagte faling van die enddruklaer van die Hoëdruk Turbo-eenheid het voorgekom gedurende 'n Korrelbed Mikro Model toetslopie. Die Korrelbed Mikro Model maak gebruik van 'n geslote Brayton termodinamiese siklus, wat dit moontlik maak om 'n groter enddrukkrag op die laer van die Hoëdruk Turbo-eenheid uit te oefen as in die geval waar dieselfde turboaanjaer op 'n turbodieselenjin gebruik word.

'n Literatuurstudie van teoretiese enddrukkrag berekeningsmetodes op turbomasjiene is gedoen wat vervolgens gebruik is om die enddrukkrag van die Hoëdruk Turbo-eenheid teoreties te voorspel. Die berekeningsmetodes van Lobanoff & Ross, Stepanoff, Gülich, Japikse en Liebner is ondersoek.

Eksperimentele enddrukkrag metings is gedoen deur metaalfilm rekstrokies op die enddruklaer van die Hoëdruk Turbo-eenheid te installeer. Datavaslegging van die gemete enddrukkrag en prosesparameters benodig vir die berekening van die enddrukkrag is gedoen gedurende 'n Korrelbed Mikro Model toetslopie. Daarna is die teoretiese berekeningsmetodes se resultate vergelyk met die eksperimentele enddrukkrag metings. Daar is bevind dat die metodes van Gülich, Lobanoff & Ross asook Stepanoff goed vergelyk met die eksperimentele data.

Verder is daar ook bereken dat die enddrukkrag op die laer van die Hoëdruk Turbo-eenheid in die Korrelbed Mikro Model ongeveer 1,4 maal hoër is as in die normale turbodieselenjin toepassing.

List of Figures

Figure 1.1: Layout of dissertation..... 3

Figure 2.1: Thrust on a single-suction open pump impeller without radial vanes on rear shroud... 5

Figure 2.2: Axial thrust of an open centrifugal pump impeller..... 8

Figure 2.3: Illustration of an open centrifugal pump impeller..... 8

Figure 2.4: Control volume for thrust force calculation..... 10

Figure 2.5: Thrust calculation nomenclature of an open impeller..... 12

Figure 2.6: Thrust measurement with a Wheatstone bridge on a tilting pad thrust bearing..... 14

Figure 2.7: Commercially available force washer..... 15

Figure 2.8: Piezo-electric strain sensors..... 15

Figure 3.1: Nomenclature applied to complete turbocharger for the thrust calculation by Lobanoff and Ross..... 18

Figure 3.2: Definition and direction of positive velocities and angles for calculation of thrust exerted due to a change in fluid momentum..... 20

Figure 3.3: Nomenclature applied to complete turbocharger for the thrust calculation by Stepanoff..... 22

Figure 3.4: Nomenclature applied to complete turbocharger for the thrust calculation by Japikse.. 24

Figure 3.5: Nomenclature applied to complete turbocharger for the thrust calculation by Gülich... 27

Figure 3.6: Nomenclature applied to complete turbocharger for the thrust calculation based on method by Liebner..... 29

Figure 4.1: HPTU turbocharger center casing and thrust bearing dimensions..... 32

Figure 4.2: Turbocharger centre casing with thrust bearing and thrust washers..... 33

Figure 4.3: Terminology used to describe sections on the thrust bearing..... 34

Figure 4.4: Finite element analysis maximum principle strain results for thrust of 200N..... 35

Figure 4.5: Turbocharger centre casing with thrust bearing and piezo-electric sensors..... 35

Figure 4.6: Quarter bridge circuit with one active gauge R_1..... 38

Figure 4.7: Half bridge circuit with two active gauges R_1 and R_2..... 38

Figure 4.8: Full bridge circuit with all gauges active..... 38

Figure 4.9: Quarter bridge with lead wire resistances..... 39

Figure 4.10: Three wire quarter bridge circuit..... 40

Figure 4.11: Half bridge with lead wire resistances..... 40

Figure 4.12: Full bridge with lead wire resistances..... 41

Figure 4.13: Finite element analysis vector plot of maximum and minimum principle strains for the thrust bearing for a thrust force of 400N in the "turbine to compressor" direction..... 44

Figure 4.14: Installation positions for strain gauges with grid alignment markings..... 46

Figure 4.15: Wiring of the thrust measuring system..... 46

Figure 4.16: Thrust bearing installed inside the turbocharger centre casing..... 47

Figure 4.17: Calibrating the thrust measuring system with dead weights..... 47

Figure 4.18: Dead weight calibration graph for "turbine to compressor" direction..... 48

Figure 4.19: Dead weight calibration graph for "compressor to turbine" direction..... 48

Figure 4.20: Thermal output of the strain gauge bridge..... 49

Figure 4.21: Cantilever beam for verification of amplifier reading..... 50

Figure 4.22: HPTU installed inside PBMM with thrust measurement system..... 52

Figure 4.23: PBMM HPT inlet temperature- and LPC inlet pressure set points for thrust measurement test..... 53

Figure 4.24: Thrust test 1 results..... 54

Figure 4.25: Installation positions for strain gauges with grid alignment markings..... 55

Figure 4.26: Connection of the strain gauge bridge to the Vishay amplifier..... 57

Figure 4.27: Thermal output of the strain gauge bridge without load..... 58

Figure 4.28: Thermal output of the strain gauge bridge with and without load..... 59

Figure 4.29: Load calibration of the thrust measurement system with a load cell..... 60

Figure 4.30: Load calibration for the direction "turbine to compressor"..... 60

Figure 4:31: Load calibration for the direction "compressor to turbine"..... 61

Figure 5.1: Thrust bearing temperature during Thrust Test 2..... 65

Figure 5.2: Thermal calibration data during Thrust Test 2..... 65

Figure 5.3: Calculation of thermal component and load component of amplifier signal..... 66

Figure 5.4: Thrust Test 2 experimentally measured thrust..... 66

Figure 5.5: Thrust Test 2 HPTU pressures..... 67

Figure 5.6: Thrust Test 2 HPTU temperatures..... 67

Figure 5.7: Thrust Test 2 mass flow rate..... 67

Figure 5.8: Thrust Test 2 HPTU rotor speed..... 68

Figure 5.9: Thrust Test 2 HPTU thrust bearing temperature..... 68

Figure 5.10: Lobanoff & Ross methodology compared with experimentally measured thrust..... 69

Figure 5.11: Stepanoff methodology compared with experimentally measured thrust..... 70

Figure 5.12: Stepanoff methodology with momentum included compared with experimentally measured thrust. 70

Figure 5.13: Japikse methodology compared with experimentally measured thrust..... 71

Figure 5.14: Japikse methodology with altered values compared with experimentally measured thrust..... 71

Figure 5.15: Gülich methodology compared with experimentally measured thrust..... 72

Figure 5.16: Gülich methodology with altered values compared to experimentally measured thrust 72

Figure 5.17: Liebner methodology compared with experimentally measured thrust 73

Figure 5.18: Comparison between the methods of Gülich, Stepanoff and Lobanoff & Ross 74

Figure 5.19: Pressure difference condition for HPTU during Thrust Test 2 74

Figure A1.1: Nomenclature applied to complete turbocharger for the thrust calculation by Lobanoff and Ross 80

Figure A2.1: Nomenclature applied to complete turbocharger for the thrust calculation by Stepanoff 85

Figure A3.1: Nomenclature applied to complete turbocharger for the thrust calculation by Japikse 90

Figure A4.1: Nomenclature applied to complete turbocharger for the thrust calculation by Gülich 99

Figure A5.1: Nomenclature applied to complete turbocharger for the thrust calculation by Gülich 103

Figure A6.1: Nomenclature applied to complete turbocharger for the thrust calculation based on method by Liebner 107

Figure A7.1: Nomenclature applied to turbocharger for the thrust calculation by Gülich 109

Figure B1.1: Thrust bearing with strain gauges positioned on Mylar hinges 114

Figure B1.2: Strain gauges clamped down on thrust bearing with pressure pads 114

Figure B2.1: Digital readout module 115

Figure B2.2: Selectors, dials and potentiometers of KWS 3073 strain gauge amplifier card 116

Figure B3.1: Vishay 2100 amplifier 118

Acknowledgements

I want to thank God almighty for giving me the ability to perform a study like this. Further I want to thank my supervisor Mr. Johan Roberts for all of his efforts and time he put into this study, my family and everyone else that made any form of contribution towards this study.

Table of Contents

Abstract ii

Uittreksel iii

Acknowledgements iv

Table of Contents v

List of Figures vii

List of Tables xi

1. Introduction 1
1.1 Preface 1
1.2 Problem definition 1
1.3 Objectives of this study 2
1.4 Layout of dissertation 2

2. Literature study 4
2.1 Introduction 4
2.2 Thrust calculation methodologies 4
2.2.1 Method 1 by Lobanoff and Ross 3
2.2.2 Method 2 by Stepanoff 7
2.2.3 Method 3 by Japikse 9
2.2.4 Method 4 by Gülich 12
2.2.5 Other 13
2.3 Thrust measurement techniques 13
2.3.1 Method 1 13
2.3.2 Method 2 14
2.3.3 Other methods 14
2.4 Summary 15

3. Theoretical thrust calculations 17
3.1 Introduction 17
3.2 Method 1 by Lobanoff and Ross 18
3.3 Method 2 by Stepanoff 21
3.4 Method 3 by Japikse 24
3.5 Method 4 by Gülich 26
3.6 Method 5 based on method suggested by Liebner 28
3.7 CFD method 29
3.8 Summary 30

4. Thrust measurement on the HPTU 32
4.1 Introduction 32
4.2 Thrust measurement concepts 32
4.2.1 Five axis electro-magnetic bearings 32
4.2.2 Force washers 33
4.2.3 Piezo-electric strain sensors 34
4.2.4 Strain gauges 35

4.3 Strain gauge measuring systems theory 36
4.3.1 Types of strain gauges 37
4.3.2 Bridge configurations 37
4.3.3 Cable errors 39
4.3.4 Temperature effects 41
4.3.5 Types of adhesives 43
4.3.6 Types of covering agents 43
4.4 Installation of first thrust measurement system 43
4.4.1 Installation of strain gauges on thrust bearing for Thrust Test 1 43
4.4.2 Calibration of the strain gauge thrust measuring system 1 46
4.4.3 Preparation for Thrust test 1 with thrust measuring system 1 installed in PBMM 51
4.4.4 Thrust Test 1 52
4.4.5 Thrust Test 1 results 53
4.5 Installation of thrust measurement system 2 54
4.5.1 Installation of strain gauges on thrust bearing for Test 2 54
4.5.2 Calibration of the strain gauge thrust measuring system 2 56
4.5.3 Preparation for Thrust test 2 with thrust measuring system 2 installed in PBMM 61
4.5.4 Thrust Test 2 61
4.6 Summary 62

5. Thrust Test 2 & comparison 64
5.1 Introduction 64
5.2 Determination of measured thrust load data 64
5.3 Theoretical thrust calculation parameter graphs for Thrust Test 2 66
5.4 Comparison of experimental thrust and thrust calculation methodologies 68
5.4.1 Method 1 by Lobanoff and Ross 69
5.4.2 Method 2 by Stepanoff 69
5.4.3 Method 3 by Japikse 70
5.4.4 Method 4 by Gülich 72
5.4.5 Method 4 by Liebner 73
5.5 Summary 73

6. Conclusion & recommendations 77
6.1 Conclusions 77
6.2 Recommendations for further studies 78

7. Appendix 80
Appendix A1: Lobanoff and Ross thrust calculation 80
Appendix A2: Stepanoff thrust calculation 85
Appendix A3: Japikse thrust calculation 90
Appendix A4: Middle rotation factor calculation 99
Appendix A5: Gülich thrust calculation 103
Appendix A6: Liebner thrust calculation 107
Appendix A7: Gülich thrust calculation a turbo diesel engine 109

Appendix B1: Strain gauge installation procedure 113
Appendix B2: Balancing of the HBM amplifier 115
Appendix B3: Balancing of the Vishay amplifier 117

8. Bibliography 119

List of Tables

Table 3.1: HPTU turbocharger geometry..... 17

Table3.2: Test data input parameters..... 18

Table 3.3: Solution of thrust calculation with the method of Lobanoff & Ross..... 21

Table 3.4: Solution of thrust calculation with the method of Stepanoff..... 24

Table 3.5: Solution of thrust calculation with the method of Japikse..... 26

Table 3.6: Solution of middle rotation factor calculation (k_0)..... 28

Table 3.7: Solution of thrust calculation with the method of Gülich..... 28

Table 5.1: Turbo thrust calculated for a turbo diesel engine arrangement..... 76

Table A1.1: Lobaoff & Ross thrust calculation solution..... 84

Table A2.1: Stepanoff thrust calculation solution..... 89

Table A3.1: Japikse thrust calculation solution..... 96

Table A4.1: Middle rotation factor calculation solution..... 102

Table A5.1: Gülich thrust calculation solution..... 106

Table A6.1: Liebner thrust calculation solution..... 108

Table A7.1: Gülich thrust calculation solution for turbo diesel engine..... 112

1. Introduction

1.1 Preface:

PBMR Pty (Ltd) is designing a nuclear power generation plant, also known as the Pebble Bed Modular Reactor (PBMR), to supply in the projected power consumption increase in South Africa [21]. A physical model was constructed to demonstrate the control strategies of Design Proposal 1 (DP1) of the PBMR. The physical model is called the Pebble Bed Micro Model (PBMM).

To save on manufacturing costs of the PBMM, commercially available turbochargers were used in the design of the PBMM instead of custom manufactured turbo machinery [9]. These commercial turbochargers used for the PBMM normally operate on earth moving equipment. The thermodynamic cycle of an engine, as used on earth moving equipment, is an open cycle where air is taken from the atmosphere, mixed with fuel, burned and exhausted to the atmosphere. Therefore the pressure at the inlet to the compressor and at the outlet of the turbine of the turbocharger is almost atmospheric pressure. Thus the differential pressure between the inlet of the compressor and the outlet of the turbine is marginal. The PBMM operates in a closed cycle, thus the working fluid is cycled over and over. In a closed cycle the differential pressure between the compressor inlet and turbine outlet can differ substantially and it is possible to exert large thrust forces on the turbocharger thrust bearing.

1.2 Problem definition:

A premature thrust bearing failure (approximately 60 operating hours) was experienced on the High Pressure Turbo Unit (HPTU) while operating at a high pressure and high mass flow rate. The primary cause for the thrust bearing failure was attributed to the "higher than ambient hydrostatic pressures that exist in the PBMM (Pebble Bed Micro Model) application" [25] and excessive aeration of the lubricating oil. Other possible causes for the failure such as incorrect assembly, misalignment of the shaft assembly, rotor balancing or insufficient bearing cooling was ruled out since it was a new turbocharger, certified for correct assembly. Furthermore, when the turbocharger was operated during the period prior to the failure, the vibration level was well within the normal operating limits. Over-heating of the thrust bearing would have caused coking of oil on the bearing or discolouring of the bearing itself, which was not observed. In order to keep the thrust bearing loading within tolerable limits, the differential pressure between the compressor outlet and turbine inlet may not exceed 25" Hg (84.6kPa) [23]. This is the design criterion of the manufacturer, with the assumption that the pressure at compressor inlet and turbine outlet is atmospheric pressure. Data from PBMM tests showed that the 84kPa pressure difference condition was not exceeded when the PBMM was operated within its design pressure ranges. The pressure difference condition ranged at levels around 40-

70% of its recommended level, when the failure occurred. However, the pressure at the compressor inlet and turbine outlet differed by approximately 50kPa.

The criterion mentioned above is an over-simplification of the problem to calculate the thrust on the rotor of a turbocharger. Therefore, a detailed study was needed to address the methodology of thrust calculation in centrifugal turbochargers as well as methods to measure this thrust in the PBMM application.

1.3 Objectives of this study:

The objectives of this study can be summarized as follows:

- Describe thrust calculation methodologies as applied in centrifugal turbo machine design.
- Devise a method to measure the thrust force exerted on the thrust bearing of the HPTU of the PBMM.
- Compare the thrust load calculation methodologies with experimental measurements on the turbo unit.
- Substantiate whether the thrust of the HPTU exceeded the likely design capacity of its thrust bearing, causing the failure, mentioned before.

1.4 Layout of dissertation:

This dissertation is composed as follows (refer to Figure 1.1):
Chapter 2: Literature study, Thrust calculation methodologies as well as thrust measuring techniques are discussed. In Chapter 3: The different thrust calculation methodologies from Chapter 2 are applied to predict the thrust of the HPTU. Chapter 4: Measuring thrust - a feasible method from the literature in Chapter 2 is devised to measure the actual thrust exerted on the bearing during operation of the PBMM. Chapter 5 comprises the test data that was recorded during the operation of the PBMM. A comparison between the theoretical thrust values from Chapter 3 and the measured data is performed. A conclusive summary of the dissertation and suggestions for further research is given in Chapter 6.

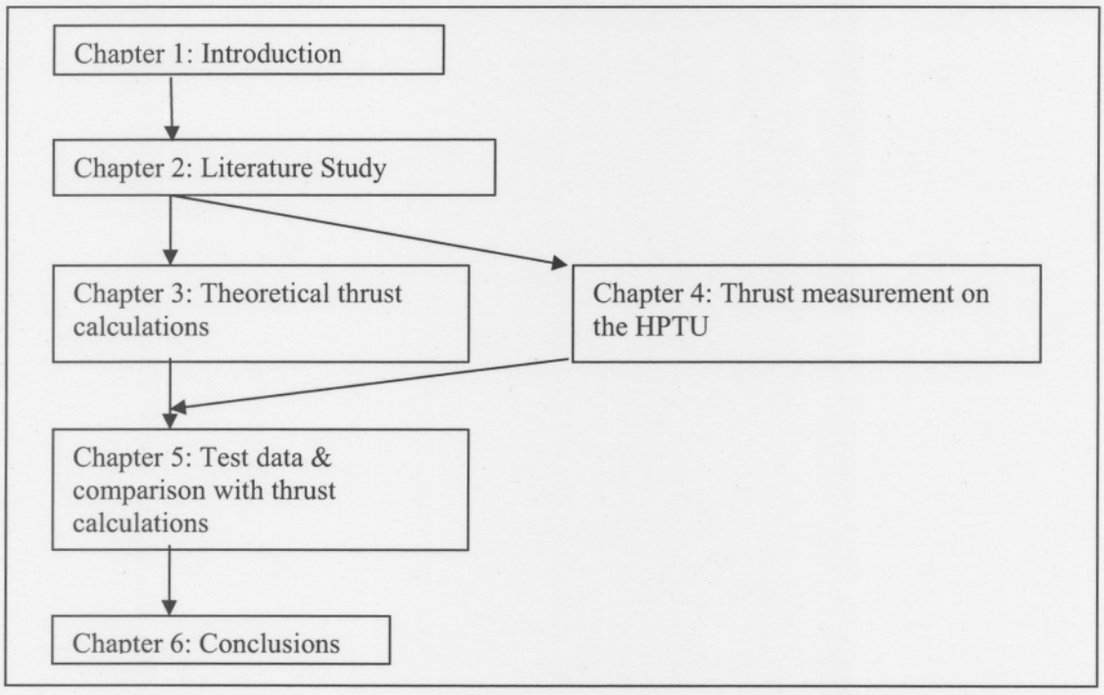


Figure 1.1: Layout of dissertation

2. Literature study

2.1 Introduction:

Although a countless number of turbo machines are successfully operated in a wide variety of applications, published articles on thrust calculation methodologies are very scarce. Some methods are considered to be proprietary by manufacturers and are not published [2]. However, a number of thrust calculation methods were found in literature that are used to predict thrust in centrifugal- pumps and compressors. These thrust calculation methods vary vastly in level of calculation difficulty and number of input parameters. Current thrust calculation techniques involve the integration of the product of the pressure field acting on the impeller area. Calculation of the pressure field introduces uncertainty into the results. For a specific test, the axial thrust was calculated as 460lbf. The actual test results gave 400lbf, which equates to an error of 15%. Several factors have an influence on the pressure field such as the position of the impeller relative to side walls and the shroud, geometry and surface roughness [2]. Additional factors include Reynolds-number, rate and direction of leakage flow through the impeller side room and pre-swirl with which the leakage enter the side room [10], [12]. Some empirical thrust calculations define a "theoretical thrust" from the static pressure rise due to the effect of rotating velocity of the fluid between the casing and impeller. From comparison between the "theoretical thrust" and test data a dimensionless corrective term is derived. This corrective term is used to predict thrust in geometrically similar pumps. The corrective term is written as a function of leakage flow, Reynolds-number and labyrinth clearance [1].

From the literature above it can be seen that the theoretically calculated thrust and experimental data can vary substantially. Due to possible large differences in theoretical thrust and experimental data, a number of thrust calculation methods will be applied to the HPTU and verified against the experimentally measured thrust.

As mentioned above, calculated thrust values need to be benchmarked against experimental test results. Therefore it is necessary to perform a literature study on thrust measuring techniques as well.

2.2 Thrust calculation methodologies:

2.2.1 Method 1 by Lobanoff and Ross [19]:

Thrust in direction A (refer to Figure 2.1) is calculated as [19]:

$$T_A = (A_S \cdot P_S) + \left[(A_3 - A_E) \cdot \frac{P_D}{2} \right] + F_X \qquad (2.1)$$

where A_S, A_3 and A_E (in^2 or m^2) are the areas calculated from diameters D_S, D_3, D_E respectively. P_S (psi or Pa) is the suction- or inlet pressure. P_D is the calculated differential pressure between outlet pressure (P_3)

and inlet pressure (P_E). F_X (lbf or N) denotes the thrust force due to the change of fluid momentum inside the impeller.

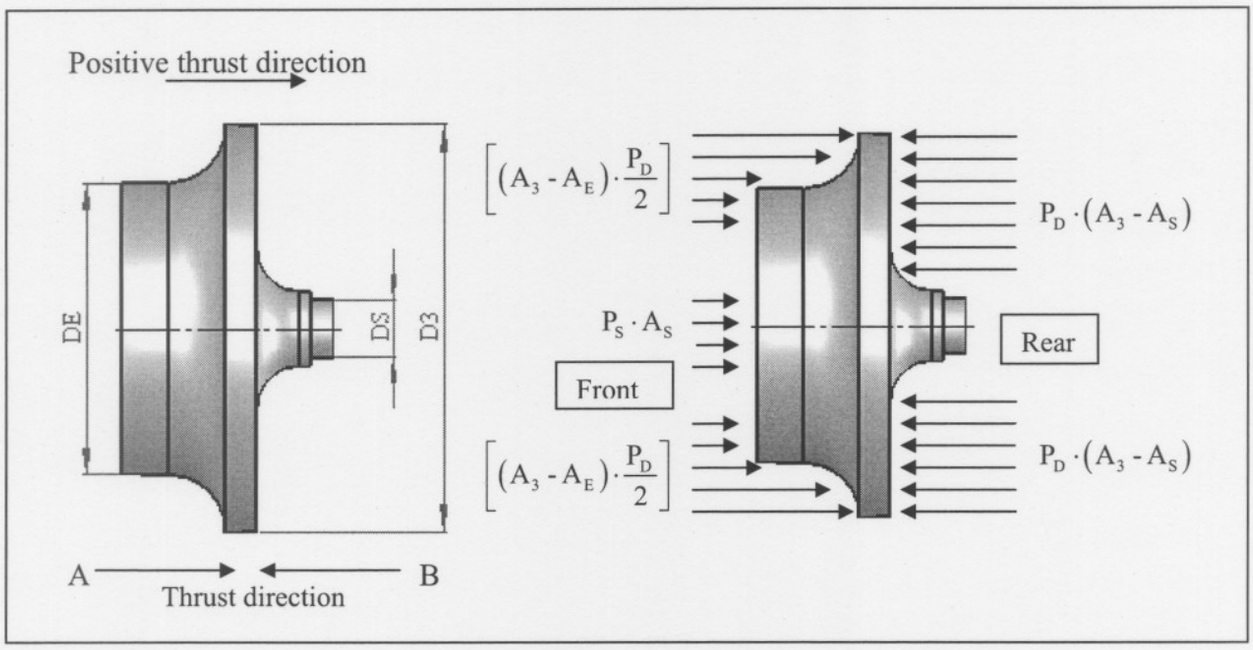


Figure 2.1: Thrust on a single-suction open pump impeller without radial vanes on rear shroud

The first term of Equation 2.1 is the suction pressure that exerts a force on the shaft area. In the second term, the average pressure between inlet and outlet exerts a force on the projected area from inlet to outlet. Lastly the force due to the momentum change of the fluid inside the impeller in the axial direction. F_X is calculated as follows for imperial units [19]:

$$F_X = \frac{\left(Q^2 \cdot spgr\right)}{A_E \cdot 722} \tag{2.2}$$

with Q the volume flow rate (Gallon/minute or GPM), spgr is the specific gravity of the fluid (dimensionless). 722 is a unit conversion factor. The unit for F_X is pound-force. Specific gravity is the ratio of the densities of the actual working fluid and water [3]. For gasses the specific gravity is calculated as the ratio of the densities of the actual working fluid and air [3].

Due to the rotation of the impeller, velocities in the impeller are referenced relative to the rotating impeller and relative to a fixed object like the turbo casing. When the velocity is referenced relative to a fixed object it is termed an absolute velocity and when referenced to a moving object it is termed relative. In the equations to follow it is important to substitute the absolute velocity.

From conservation of mass it follows that:

$$\dot{m} = \rho \cdot C \cdot A : [kg/s] \text{ mass flow rate}$$
$$\dot{m} = \rho \cdot Q : [kg/s] \text{ mass flow rate} \tag{2.3}$$

with :

$\rho \equiv$ density (kg/m^3)

$A \equiv$ Area (m^2)

$C \equiv$ Absolute velocity (m/s)

$Q \equiv$ Volume flow rate (m^3/s)

Equation 2.2 can be converted as follows for metric units:

$$F_X = \frac{d(m \cdot C)}{dt} : [N] \text{ by definition of force}$$

$$F_X = (\dot{m}_{inlet} \cdot C_{inlet} \cdot \cos(\phi_{inlet})) - (\dot{m}_{outlet} \cdot C_{outlet} \cdot \cos(\phi_{outlet})) \text{ if integrated over the control volume (impeller)}$$

$$F_X = \left(\rho_{inlet} \cdot Q_{inlet} \cdot \left(\frac{Q_{inlet}}{A} \right) \cdot \cos(\phi_{inlet}) \right) - \left(\rho_{outlet} \cdot Q_{outlet} \cdot \left(\frac{Q_{outlet}}{A_{outlet}} \right) \cdot \cos(\phi_{outlet}) \right)$$

or

$$F_X = \left(\rho_{inlet} \cdot \left(\frac{Q_{inlet}^2}{A_{inlet}} \right) \cdot \cos(\phi_{inlet}) \right) - \left(\rho_{outlet} \cdot \left(\frac{Q_{outlet}^2}{A_{outlet}} \right) \cdot \cos(\phi_{outlet}) \right)$$

where

$m \equiv$ Mass (kg)

$C \equiv$ Absolute velocity vector (m/s)

$t \equiv$ Time (s)

ϕ_{outlet} and ϕ_{inlet} denotes the angle to calculate the axial component of the absolute velocity C.

for a centrifugal pump impeller where the fluid enters the impeller parrallel to the machine axis and exits at a 90 degree angle, $\phi_{inlet} = 0$ and $\phi_{outlet} = 90$

$$F_X = \left(\rho_{inlet} \cdot \left(\frac{Q_{inlet}^2}{A_{inlet}} \right) \cdot \cos(0^\circ) \right)$$

$$F_X = \rho_{inlet} \cdot \left(\frac{Q_{inlet}^2}{A_{inlet}} \right) \qquad (2.4)$$

For the thrust calculation in direction B, due to the pressure at the back of the impeller, the following formula is used [19]:

$$T_B = \frac{3}{4} \cdot P_D \cdot (A_3 - A_S) \qquad (2.5)$$

In practice, the pressure distribution on the rear side of the impeller has a nonlinear profile. For simplification the pressure distribution on the rear is assumed to be a constant at 75% of the differential pressure P_D [19].

It should be noted that the thrust force is calculated as a vector and a vector has a specific direction associated with it. Thus to calculate the net thrust, the thrust in direction B is subtracted from the thrust in direction A, as in Equation 2.6. A positive value for T_{net} indicates that the net thrust is exerted in direction A while a negative value indicates that the net thrust is in direction B.

$$T_{net} = T_A - T_B \tag{2.6}$$

The thrust calculation method, as described above, was applied to centrifugal pumps with a single suction inlet and without any ribs on the rear shroud to reduce thrust. Equation 2.2 also applies to incompressible gas flow, provided the specific gravity or density relative to water is used. If the specific gravity of a gas is substituted in Equation 2.2, the density will be relative to another gas and not relative to water and the same order of force is obtained. If the actual density of nitrogen in a gas phase is substituted in Equation 2.4, a substantially lower thrust force will be obtained than with water. Thus if Equation 2.4 is used instead of Equation 2.2, this thrust calculation method applies to liquids and gasses. The rest of the forces result from pressures acting on areas and is valid for both liquids and gasses.

2.2.2 Method 2 by Stepanoff [27]:

Stepanoff [27] states that the thrust of an open centrifugal pump impeller (Figure 2.3) is calculated by subtracting the thrust force on the front of the impeller from the thrust force on the rear of the impeller. Thrust on the rear of the impeller is given as:

$$T_b = (A_2 - A_s) \cdot \left[H_v - \frac{1}{8} \cdot \frac{(u_2^2 - u_s^2)}{2g} \right] \cdot \gamma \tag{2.7}$$

where

$A_s \equiv$ Shaft area (m^2)
$A_2 \equiv$ Impeller rear shroud area (m^2)
$Hv \equiv$ Pressure head developed at the impeller periphery (m)
$u_s \equiv$ Shaft peripheral velocity (m/s)
$u_2 \equiv$ Outer diameter peripheral velocity (m/s)
$g \equiv$ gravitational acceleration ($9.81 m/s^2$)
$\rho \equiv$ Fluid density (kg/m^3)
$\gamma \equiv$ Specific weight of the fluid (kg/m^2s^2)
$T_b \equiv$ Thrust force on rear of impeller (N)

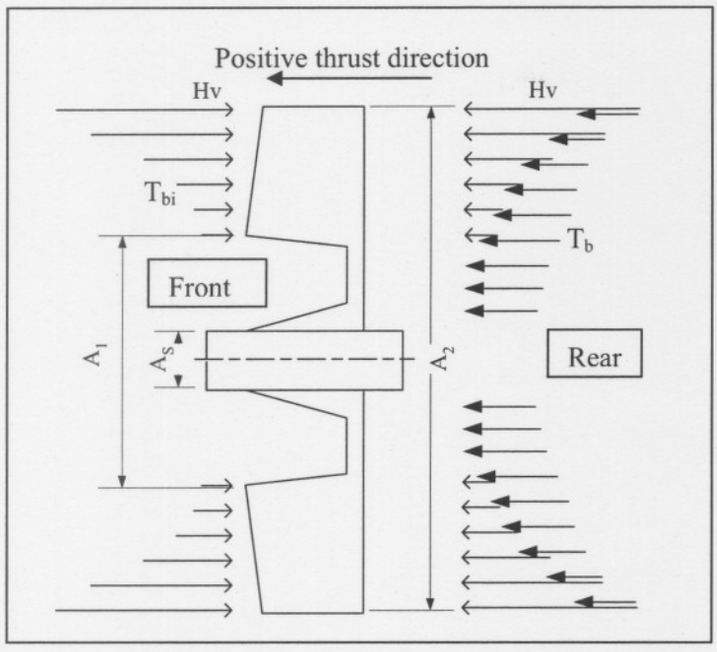


Figure 2.2: Axial thrust of an open centrifugal pump impeller

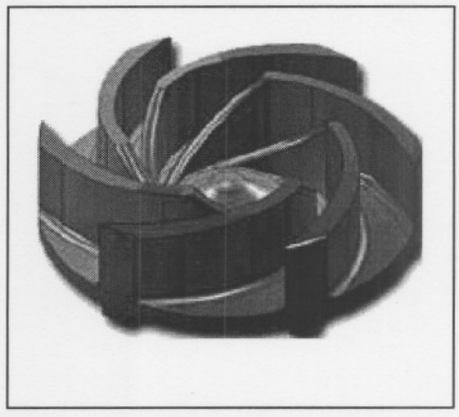


Figure 2.3: Illustration of an open centrifugal pump impeller

γ is calculated by multiplying the density of the fluid with gravitational acceleration $\gamma = \rho \cdot g$. The thin arrows in Figure 2.2 depict the parabolic head developed by the fluid as it moves through the impeller on the vaned side, while the bold arrows resemble the unbalanced portion of the head developed on the rear shroud. The head developed on the rear shroud is given by vector addition of the bold arrows and the thin arrows. Therefore, the thrust force on the front of the impeller is only partly balanced by the thrust on the rear of the impeller. Stepanoff calculates the head loss due to fluid rotation as the factor: $\frac{1}{8} \cdot \frac{\left(u_2^2 - u_s^2\right)}{2g}$.

The thrust on the vaned side of the impeller is calculated as [27]:

$$T_{bi} = \left(A_2 - A_1\right) \cdot \frac{H_v}{2} \cdot \gamma \tag{2.8}$$

A_1 is defined as shown in Figure 2.2. The parabolic pressure head (H_v) acting inside the impeller is simplified to an assumed constant value of $\frac{H_v}{2}$. Again the net thrust is obtained by subtracting T_{bi} from T_b [27]:

$$T_{net} = T_b - T_{bi} \tag{2.9}$$

A positive value of T_{net} indicates that the thrust force acts from the rear side to the front of the impeller. From the equations above, it is evident that Stepanoff ignores the pressure forces on the unvaned part of the impeller.

In some applications it is required to pump suspended particles. To prevent that the suspended particles obstruct the impeller, parts of the back shroud is cut out. Due to the smaller area of the back shroud and

short circuiting of the suction and pressure paths at the eye area, such impellers develop lower thrust forces [27].

This thrust calculation method of Stepanoff is applied to incompressible flow in centrifugal pumps. For incompressible flow, γ is a constant due to the density being constant. For compressible flow of gasses, γ is not constant because of the varying density. Thus to make this method applicable to gasses, some assumption will have to be made regarding the density to be used in the calculation of γ. It is assumed with this type of radial pump that the inlet velocity is in the radial direction as well as the outlet velocity. Thus there is no change of momentum fluid inside the impeller.

2.2.3 Method 3 by Japikse [17]:

Japikse [17] derives the thrust calculation of a centrifugal compressor from conservation of momentum on a control volume. The momentum equation for the control volume of Figure 2.4 in the axial direction is written as:

$$\iint \rho \mathbf{C}(\mathbf{C}\cdot d\mathbf{A}) = \oint p \cdot d\mathbf{A} + \mathbf{F} \tag{2.10}$$

It is possible to evaluate Equation 2.10 if detailed velocities and pressures of the control volume are known. When detailed pressures and velocities are not known, an approximation can be made by describing the static pressure field as a function of the radius along the outlet, front- and rear cavity in terms of a fraction of the local wheel speed. This approximation is given as:

$$p(r) = p_1' + (1-F^2)\cdot\left(\frac{\rho}{2}\right)\cdot\left[U^2(r) - U_1'^2\right]$$

or re - arranged as :

$$p(r) = \left(\frac{\rho}{2}\right)\cdot(1-F^2)\cdot U^2(r) + \left[p_1' - \left(\frac{\rho}{2}\right)\cdot(1-F^2)\cdot U_1'^2\right] \tag{2.11}$$

$$p(r) = Ar^2 + B$$

with

$p(r) \equiv$ the static pressure field as a function of radius

$p_1' \equiv$ the static pressure at station 1'

$F \equiv$ front cavity speed ratio

$\rho \equiv$ density

$U_1' \equiv$ tangential velocity at station 1'

and

$$A = \left(\frac{\rho}{2}\right)(1-F^2)(2\pi\omega)^2$$

$$B = p_1' - \left(\frac{\rho}{2}\right)(1-F^2)U_1'^2$$

A detailed derivation of Equation 2.11 is given in Japikse [17]. The thrust force due to the axial component of momentum exerted on the impeller can be calculated with [17]:

$$F_{momentum} = \left(\dot{m} \cdot C_1 \cdot \sin\Phi_1\right) - \left(\dot{m} \cdot C_2 \cdot \sin\Phi_2\right) \tag{2.12}$$

For the nomenclature used in Equation 2.12, refer to Figure 2.4. Pressures acting along the control volume boundaries also amount to the thrust force exerted and are calculated as follows:

$$F_1 = p_{1h} \cdot \pi \cdot r_{1h}^2 \tag{2.13}$$

Equation 2.13 calculates the thrust force component due to the inlet hub pressure $\left(p_{1h}\right)$ acting on the shaft area $\left(\pi r_{1h}^2\right)$ exposed at the inlet. A second thrust force component results from the average inlet pressure acting on the inlet projected blade area [17]:

$$F_2 = \frac{p_{1h} + p_{1t}}{2} \cdot \pi \cdot \left(r_{1t}^2 - r_{1h}^2\right) \tag{2.14}$$

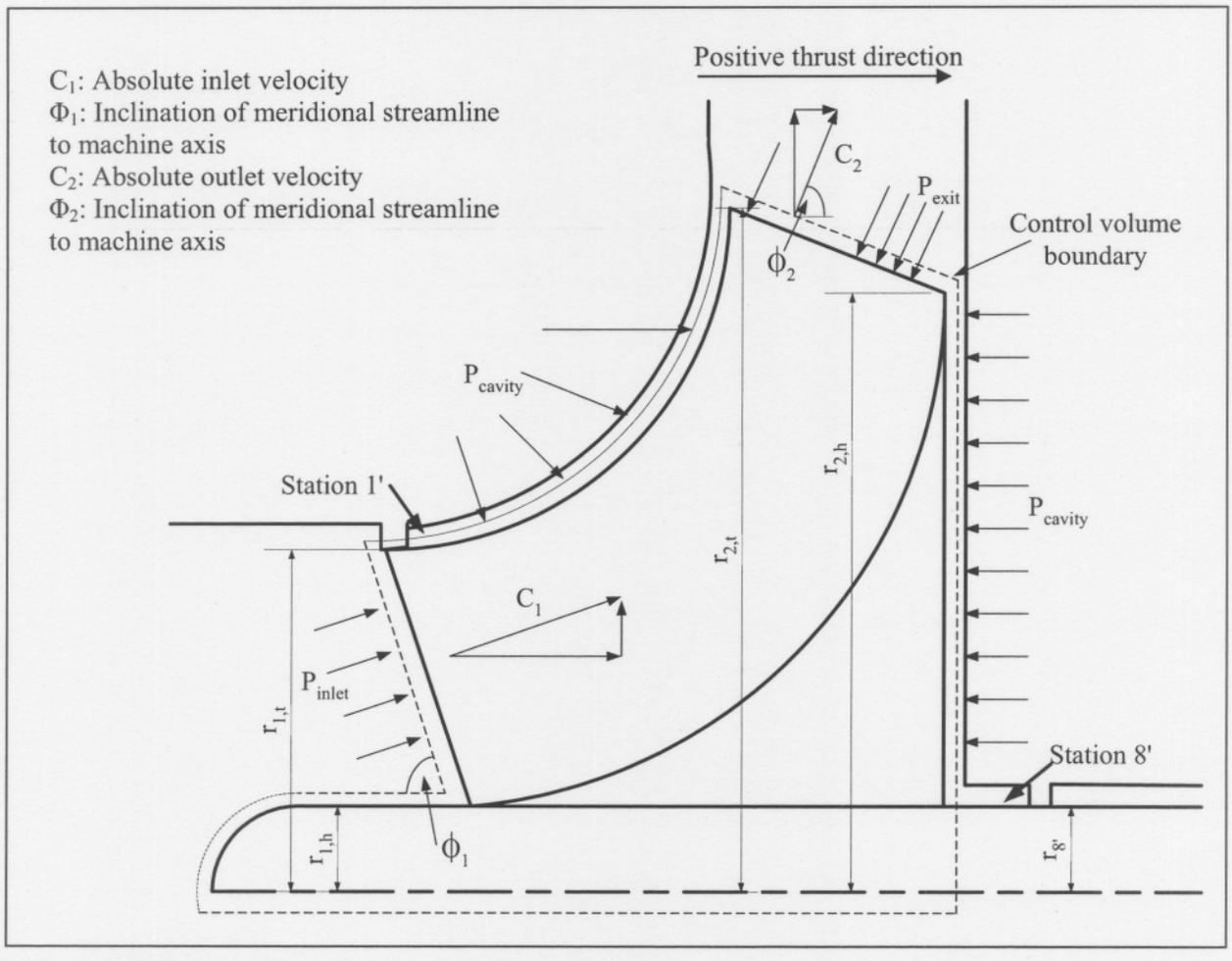


Figure 2.4: Control volume for thrust force calculation

Equation 2.11 is used to calculate the pressure as a function of radius. The third thrust force component is due to the pressure on the front cavity (from inlet tip radius to outlet tip radius). The resulting equation for this thrust force component is Equation 2.15:

$$F = \underbrace{\text{Pressure}}_{\text{Eq. 2.11}} \times \text{Area}$$

$$F_3 = \left[\underbrace{\left(\frac{\pi}{2} \cdot \left(r_{2t}^4 - r_{1t}^4 \right) \right)}_{\text{Area} \times r^2} \cdot \underbrace{\left(\frac{\rho}{2} \right) \cdot \left(1 - F_f^2 \right) \cdot \left(2\pi\omega \right)^2}_{A_f} \right] + \left[\underbrace{\left(\pi \cdot \left(r_{2t}^2 - r_{1t}^2 \right) \right)}_{\text{Area}} \cdot \underbrace{\left[p_1' - \left(\frac{\rho}{2} \right) \cdot \left(1 - F_f^2 \right) \right] \cdot U_1'^2}_{B_f} \right] \tag{2.15}$$

where r (m) is a radius at a specified location, ρ (kg/m^3) is the fluid density, F_f (dimensionless) is the front cavity speed ratio, ω (rad/s) the rotational speed of the impeller, p_1' (Pa) is the static pressure just inside the inlet tip seal (See Figure 2.4) and U_1' (m/s) the tangential velocity of the blades [17]. Subscripts 2t and 1t refer to the outlet- and inlet tip radii.

The thrust force component, acting on the rear cavity, is derived similarly to Equation 2.15 as [17]:

$$F_4 = -\left[\underbrace{\left(\frac{\pi}{2} \cdot \left(r_{2h}^4 - r_{8h}^4 \right) \right)}_{\text{Area} \times r^2} \cdot \underbrace{\left(\frac{\rho}{2} \right) \cdot \left(1 - F_r^2 \right) \cdot \left(2\pi\omega \right)^2}_{A_r} \right] - \left[\underbrace{\left(\pi \cdot \left(r_{2h}^2 - r_{8h}^2 \right) \right)}_{\text{Area}} \cdot \underbrace{\left[p_8' - \left(\frac{\rho}{2} \right) \cdot \left(1 - F_r^2 \right) \cdot U_8'^2 \right]}_{B_r} \right] \tag{2.16}$$

with subscripts r_{2h} and r_{8h} (m) the radii at the outlet hub and shaft at the back of the impeller respectively. F_r (dimensionless) denotes the rear cavity speed ratio, p_8' (Pa) is the static pressure next to the shaft seal on the impeller side and U_8' (m/s) is the tangential velocity of the shaft. A typical value for the cavity speed ratio (F_f, F_r) is 0.75 for a compressor, but it can vary from 0.3 to 0.9 [17]. Satisfactory results have been obtained for the thrust calculation if an average density between compressor inlet and outlet is substituted for the front cavity. For the rear cavity, an average density is calculated between impeller outlet and the shaft (station 8') [4].

The last thrust force component results from the outlet static pressure (p_2) acting on the outlet of the impeller from outlet tip (r_{2t}) to outlet hub (r_{2h}) and is calculated as follows [17]:

$$F_5 = -p_2 \cdot \pi \cdot \left(r_{2t}^2 - r_{2h}^2 \right) \tag{2.17}$$

To obtain the net thrust that the impeller exerts, the force due to change in momentum $(F_{momentum})$ and the five pressure force components $(F_1 \text{ to } F_5)$ are summed:

$$F_{net} = F_{momentum} + F_1 + F_2 + F_3 + F_4 + F_5 \tag{2.18}$$

2.2.4 Method 4 by Gülich [11]:

According to Gülich [11] the thrust for a single suction open impeller centrifugal pump is calculated with the following formula if a linear increase of pressure with radius in the impeller is assumed:

$$F_{ax} = \underbrace{\frac{\pi}{4} \cdot d_2^2}_{Area} \cdot \underbrace{\left[\Delta p_{La} \cdot \left(1 - \frac{d_D^2}{d_2^2} \right) - \frac{\rho}{4} \cdot \overline{k}_{Ts}^2 \cdot u_2^2 \cdot \left(1 - \frac{d_D^2}{d_2^2} \right)^2 - \frac{\Delta p_{La}}{2} \cdot \left(1 - \frac{d_1^2}{d_2^2} \right)^2 \right]}_{Pressure} \tag{2.19}$$

d_D, d_1 and d_2 (m) denotes the shaft sealing diameter, impeller inlet diameter and impeller outlet diameter respectively (See Figure 2.5). Δp_{La} (Pa) is the differential static pressure between the impeller outlet and impeller inlet. ρ (kg/m^3) is the density of the fluid being pumped and u_2 (m/s) is the peripheral velocity at the impeller outlet diameter d_2. $\overline{k}_{Ts}$ is a dimensionless parameter, called the rear side room rotation factor. It is calculated with Equation 2.20 after at least one static pressure, p, at a known radius, r, has been determined experimentally [11].

$$\overline{k}_{Ts} = \sqrt{\frac{2 \cdot (p_2 - p)}{\rho \cdot u_2^2 \cdot \left(1 - \frac{r^2}{r_2^2} \right)}} \tag{2.20}$$

As mentioned before, p in Equation 2.20 denotes a static pressure, measured at any radius r smaller than r_2. In addition to Equation 2.19 the thrust force, due to the change in fluid momentum, is added [11].

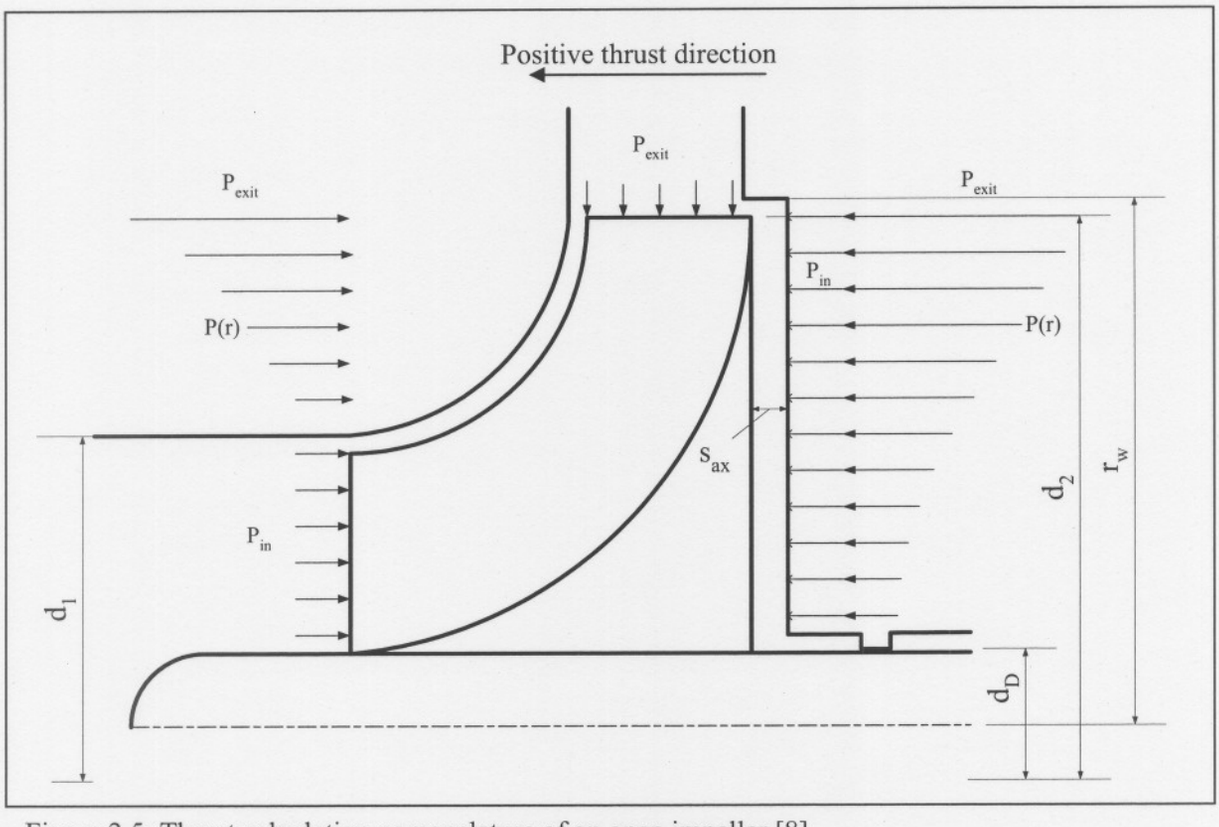


Figure 2.5: Thrust calculation nomenclature of an open impeller [8].

2.2.5 Other Methods:

Similar to Japikse [17], Liebner [18] suggests that the thrust on a turbocharger thrust bearing is calculated by applying the conservation of momentum law (see Figure 2.4) on two control volumes that include only the compressor- and turbine impellers. The pressure forces are calculated from the static pressure fields of both the turbine and compressor. A change of fluid momentum also exerts a thrust force that must be added to the pressure force. The resultant of the pressure force components and momentum component is the thrust force acting on the thrust bearing.

An alternative method for the prediction of thrust on an impeller is the use of Computational fluid dynamics (CFD) numerical simulation [12]. The CFD method implies that the flow field inside and around the impeller is divided into a finite number of volumes and that the governing equations are applied to each volume in discretized form. It should be noted that the flow field does not consist of the impeller geometry but of the flow paths. A linear k-ω turbulence model is used to simulate Eddy viscosity. At mesh vertices the Least-squares method is applied to calculate gradients and an explicit scheme is used for time integration. Results from the numerical CFD simulation includes axial thrust load from the compressor and details of the leakage flows. This simulation was validated by demonstration that the solution was grid independent. No experimental validation occurred at the time of print due to the lack of experimental data for the specific compressor.

NREC ETI, Inc. developed turbo machinery design software named NREC Concepts®. This software computes the axial thrust that is exerted on an impeller as the sum of seven forces namely:

- "Force due to the momentum of the flow entering the impeller" [20].
- "Force due to the momentum of flow leaving the impeller" [20].
- "Force due to the pressure over the impeller inlet" [20].
- "Force due to the pressure over the impeller outlet" [20].
- "Force due to the pressure in the leakage path behind the impeller hub" [20].
- "Force due to the pressure along the impeller shroud. For an open impeller it is the force due to the pressure along the shroud side of the blade passage" [20].
- "Force on the exposed part of the shaft coming out of the front of the impeller" [20].

This method is exactly the application of Japikse's thrust calculation method.

2.3 Thrust measurement techniques:

2.3.1 Method 1:

Figure 2.6 illustrates the use of strain gauges wired in the form of a Wheatstone bridge. The Wheatstone bridge forms a strain gauge load cell that gives a cumulative averaged reading of all strain gauges when the thrust bearing is deformed by the thrust force. A strain gauge amplifier provides the excitation voltage

for the Wheatstone bridge and amplifies the output voltage from the Wheatstone bridge. The output strain value can be related to a thrust force value. Duncan [7] used this method to measure the thrust force of a pump. It had been calibrated on a compression test machine.

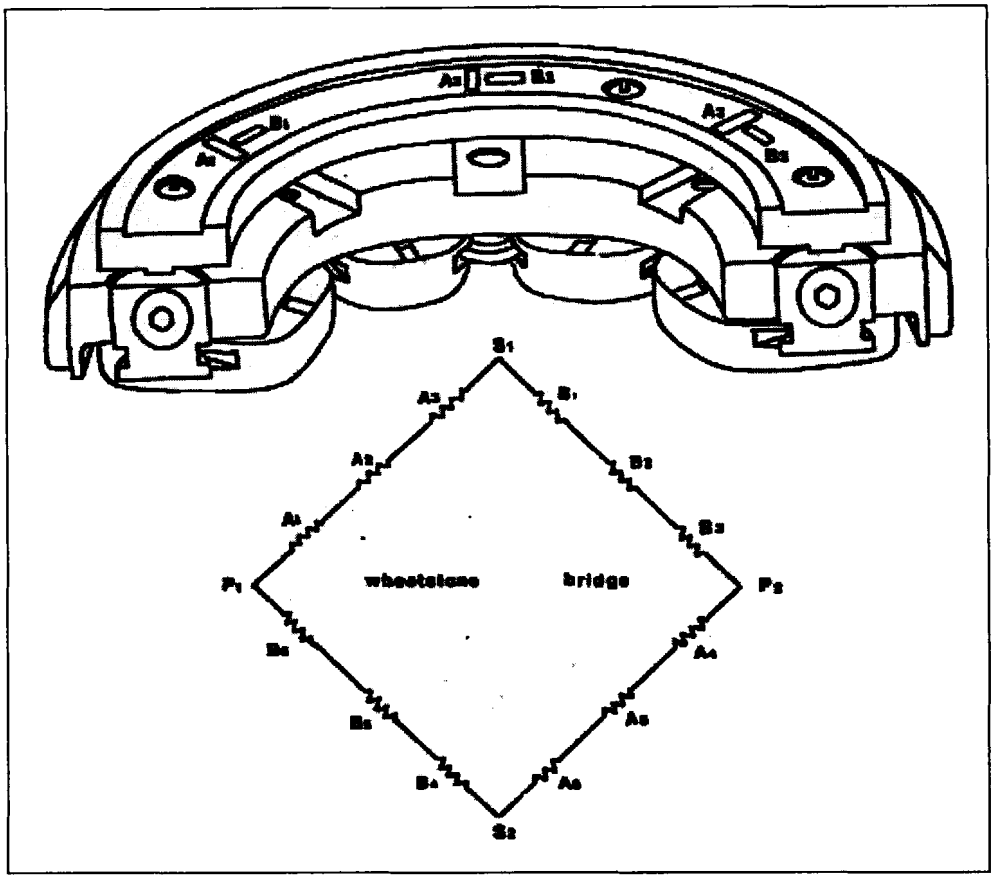


Figure 2.6: Thrust measurement with a Wheatstone bridge on a tilting pad thrust bearing. Adapted from Duncan [7].

2.3.2 Method 2:

Five axis magnetic bearing technology offers an accurate method of thrust force measurement. Thrust can be measured with magnetic bearings because any change in the axial magnetic stator current is related to the thrust force exerted. Electro-magnetic bearings can also be utilized to measure thrust forces under steady state as well as transient conditions [2].

2.3.3 Other methods:

Force washers as illustrated in Figure 2.7 can also be used to measure a force. Forces in the order of 0.04448kN to 444.8kN can be measured with thrust washers [22]. A disadvantage is that these force washers can measure compression forces only. This thrust washer can be bolted between a bolt head and the component to measure the force.

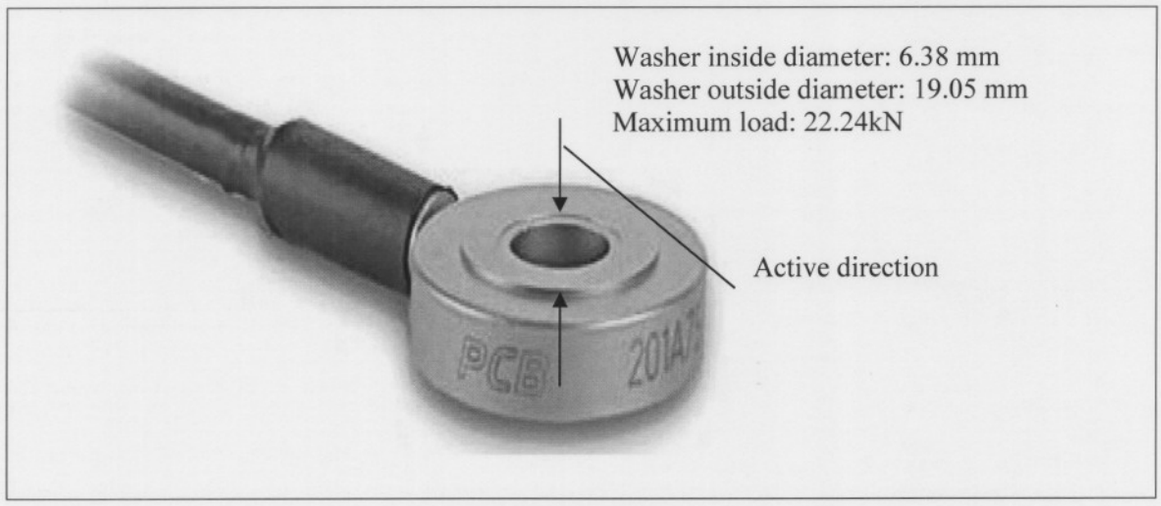


Figure 2.7: Commercially available force washer

An alternative for strain measurement with strain gauges are piezo-electric strain sensors (see Figure 2.8). These sensors can operate at temperatures of -54 to 121°C and measure up to 300με with a sensitivity of 10mV/με [22].

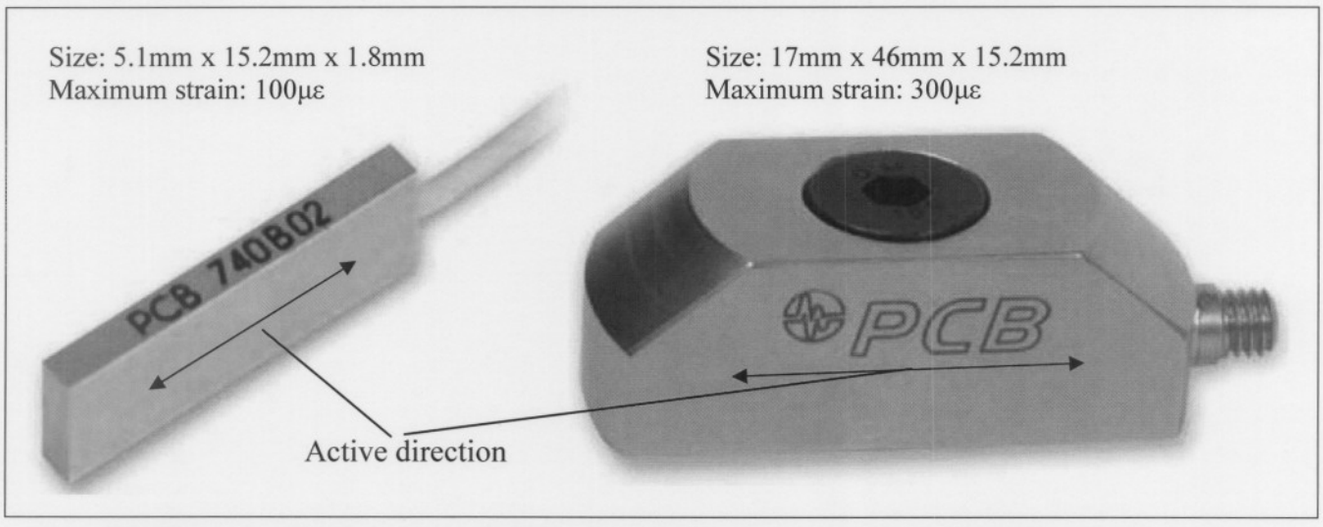


Figure 2.8: Piezo-electric strain sensors [22]

2.4 Summary:

Several thrust calculation methodologies have been discussed in Sections 2.2.1 to 2.2.5. A first method by Lobanoff and Ross [19] was applied on centrifugal pumps with open impellers and assumes a constant pressure distribution and includes the thrust force that results from the change of momentum. Input parameters include pressures at inlet and outlet of the impeller, impeller size (inlet and outlet areas), volume flow rate and specific gravity of the fluid.

Stepanoff [27] gave a similar method to Lobanoff and Ross [19] for thrust calculation in centrifugal pumps with open impellers but the multiplication factor for the pressure values differs and a parabolic

pressure distribution is assumed. The thrust force due to a change in fluid momentum is ignored by Stepanoff.

A method suggested by Japikse [17] models the parabolic pressure field of a centrifugal compressor and changes the cavity speed ratio factor (F) to adjust calculated thrust values to measured data. All forces resulting from pressures and momentum are taken into account for the thrust calculation; therefore this method has a comprehensive list of input parameters that includes geometry such as impeller areas and vane angles, pressures, velocities and fluid properties.

In the thrust calculation method for centrifugal pumps with open impellers presented by Gülich [11], a parabolic pressure distribution is assumed. The pressure loss due to fluid rotation is accounted for by calculating a factor $\left(\overline{k}_{Ts}\right)$ from an experimentally measured pressure. Thrust resulting from a change in fluid momentum should be added. Parameters needed as input include pressures, geometry like impeller areas, fluid density, and peripheral velocities.

Computational Fluid dynamic (CFD) simulation can also be utilized for modelling compressor thrust but the results of the article still have to be verified against experimental measurements.

From literature two methods for experimental thrust measuring have been found namely: strain gauges wired in a Wheatstone bridge to form a strain gauge load cell or magnetic bearing technology from which the axial magnetic stator current can be measured and related to the axial thrust.

A force washer is an alternative method that can be implemented to measure force by installing such a force washer on a thrust bearing mounting bolt.

Piezo-electric strain sensors can be used as an alternative for strain gauges in strain measurement. The strain can then be related to a thrust force exerted on the thrust bearing.

3. Theoretical thrust calculations

3.1 Introduction:

The literature on thrust calculation methodologies was discussed in the preceding chapter. Some of these methodologies are applied to theoretically predict the thrust force exerted during the operation of the HPTU, that consists of a centrifugal- compressor and turbine. Most of the thrust calculation methods discussed in Chapter 2 were applied to centrifugal pumps with open impellers and had to be adapted to apply to the compressible flow of the centrifugal compressor and turbine of the HPTU. In centrifugal pumps it is assumed that the density of the fluid is constant, while the density varies in a compressor or turbine. Some of the methodologies cited are therefore not directly applicable to the calculation of the thrust of compressible fluid turbo machines like the HPTU.

In the subsequent sections, detailed thrust calculations are performed with some of the methods discussed in Chapter 2. The different thrust calculation methodologies were programmed using Engineering Equation Solver (EES), which solves the set of simultaneous algebraic equations. Table 3.1 list the geometry of the impellers of the HPTU that are used in all of the thrust calculations to follow.

Compressor		**Turbine**	
Inlet diameter: $D_{1,c}$	0.0678m	Inlet diameter: $D_{1,t}$	0.082m
Outlet diameter: $D_{2,c}$	0.094m	Outlet diameter: $D_{2,t}$	0.075m
Shaft diameter: $D_{8',c}$	0.0134m	Shaft diameter: $D_{8',t}$	0.02m
Outlet blade height: $b_{2,c}$	0.0065m	Inlet blade height: $b_{1,t}$	0.0155m
Inlet flow angle: $\Phi_{1,c}$	0°	Inlet flow angle; $\Phi_{1,t}$	90°
Outlet flow angle: $\Phi_{2,c}$	90°	Outlet flow angle: $\Phi_{2,t}$	0°

Table 3.1: HPTU turbocharger geometry.

To compare the solution of the different thrust calculation methodologies, a single arbitrary data point from a previous PBMM test run is used as input to the thrust calculation methodologies. The single data point contains parameters like the inlet- and outlet- temperatures and pressures of the compressor and turbine, mass flow rate, rotor rotational speed and lubrication chamber pressure. The values of these parameters are listed in Table 3.2. The measuring instruments for the parameters listed in Table 3.2, have an accuracy of ±1% of its full scale range, commensurate with normal industrial standards, and all data were captured with the data acquisition system of the PBMM, except the strain data and the vibration spectra.

Compressor		Turbine	
Inlet pressure: $P_{inlet,c}$	43060Pa (gauge)	Inlet pressure: $P_{inlet,t}$	109195Pa (gauge)
Outlet pressure: $P_{outlet,c}$	113834Pa (gauge)	Outlet pressure: $P_{outlet,t}$	65645Pa (gauge)
Inlet temperature: $T_{inlet,c}$	287.15K	Inlet temperature: $T_{inlet,t}$	792.135K
Outlet temperature: $T_{outlet,c}$	337.849K	Outlet temperature: $T_{outlet,t}$	706K
Rotor Speed: N	56123RPM	Mass flow rate: $\dot{m}$	0.302kg/s
Lubrication chamber pressure: $P_{lub-chamber}$	86500Pa (absolute)		

Table3.2: Test data input parameters

3.2 Method 1 by Lobanoff and Ross [19]:

Equations 2.1 to 2.6, as introduced in Chapter 2, describe the method for thrust calculation by Lobanoff and Ross [19] for a centrifugal pump. This method is adapted to apply to both the compressor and turbine, and to yield a positive thrust value for a net thrust in the direction: "turbine to compressor".

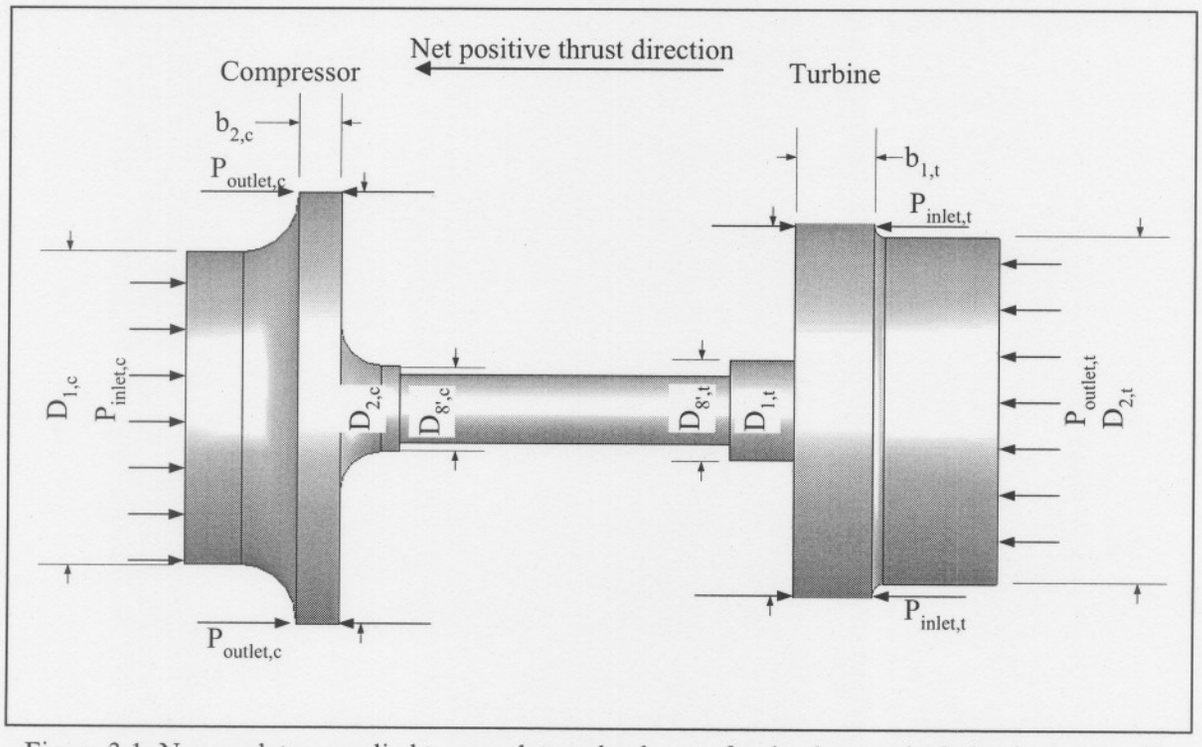


Figure 3.1: Nomenclature applied to complete turbocharger for the thrust calculation by Lobanoff and Ross.

Figure 3.1 shows the nomenclature used in the equations of Appendix A1 to calculate the thrust on both the compressor and turbine. All parameters from Table 3.1 and those applicable to this method from Table 3.2 are used as input for the thrust calculation. A built-in function in EES was used to evaluate the density of the fluid at different pressures and temperatures. Imperial units were used in the literature while

this thrust calculation is performed with metric units. With the positive flow angles as defined in Figure 3.2, the thrust force due to a change in fluid momentum for a control volume that includes the compressor wheel is derived as follows for a global coordinate system with x-axis defined "compressor to turbine" as positive and for the y-axis, upward is positive:

The force on the fluid due to a change in momentum inside the compressor is:

$$F_{momentum,fluid,c} = \dot{m} \cdot C_{2,c} \cdot \cos\Phi_{2,c} - \dot{m} \cdot C_{1,c} \cdot \cos\Phi_{1,c}$$

If $\phi_{2,c} < 90$ the outlet momentum will subtract from the inlet momentum (smaller momentum change from inlet to outlet). If $\phi_{2,c} > 90$ the outlet momentum will add to the inlet momentum (larger momentum change from inlet to outlet). The force from the fluid on the compressor impeller is just in the opposite direction (sign) that gives:

$$F_{momentum,c} = \underbrace{\dot{m} \cdot C_{1,c} \cdot \cos(\Phi_{1,c})}_{\text{into compressor control volume}} - \underbrace{\dot{m} \cdot C_{2,c} \cdot \cos(\Phi_{2,c})}_{\text{out of compressor control volume}} \quad (3.1)$$

and for the turbine control volume the force on the fluid due to a change in momentum inside the turbine is calculated with:

$$F_{momentum,fluid,t} = \dot{m} \cdot C_{2,t} \cdot \cos\Phi_{2,t} - (-)\dot{m} \cdot C_{1,t} \cdot \cos\Phi_{1,t}$$

If $\phi_{1,t} < 90$ the inlet momentum will add to the outlet momentum (larger momentum change from inlet to outlet) and conversely if $\phi_{1,t} > 90$ the inlet momentum will subtract from outlet (smaller momentum change from inlet to outlet). The force from the fluid on the turbine impeller acts in the opposite direction, therefore the sign is changed to:

$$F_{momentum,t} = \underbrace{-\dot{m} \cdot C_{1,t} \cdot \cos(\Phi_{1,t})}_{\text{into turbine control volume}} - \underbrace{\dot{m} \cdot C_{2,t} \cdot \cos(\Phi_{2,t})}_{\text{out of turbine control volume}} \quad (3.2)$$

$\dot{m} \equiv$ Mass flow rate (kg/s)
$C_{1,c} \equiv$ Compressor absolute inlet velocity for a non - inertial control volume (m/s)
$C_{2,c} \equiv$ Compressor absolute outlet velocity for a non - inertial control volume (m/s)
$\phi_{1,c} \equiv$ Inclination angle of meridional streamline to compressor axis at inlet (degrees)
$\phi_{2,c} \equiv$ Inclination angle of meridional streamline to compressor axis at outlet (degrees)
$C_{1,t} \equiv$ Turbine absolute inlet velocity for a non - inertial control volume (m/s)
$C_{2,t} \equiv$ Turbine absolute outlet velocity for a non - inertial control volume (m/s)
$\phi_{1,t} \equiv$ Inclination angle of meridional streamline to turbine axis at inlet (degrees)
$\phi_{2,t} \equiv$ Inclination angle of meridional streamline to turbine axis at outlet (degrees)

Equation 2.2 becomes invalid if metric units are used due to the conversion factor. Equations 3.1 and 3.2 are derived to calculate the thrust due to a change of fluid momentum inside the impellers (compressor and turbine), by applying conservation of momentum for a non-inertial control volume. The mass flow rate used in Equation 3.1 and 3.2 will change if the density of the fluid changes and is applicable for compressible fluids as well as incompressible fluids. The specific gravity of water is unity by definition

and for nitrogen in a gas phase it is 0.97 by definition. Thus for the same volume flow rate and area, the thrust exerted by water and the thrust exerted by nitrogen in a gas phase will differ by 4% when Equation 2.2 is used. If Equation 2.4 is used, the difference will be 99.95% due to the difference in density between water (1000kg/m^3) and nitrogen (±0.5kg/m^3). Therefore, Equation 2.2 is not suitable for compressible flow machines; Equations 3.1 and 3.2, which are based on Equation 2.4, are used for this thrust calculation with a compressible flow compressor and turbine. The detail thrust calculation with the method of Lobanoff and Ross applied on a compressible flow centrifugal compressor and turbine can be seen in Appendix A1.

The main equation for the thrust calculation with the method of Lobanoff & Ross is:

$$Net_{turbo,thrust} = \left[\left(P_{outlet,t} \cdot A_{8',t}\right) + \left[\left(A_{1,t} - A_{2,t}\right) \cdot \frac{\Delta P_t}{2}\right] - F_{momentum,t}\right] - \left[\frac{3 \cdot \Delta P_t}{4} \cdot A_{1,t} - A_{8',t}\right]$$
$$- \left[\left(P_{inlet,c} \cdot A_{8',c}\right) + \left[\left(A_{2,c} - A_{1,c}\right) \cdot \frac{\Delta P_c}{2}\right] + F_{momentum,c}\right] + \left[\frac{3 \cdot \Delta P_c}{4} \cdot \left(A_{2,c} - A_{8',c}\right)\right] : [N] \qquad (3.3)$$

Net thrust exerted on turbocharger thrust bearing

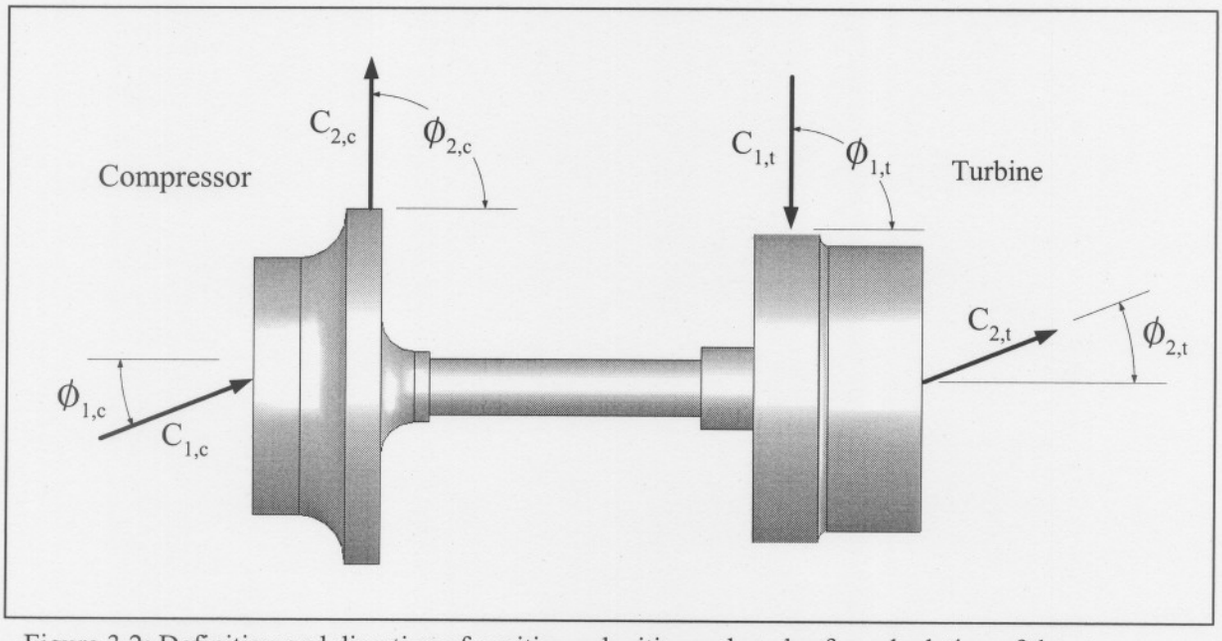


Figure 3.2: Definition and direction of positive velocities and angles for calculation of thrust exerted due to a change in fluid momentum.

$A_{1,c} = 0.00361$ [m^2]	$\rho_{2,t} = 0.3132$ [kg/m^3]	$T_{B,c} = 360.9$ [N]
$A_{2,c} = 0.00694$ [m^2]	$C_{1,c} = 165.5$ [m/s]	$F_{momentum,t} = -65.91$ [N]
$A_{8',c} = 0.000141$ [m^2]	$C_{2,c} = 138.6$ [m/s]	$T_{A,t} = 105.3$ [N]
$A_{1,t} = 0.005281$ [m^2]	$C_{1,t} = 162.9$ [m/s]	$T_{B,t} = 162.2$ [N]
$A_{2,t} = 0.004418$ [m^2]	$C_{2,t} = 218.3$ [m/s]	$T_{net,c} = -187$ [N]
$A_{8',t} = 0.0003142$ [m^2]	$\Delta P_c = 70774$ [Pa]	$T_{net,t} = -56.9$ [N]
$\rho_{1,c} = 0.5053$ [kg/m^3]	$\Delta P_t = 43550$ [Pa]	$Net_{turbo,thrust} = 130.1$ [N]
$\rho_{2,c} = 1.135$ [kg/m^3]	$F_{momentum,c} = 49.99$ [N]	
$\rho_{1,t} = 0.4643$ [kg/m^3]	$T_{A,c} = 173.9$ [N]	

Table 3.3: Solution of thrust calculation with the method of Lobanoff & Ross.

For the set of input parameters regarding geometry, pressures, temperatures and mass flow rate, the net thrust exerted on the thrust bearing is 130.1N. This negative value indicates that the resultant thrust force acts in the direction "compressor to turbine". This method by Lobanoff and Ross does not account for effects like the position of the impeller relative to the side walls, Reynolds-number, surface roughness and leakage flows. The input parameters for this method are measurable and relatively easy to obtain, therefore it is an uncomplicated method for computation of thrust.

3.3 Method 2 by Stepanoff [27]:

In Section 2.2.2 of Chapter 2 the method of Stepanoff (Equations 2.7-2.9) for thrust calculation in open centrifugal pumps is discussed. Similar to the method by Lobanoff and Ross, the method by Stepanoff must be adapted to apply to a centrifugal compressor and turbine due to the compressibility of the fluid. Figure 3.3 illustrates the nomenclature used for the thrust calculation with the method of Stepanoff applied to the centrifugal compressor and turbine.

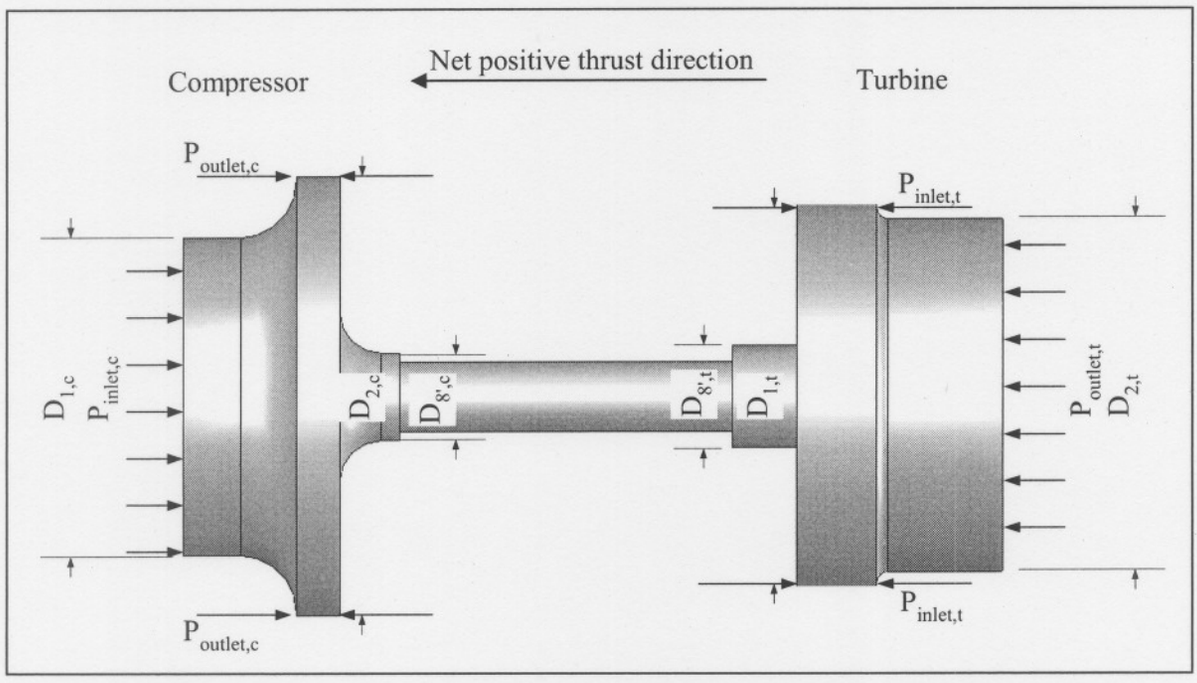


Figure 3.3: Nomenclature applied to complete turbocharger for the thrust calculation by Stepanoff.

The applicable geometrical parameters and test data parameters from Tables 3.1 and 3.2 are used as input for this thrust calculation. Different from other methods, the pressure is converted to a pressure head (typically used with pumps). As mentioned before, this method has to be modified to apply to compressible fluids. Density is used in the calculation of the pressure head, specific weight of the fluid and thrust. Thus as a first order estimate, the varying densities of the fluid is replaced by a weighted constant density on the rear shroud of the compressor and turbine. Equations 3.4 and 3.5 are derived as follows:

It is assumed that the pressure and density (ρ) on the rear of the shroud vary proportional to the square of the ratio of the shaft diameter ($D_{8',c}$ or $D_{8',t}$) and outlet diameter ($D_{2,c}$ for the compressor) or inlet diameter ($D_{1,t}$ for the turbine). This is due to the fact that the velocity increases linearly as the radius increases and pressure decrease proportional to the square of the velocity (Equation 2.10).

$$\frac{\rho_{8',c}}{\rho_{2,c}} \propto \left(\frac{D_{8',c}}{D_{2,c}}\right)^2 \text{ for the compressor}$$

and

$$\frac{\rho_{8',t}}{\rho_{1,t}} \propto \left(\frac{D_{8',t}}{D_{1,t}}\right)^2 \text{ for the turbine}$$

The weighted constant density assumed for the rear shroud is calculated as the weighted average density between the outlet density (compressor) or inlet density (turbine) and the density at the shaft.

$$\rho_{weighted,c} = \frac{\rho_{outlet,c}\left(\frac{D_{8',c}}{D_{2,c}}\right)^2 + \rho_{outlet,c}}{2}$$

$$\rho_{weighted,c} = \frac{\rho_{outlet,c}\left[\left(\frac{D_{8',c}}{D_{2,c}}\right)^2 + 1\right]}{2} : [kg/m^3]$$ Weighted average density on rear shroud of compressor (3.4)

$$\rho_{weighted,t} = \frac{\rho_{inlet,t}\left(\frac{D_{8',t}}{D_{1,t}}\right)^2 + \rho_{inlet,t}}{2}$$

$$\rho_{weighted,t} = \frac{\rho_{inlet,t}\left[\left(\frac{D_{8',t}}{D_{1,t}}\right)^2 + 1\right]}{2} : [kg/m^3]$$ Weighted average density at the rear of turbine (3.5)

For the vaned side of both the compressor and turbine, the arithmetic mean density between inlet and outlet was substituted in the calculation of specific weight of the fluid and the thrust. The complete thrust calculation is shown in Appendix A2. For the test data in Table 3.2, the net thrust exerted on the thrust bearing is calculated as -4.176N with Equation 3.6.

$$Net_{turbo,thrust} = \left[\left(A_{1,t} - A_{2,t}\right)\cdot\frac{Hv_t}{2}\cdot\gamma_{front,t}\right] - \left[\left(A_{1,t} - A_{8',t}\right)\cdot\left(Hv_t - \frac{1}{8}\cdot\left[\frac{u_{1,t}^2 - u_{8',t}^2}{2\cdot g}\right]\right)\right]\cdot\gamma_{rear,t}$$

$$-\left[\left(A_{2,c} - A_{1,c}\right)\cdot\frac{Hv_c}{2}\cdot\gamma_{front,c}\right] + \left[\left(A_{2,c} - A_{8',c}\right)\cdot\left(Hv_c - \frac{1}{8}\cdot\left[\frac{u_{2,c}^2 - u_{8',c}^2}{2\cdot g}\right]\right)\right]\cdot\gamma_{rear,c} : [N] \quad (3.6)$$

Net thrust exerted on turbocharger thrust bearing

A negative sign implies that the net thrust is acting in the direction: "compressor to turbine". Stepanoff ignores effects like the position of the impeller relative to the stationary side walls, Reynolds-number, surface roughness, leakage flows and thrust resulting from a change of momentum fluid inside the impeller.

$A_{1,c} = 0.00361\ [m^2]$	$\rho_{2,t} = 0.3132\ [kg/m^3]$	$u_{8',c} = 39.38\ [m/s]$
$A_{2,c} = 0.00694\ [m^2]$	$\rho_{avg,t} = 0.3887\ [kg/m^3]$	$u_{1,t} = 241\ [m/s]$
$A_{8',c} = 0.000141\ [m^2]$	$\rho_{weighted,t} = 0.2459\ [kg/m^3]$	$u_{8',t} = 58.77\ [m/s]$
$A_{1,t} = 0.005281\ [m^2]$	$\omega = 5877\ [rad/s]$	$T_{A,c} = 136.9\ [N]$
$A_{2,t} = 0.004418\ [m^2]$	$\gamma_{front,c} = 8.047\ [kg/m^2s^2]$	$T_{B,c} = 376.4\ [N]$
$A_{8',t} = 0.0003142\ [m^2]$	$\gamma_{rear,c} = 5.681\ [kg/m^2s^2]$	$T_{net,c} = -239.5\ [N]$
$\rho_{1,c} = 0.5053\ [kg/m^3]$	$\gamma_{front,t} = 3.813\ [kg/m^2s^2]$	$T_{A,t} = 39.46\ [N]$
$\rho_{2,c} = 1.135\ [kg/m^3]$	$\gamma_{rear,t} = 2.413\ [kg/m^2s^2]$	$T_{B,t} = 283.1\ [N]$
$\rho_{avg,c} = 0.8202\ [kg/m^3]$	$Hv_c = 10222\ [m]$	$T_{net,t} = -243.7\ [N]$
$\rho_{weighted,c} = 0.5791\ [kg/m^3]$	$Hv_t = 23976\ [m]$	$Net_{turbo,thrust} = -4.176\ [N]$
$\rho_{1,t} = 0.4643\ [kg/m^3]$	$u_{2,c} = 276.2\ [m/s]$	

Table 3.4: Solution of thrust calculation with the method of Stepanoff.

3.4 Method 3 by Japikse [17]:

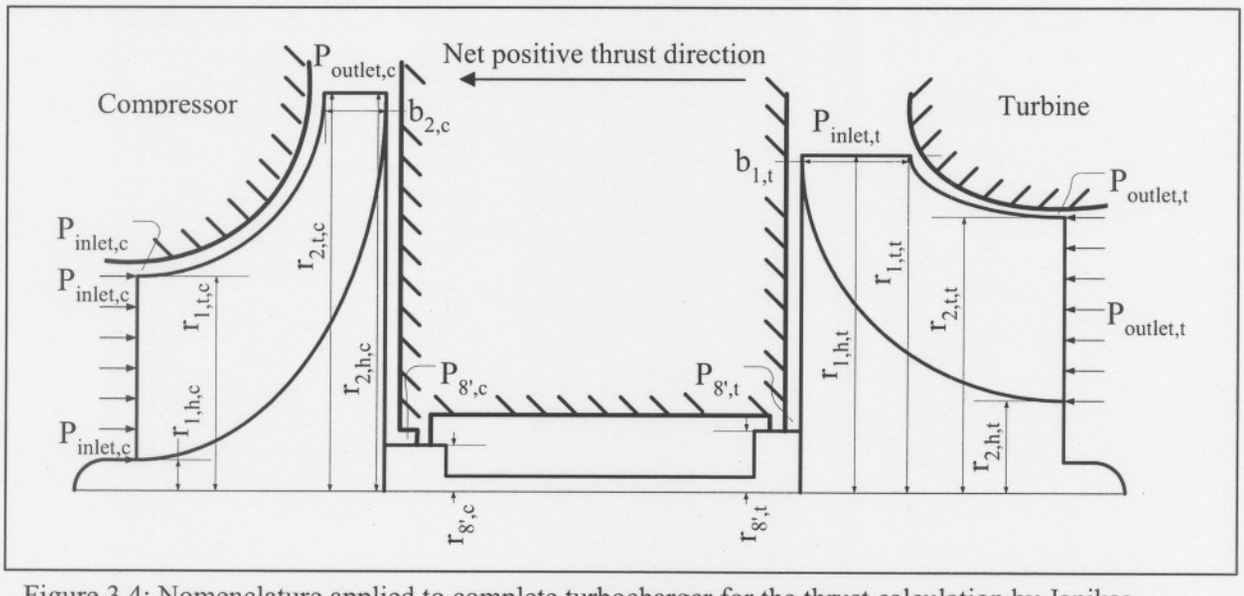


Figure 3.4: Nomenclature applied to complete turbocharger for the thrust calculation by Japikse

The only thrust calculation method discussed in Chapter 2 that was applied to a centrifugal compressor, is the method given by Japikse [17] in Section 2.2.3. Japikse's method requires more input parameters than the previous two methods in Sections 3.2 and 3.3; therefore it takes more effort to reach a solution. Figure 3.4 shows a sectional diagram for the turbo rotor with the nomenclature used in the subsequent thrust calculation.

It is assumed that the tip and hub pressure at inlet of the compressor and the outlet of the turbine is constant. The specific turbocharger used as the HPTU (High Pressure Turbo unit) of the PBMM has no seal at Station 1' (Refer to Figure 2.4, Chapter 2) on neither the compressor nor the turbine. Therefore it

is assumed that for the compressor, the pressure at station 1' is equal to the inlet pressure ($P_{inlet,c}$) and for the turbine that the pressure at station 2' equals the outlet pressure ($P_{outlet,t}$). Due to the difficulty to measure the true static pressure at $P_{8',c}$ and $P_{8',t}$ in the HPTU, it was assumed that the pressure is proportional to the square of the radius as before. With this assumption the pressure at $P_{8',c}$ and $P_{8',t}$ was calculated with Equations 3.7 and 3.8.

$$P_{8',c} = P_{outlet,c}\left[\left(\frac{r_{8',c}}{r_{2,h,c}}\right)^2\right] : [Pa]\ \text{Compressor shaft seal pressure} \tag{3.7}$$

$$P_{8,acsent,t} = P_{inlet,t}\left[\left(\frac{r_{8',t}}{r_{2,h,t}}\right)^2\right] : [Pa]\ \text{Turbine shaft seal pressure} \tag{3.8}$$

In order to substitute values for the cavity speed ratios ($F_{f,c}$, $F_{r,c}$, $F_{f,t}$ and $F_{r,t}$) that will produce accurate results, some past empirical experience is needed [17]. For a compressor, a good starting value would be if F equals 0.75 [17]. Therefore a value of 0.75 was assigned to $F_{f,c}$, $F_{r,c}$, $F_{f,t}$ and $F_{r,t}$. Alteration in any of the values for $F_{f,c}$, $F_{r,c}$, $F_{f,t}$ and $F_{r,t}$, greatly affects the solution for the thrust. Therefore, it may be necessary to alter the value of a single parameter when performing data fitting.

The calculation of the thrust due to a change in fluid momentum is slightly modified from the definitions used by Japikse. Equations 3.1 and 3.2 are used to calculate the thrust due to a change in fluid momentum along with the definitions of Figure 3.2; the same as for the Method 1 by Lobanoff and Ross.

For the front A-factor and B-factor of both the turbine and compressor ($A_{f,c}$, $A_{f,t}$,$B_{f,c}$,$B_{f,t}$) an average density between inlet and outlet was substituted as suggested by Baines [4]. At the shaft (station 8') a weighted density was substituted (Equations 3.4 and 3.5) in the calculation of the rear A- and B-factor.

$$\begin{aligned} Net_{turbo,thrust} = &-F_{momentum,t} + Pressure_{1,t} + Pressure_{2,t} + Pressure_{3,t} + Pressure_{4,t} + Pressure_{5,t} \\ &+ Pressure_{6,t} + Pressure_{7,t} - F_{momentum,c} - Pressure_{1,c} - Pressure_{2,c} - Pressure_{3,c} - Pressure_{4,c} \\ &-Pressure_{5,c} - Pressure_{6,c} - Pressure_{7,c} : [N]\ \text{Net thrust exerted on turbocharger thrust bearing} \end{aligned} \tag{3.9}$$

The solution obtained for the thrust calculation with the method of Japikse (Equation 3.9, for the detail refer to Appendix A3) is given in Table 3.5. For the same pressures and temperatures as used in the previous thrust calculation methods, the thrust force exerted on the thrust bearing with the method of Japikse is -146.1N. Japikse's thrust calculation accounts for thrust forces exerted by the pressure distribution acting on the control volume including the thrust from a change in fluid momentum inside the impeller. Effects like the gap between impeller and casing walls, Reynolds-number and surface roughness are inherently accounted for in the cavity speed ratio. The accuracy of the solution relies strongly on the value of cavity speed ratios and the density substituted in the A- and B-factors of both the compressor and turbine.

$A_{1,c} = 0.003456$ [m^2]	$U_{8',c} = 39.38$ [m/s]	$Pressure_{3,c} = 1368$ [N]
$A_{2,t} = 0.003962$ [m^2]	$C_{1,t} = 162.9$ [m/s]	$Pressure_{4,c} = 119.7$ [N]
$\rho_{1,c} = 0.5053$ [kg/m^3]	$C_{2,t} = 243.4$ [m/s]	$Pressure_{5,c} = -1324$ [N]
$\rho_{2,c} = 1.135$ [kg/m^3]	$U_{2,t} = 220.7$ [m/s]	$Pressure_{6,c} = -14.39$ [N]
$\rho_{avg,c} = 0.8202$ [kg/m^3]	$U_{8',t} = 60.24$ [m/s]	$Pressure_{7,c} = 0$ [N]
$\rho_{weighted,c} = 0.5791$ [kg/m^3]	$A_{f,c} = 2.447E+08$ [kg/m^3s^2]	$F_{momentum,t} = -73.5$ [N]
$\rho_{1,t} = 0.4643$ [kg/m^3]	$A_{r,c} = 1.727E+08$ [kg/m^3s^2]	$Pressure_{1,t} = 30.7$ [N]
$\rho_{2,t} = 0.3132$ [kg/m^3]	$B_{f,c} = 35938$ [Pa]	$Pressure_{2,t} = 260.1$ [N]
$\rho_{avg,t} = 0.3887$ [kg/m^3]	$B_{r,c} = 2117$ [Pa]	$Pressure_{3,t} = 152.6$ [N]
$\rho_{weighted,t} = 0.2466$ [kg/m^3]	$A_{f,t} = 1.159E+08$ [kg/m^3s^2]	$Pressure_{4,t} = 52.36$ [N]
$P_{8',c} = 2313$ [Pa]	$A_{r,t} = 7.357E+07$ [kg/m^3s^2]	$Pressure_{5,t} = -325.3$ [N]
$P_{8',t} = 6825$ [Pa]	$B_{f,t} = 61504$ [Pa]	$Pressure_{6,t} = -32.82$ [N]
$\omega = 5877$ [rad/s]	$B_{r,t} = 6629$ [Pa]	$Pressure_{7,t} = 0$ [N]
$C_{1,c} = 172.9$ [m/s]	$F_{momentum,c} = 52.22$ [N]	$Net_{turbo,thrust} = -146.1$ [N]
$C_{2,c} = 138.6$ [m/s]	$Pressure_{1,c} = 6.629$ [N]	
$U_{1,c} = 199.2$ [m/s]	$Pressure_{2,c} = 148.8$ [N]	

Table 3.5: Solution of thrust calculation with the method of Japikse.

3.5 Method 4 by Gülich [11]:

Gülich [11] calculates the thrust for an open centrifugal pump impeller as described in Section 2.2.4. In pumps, a constant density is used because incompressible flow is prevalent. Thus for the compressor and turbine, a weighted density (Equations 3.4 and 3.5) is assumed in the thrust calculation due to compressibility effects similar to the methods discussed in Sections 3.2 (Lobanoff and Ross) and 3.3 (Stepanoff). Figure 3.5 shows a sectional view of the impeller with the nomenclature used for the calculations that follow. Different from the other methods, $D_{1,c}$ and $D_{2,t}$ are not defined as the impeller inlet diameter for the compressor or outlet impeller diameter for the turbine but as the casing inlet- or outlet diameter.

The input parameters consist of pressures, temperatures, impeller geometry, rotor speed and middle rotation factors. Similar to the cavity speed ratio used in the method by Japikse, Gülich uses middle rotation factors of a pressure difference in side room ($\bar{k}_{Ts,c}$ and $\bar{k}_{Ts,t}$). These middle rotation factors are calculated from the density, outlet pressure, outlet radius and a pressure measured at a specific radius smaller than the impeller outlet radius (Equation 2.20). The construction of the HPTU does not facilitate a pressure measurement in the rear side room of the turbine. Due to the uncertainty that the density introduces into the calculation of the middle rotation factors, it is not feasible to attempt to measure the side room pressures. Instead, the middle rotation factors ($\bar{k}_{Ts,c}$ and $\bar{k}_{Ts,t}$) are estimated as the rotation

factor if no through flow occurs in the side room (k_0). Factors such as the Reynolds-number, surface roughness and gap between the impeller and casing wall is also accounted for by k_0.

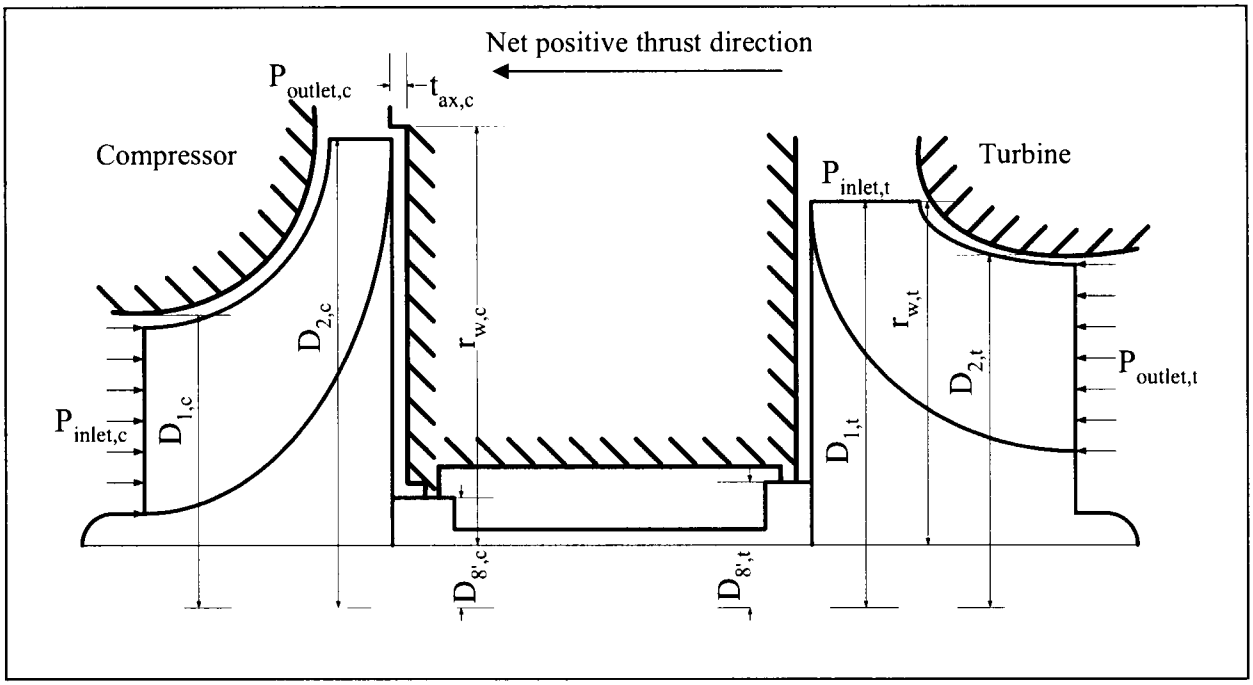


Figure 3.5: Nomenclature applied to complete turbocharger for the thrust calculation by Gülich.

$$Re = \frac{\omega \cdot r_2^2}{\nu} : [\text{dimensionless}]\ \text{Reynolds - number}$$

$$\lambda_w = \frac{0.136}{\left\{-\log\left(0.2\frac{\varepsilon_{casing}}{r_2} + \frac{12.5}{Re}\right)\right\}^{2.15}} : [\text{dimensionless}]\ \text{casing friction factor}$$

$$\lambda_R = \frac{0.136}{\left\{-\log\left(0.2\frac{\varepsilon_{rotor}}{r_2} + \frac{12.5}{Re}\right)\right\}^{2.15}} : [\text{dimensionless}]\ \text{rotor friction factor} \qquad (3.10)$$

$$k_0 = \frac{1}{1+\left(\frac{r_w}{r_2}\right)^2 \cdot \sqrt{\left(\frac{r_w}{r_2} + 5\frac{t_{ax}}{r_2}\right)\left(\frac{\lambda_w}{\lambda_R}\right)}} : [\text{dimensionless}]\ \text{Rotation factor without through flow in side room}$$

where

$\varepsilon_{casing} \equiv$ casing wall roughness [m]

$\varepsilon_{rotor} \equiv$ Rotor wall roughness [m]

$t_{ax} \equiv$ Axial gap between impeller and stationary side room wall [m]

Equation set 3.10 was applied for both the compressor and turbine to calculate the rotation factors if no through flow occurs in the side room. The solution obtained for the calculation of the middle rotation factors (Appendix A4) is given in Table 3.6.

$\omega = 5877$ [rad/s]	$\lambda_{R,c} = 0.004063$ [m]	$\lambda_{w,t} = 0.005975$ [m]
$\nu_c = 0.00001758$ [m^2/s]	$k_{0,c} = 0.4377$ [dimensionless]	$\lambda_{R,t} = 0.004403$ [m]
$Re_c = 1.571E+07$ [dimensionless]	$\nu_t = 0.0000757$ [m^2/s]	$k_{0,t} = 0.3606$ [dimensionless]
$\lambda_{w,c} = 0.00458$ [m]	$Re_t = 3.183E+06$ [dimensionless]	

Table 3.6: Solution of middle rotation factor calculation (k_0).

Now that the rotation factors, if no through-flow occurs in the side rooms, are calculated, the rest of the thrust calculation can proceed with $\bar{k}_{Ts,c}$ set equal to $k_{0,c}$ and $\bar{k}_{Ts,t}$ equal to $k_{0,t}$ in Equation 3.11 (See Appendix A5).

$$Net_{turbo,thrust} = -\frac{\pi}{4}\cdot D_{1,t}^2\cdot\left[\Delta P_t\cdot\left(1-\frac{D_{8',t}^2}{D_{1,t}^2}\right)-\frac{\rho_{weighted,t}}{4}\cdot\bar{k}_{Ts,t}^2\cdot U_{1,t}^2\cdot\left(1-\frac{D_{8',t}^2}{D_{1,t}^2}\right)^2-\frac{\Delta P_t}{2}\cdot\left(1-\frac{D_{2,t}^2}{D_{1,t}^2}\right)^2\right]$$

$$+\frac{\pi}{4}\cdot D_{2,c}^2\cdot\left[\Delta P_c\cdot\left(1-\frac{D_{8',c}^2}{D_{2,c}^2}\right)-\frac{\rho_{weighted,c}}{4}\cdot\bar{k}_{Ts,c}^2\cdot U_{2,c}^2\cdot\left(1-\frac{D_{8',c}^2}{D_{2,c}^2}\right)^2-\frac{\Delta P_c}{2}\cdot\left(1-\frac{D_{1,c}^2}{D_{2,c}^2}\right)^2\right]:[N] \qquad (3.11)$$

Net thrust exerted on turbocharger thrust bearing

$\omega = 5877$ [rad/s]	$\rho_{weighted,c} = 0.5792$ [kg/m^3]	$U_{1,t} = 241.5$ [m/s]
$\Delta P_c = 70774$ [Pa]	$\rho_{1,t} = 0.4643$ [kg/m^3]	$T_{net,c} = 414$ [N]
$\Delta P_t = 43550$ [Pa]	$\rho_{weighted,t} = 0.2462$ [kg/m^3]	$T_{net,t} = 212.6$ [N]
$\rho_{2,c} = 1.135$ [kg/m^3]	$U_{2,c} = 276.2$ [m/s]	$Net_{turbo,thrust} = 201.4$ [N]

Table 3.7: Solution of thrust calculation with the method of Gülich.

With the thrust calculation method of Gülich it was found that the thrust exerted on the thrust bearing is 201.4N. A positive sign implies that the direction of the resultant thrust is acting in the direction:" turbine to compressor". Thrust due to the change of momentum of the fluid inside the compressor is 52.2N (Equations 3.1 and 3.2) and for the turbine -73.5N. When the thrust due to a change of fluid momentum is accounted for [11], a net thrust of 180.1N is exerted on the thrust bearing. Effects such as axial gap between impeller and stationary casing wall, Reynolds-number and surface roughness are included in the rotation factors. Some uncertainty still exists around the values substituted for the density in the thrust calculation due to compressibility in the compressor and turbine. In Chapter 5 a series of data points will be compared with measured thrust data. Only then, the margin of error will become apparent.

3.6 Method 5 based on the method suggested by Liebner [18]:

From experimental measurements recorded when the PBMM is operated, the inlet- pressure and temperature of the compressor and turbine, outlet- pressure and temperature of the compressor and turbine, rotor speed and mass flow rate are known parameters. The following assumptions are made:

- A constant pressure distribution is assumed on the rear- and front side rooms of both the compressor and turbine.

- The return oil line is not completely filled with oil, therefore it is assumed that the lubrication chamber is at atmospheric pressure like the sump.
- The contribution towards thrust force of the pressure distribution from compressor inlet tip to compressor outlet tip and from turbine inlet tip to outlet tip is ignored.

Both the compressor and turbine wheel are taken as control volumes, then the forces resulting from pressures acting on the different areas (see Figure 3.6) are summed (Equation 3.12). The diameter of the shaft in the middle is 0.0127m.

$$Net_{turbo,thrust} = \frac{\pi}{4}\begin{pmatrix} -P_{inlet,c}\cdot D_{1,c}^2 + P_{outlet,c}\cdot\left(D_{2,c}^2 - D_{8',c}^2\right) + P_{lub\text{-}chamber}\cdot\left(D_{8',c}^2 - D_{shaft,middle}^2\right) \\ -P_{lub\text{-}chamber}\cdot\left(D_{8',t}^2 - D_{shaft,middle}^2\right) - P_{inlet,t}\cdot\left(D_{1,t}^2 - D_{8',t}^2\right) + P_{outlet,t}\cdot D_{2,t}^2 \end{pmatrix} : [N] \quad (3.12)$$

Net thrust exerted on turbocharger thrust bearing

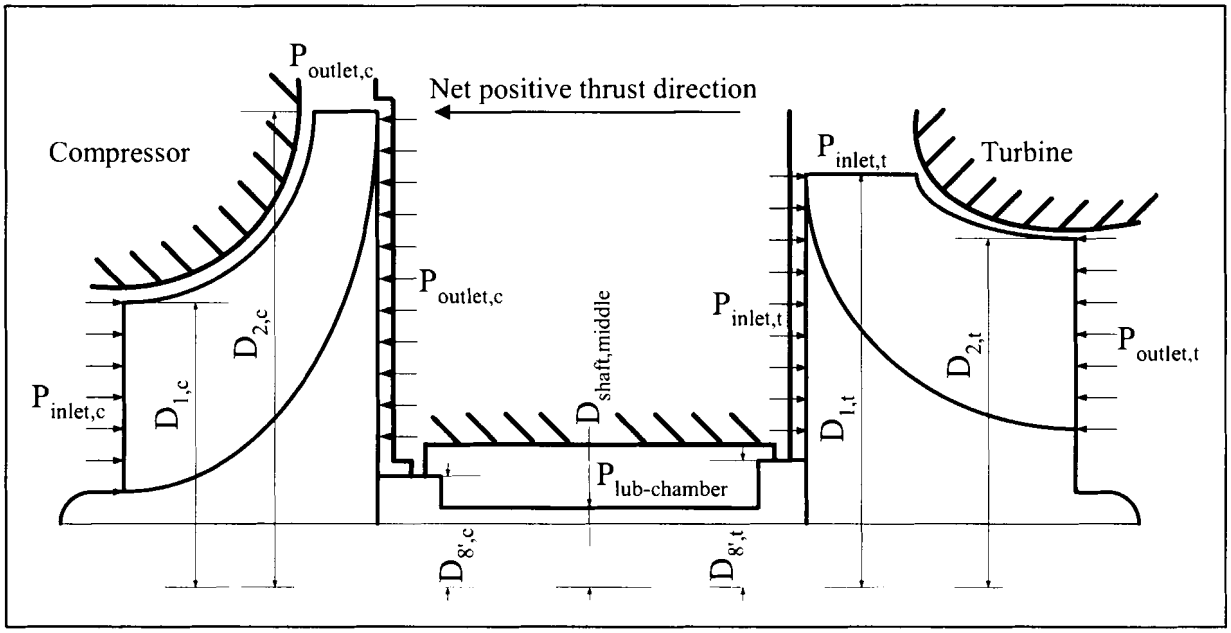


Figure 3.6: Nomenclature applied to complete turbocharger for the thrust calculation based on method by Liebner

It is obtained that the thrust exerted on the thrust bearing with the calculation method above (Equation 3.12) is 351.1N. Influences from the rotor speed, mass flow rate, side room leakage flows, surface roughness and position of the rotor relative to the casing are ignored with this thrust calculation. The thrust due to a momentum change of the fluid can be calculated with Equations 3.1 and 3.2. Thus a further -21.3N should be added for change of fluid momentum and the total thrust is calculated as 329.8N.

3.7 CFD method [12]:

Accurate geometry of the impeller is needed to model the fluid paths. Attempts had been made to digitize the impeller geometry but proved to be unsuccessful. As a first attempt, a point scanner was used, but the scanning head could not fit between the blades to scan the whole blade geometry. Then the compressor and turbine impeller was scanned with a laser scanner. The reflective powder's texture was too coarse and

gave unsatisfactory post processed CAD (Computer aided design) results. Thus accurate impeller geometry could not be obtained for input of flow paths in a CFD analysis. Specialist knowledge in the field of CFD is necessary to conduct such advanced modeling of turbo machinery. CFD modeling was thus not used as a calculation method for this study.

3.8 Summary:

Five different theoretical thrust calculation methodologies were applied on the centrifugal compressor and turbine of the high pressure turbo unit (HPTU) of the Pebble Bed Micro Model (PBMM) with the same pressure, temperature and rotor speed as input parameters from previous test data. This data point was randomly selected from test data to compare the results from different thrust calculation methodologies. Each of the thrust calculation methodologies gave a different solution to the thrust force value as described in the next paragraphs.

With the method of Lobanoff and Ross, the theoretical thrust was calculated as 130.1N. In the literature, the thrust calculation method of Lobanoff & Ross was applied to open impeller centrifugal pumps and here it was applied to a compressible flow centrifugal compressor and turbine. Thrust due to a change in fluid momentum is accounted for but not effects like Reynolds-number, surface roughness and position of the rotor relative to the casing walls. A negative sign implies that the net thrust force is acting in the direction "compressor to turbine".

When the net thrust exerted on the thrust bearing is calculated with the method of Stepanoff a value of -4.176N is obtained, which means it is acting from the "compressor to turbine" direction. The thrust calculation method of Stepanoff was also applied to open impeller centrifugal pumps originally. Thrust due to a change of fluid momentum inside the impellers is not included in the calculation method. Similar to the method of Lobanoff and Ross, the influence of Reynolds-number, surface roughness and axial gap between rotor and stationary casing walls is ignored.

Japikse's thrust calculation method predicted the thrust force as -293.1N acting in the direction from the compressor to the turbine. In the literature, this thrust calculation method of Japikse was applied to centrifugal compressors. The cavity speed ratio has its origin from analysis of the side room leakage flows and inherently accounts for effects like Reynolds-number and axial gap between rotor and casing walls. Thrust due to a change of fluid momentum in the impellers is included in the calculation method.

According to the literature on the thrust calculation method of Gülich, this method was applied to open impeller centrifugal pumps. Middle rotation factors could not be calculated with Equation 2.20 due to the difficulty to obtain an experimental pressure measurement at a specified radius. Thus it was assumed that the middle rotation factor is equal to the rotation factor if no through flow occurs in the side room. The

thrust force was calculated as 180.1N. A positive sign indicates that the thrust is exerted in the direction "turbine to compressor". The thrust resulting from a change of fluid momentum is included in the calculation [11].

As a last calculation method, the method of Liebner predicted the thrust force as 329.8N. Again, a positive sign indicates that the thrust is exerted in the direction "turbine to compressor". Thrust due to momentum change of the fluid is included. This thrust calculation is unaffected by effects such as rotor speed, mass flow rate, surface roughness, position of rotor relative to the side walls and Reynolds-number.

At this stage no comment can be given pertaining to the correctness of any of the methods due to the large variance in answers. Five different values have been obtained for the thrust, while three methods give the direction as "compressor to turbine" and two methods give the direction as "turbine to compressor". The theoretical thrust calculations need to be verified by experimental thrust measurement.

4. Thrust measurement on the HPTU

4.1 Introduction:

In the introduction of Chapter 2 it was cited that experimental measured thrust differed by 15% from the theoretical calculated thrust. The results obtained with the different thrust calculation methodologies in Chapter 3 showed a much larger variance, with the thrust ranging from as little as 1.7N up to 331N. Thus experimental thrust measurement is needed to benchmark the theoretical calculated thrust for the HPTU of the PBMM. Thrust measurement on the HPTU presents a number of challenges that needs to be addressed like:

- The limited space available inside the turbocharger center casing for sensors (see Figure 4.1),
- measurement at higher than ambient temperature,
- lubrication oil present for the hydrodynamic thrust bearing,
- Vibration of the HPTU.
- The location of the HPTU inside the pressure vessel.

The limited space available in the turbocharger centre casing restricts the use of general force measurement techniques like load cells. Therefore, this Chapter will cover the thrust measurement system design to be implemented specifically on the HPTU of the PBMM.

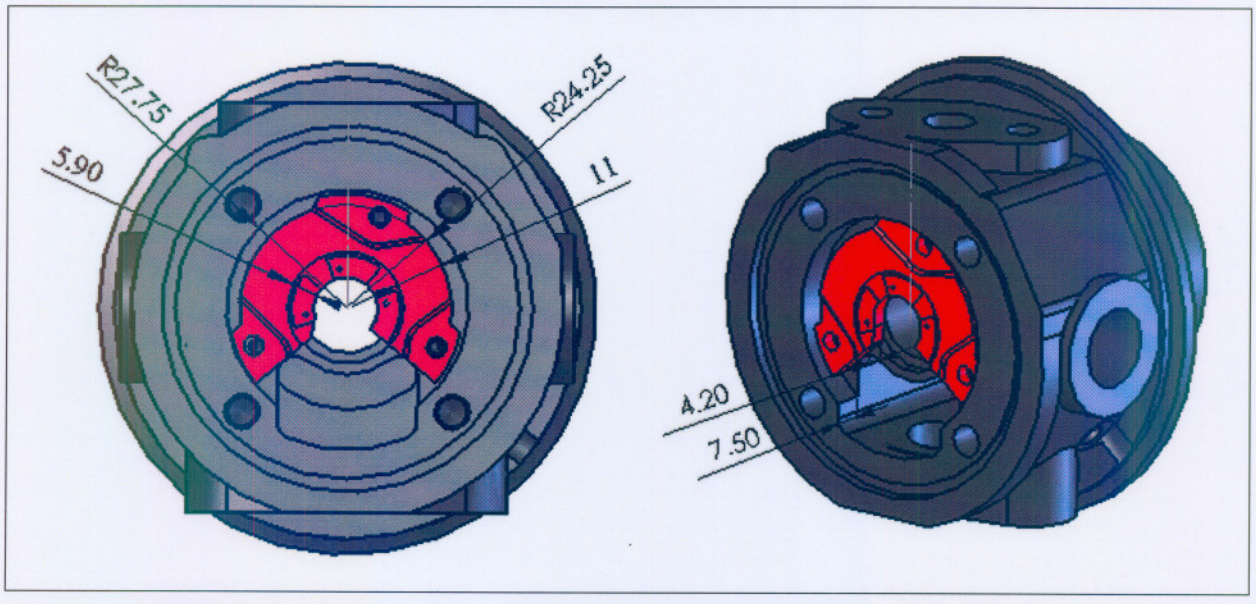


Figure 4.1: HPTU turbocharger center casing and thrust bearing dimensions.

4.2 Thrust measurement concepts:

4.2.1 Five axis electro-magnetic bearings:

In Section 2.3, thrust measuring techniques and equipment was illustrated. Five axis electro-magnetic bearings will be extremely costly to implement because this type of technology is still very expensive for small quantities that is needed. A complete new center casing with cooling will have to be manufactured

if magnetic bearings are to be used that adds to the implementation costs of a thrust measurement system. Magnetic bearings generate heat that is not normally dissipated outside the machine, like with fluid film bearings. The gas temperature inside the pressure vessel also ranges in the order of 100°C, therefore sufficient cooling should be provided to the magnetic bearings. A new centre casing will have to be exactly the same length as the existing one; otherwise new impellers will have to be manufactured as well. Thus the total length of the magnetic bearings must not have a length longer than the length of the current center casing.

4.2.2 Force washers:

Force washers are able to handle the range of the thrust force exerted on the thrust bearing as calculated in Chapter 3 very easily. It is also possible to have redundancy in the range of the thrust washer if the calculated thrust force is over- or under estimated. The first disadvantage of the force washer is that in can only measure a unidirectional compression force. Thus if such a force washer is installed between the thrust bearing and the bolt head, it will only be able to measure a force in the direction "turbine to compressor" and not in the direction "compressor to turbine" (Figure 4.2). Due to the relative stiffness of the bolt and the member of a pre-loaded bolt assembly, the load fraction seen by the member further reduces the sensitivity of this type of measurement (The force washer becomes a part of the member group of the bolted assembly). Secondly, the smallest inner diameter of a thrust washer is 6.38mm; this is bigger than the 4mm bolt that mounts the thrust bearing. The outer diameter is too big, it will interfere with the casing and the thickness will cause that the back plate of the compressor cannot mount flush onto the sealing surface. Thus the use of force washers is not suited for thrust measurement on the HPTU.

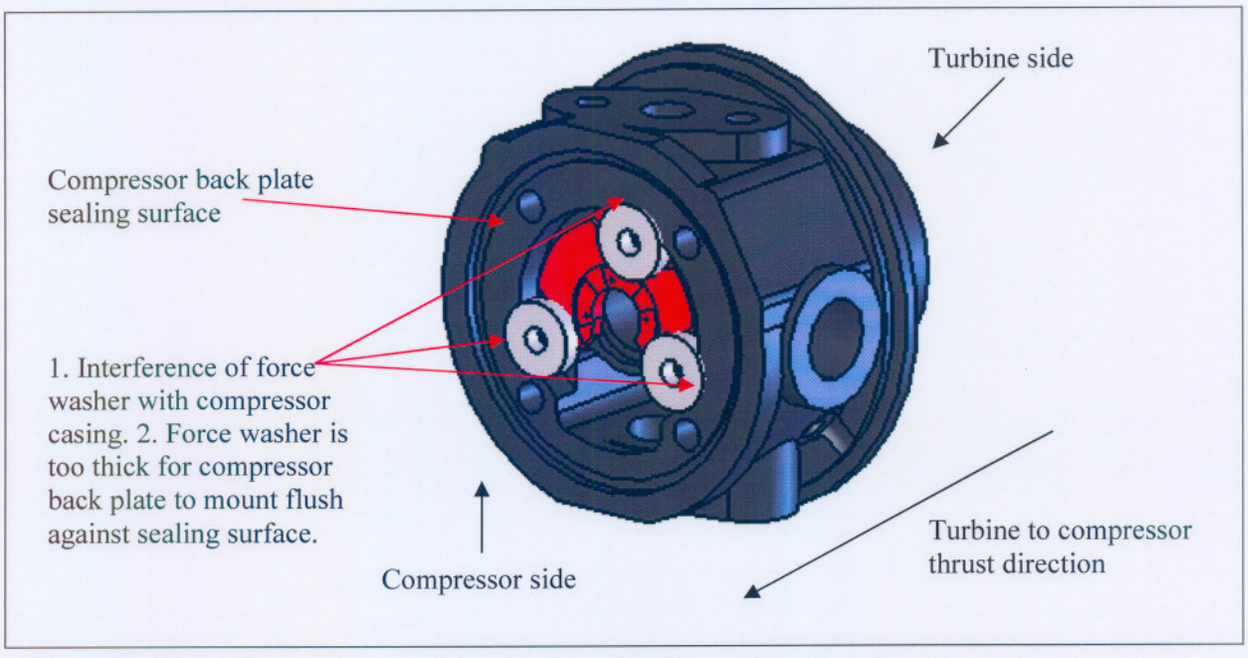


Figure 4.2: Turbocharger centre casing with thrust bearing and thrust washers.

4.2.3 Piezo-electric strain sensors:

A finite element analysis (FEA) was done to determikne the position on the thrust bearing where the largest strain occurs that is suitable to measure the thrust in both directions ("turbine to compressor" and "compressor to turbine"). This position was found to be radially outward from the recess between the "thrust shoes" (Figures 4.3 and 4.4). This radial direction also corresponds to the directions of the minimum- or maximum principal strains depending on the direction of the thrust force. The PCB 740B02 (Figure 2.8) type piezo-electric strain sensor is too big in physical size to fit in the space available on the thrust bearing for thrust measurement as indicated by Figure 4.5. If the thrust reach levels of 400N, it was simulated with finite element analysis that the strain in the areas where the sensor is positioned, ranges around 100 to 150με. Thus if the calculated thrust value of 331N is under estimated, the sensor's (PCB 740B02) range is exceeded. The sensor illustrated in Figure 2.8 with a range of 300με, is in length almost the same as the diameter of the thrust bearing and twice as thick as the bearing cavity, therefore it is not possible to fit it inside the centre casing. In conclusion, piezo-electric sensors are too big to fit in the turbocharger centre casing and might not have the sufficient range to measure the thrust; therefore it was not suited as instruments to measure the thrust for this specific application.

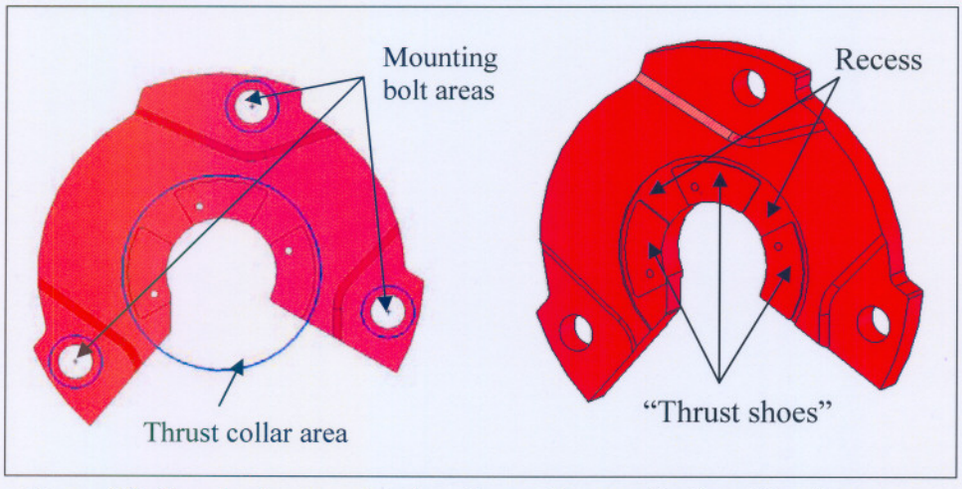


Figure 4.3: Terminology used to describe sections on the thrust bearing.

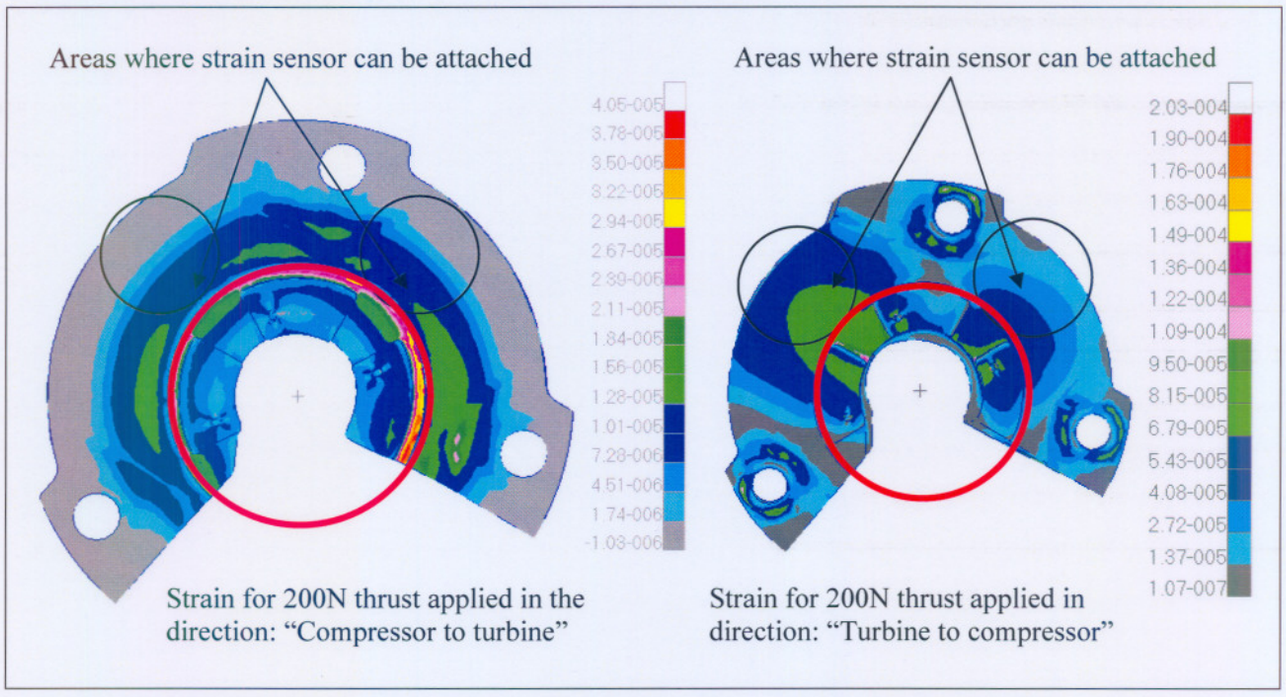


Figure 4.4: Finite element analysis maximum principle strain results for thrust of 200N.

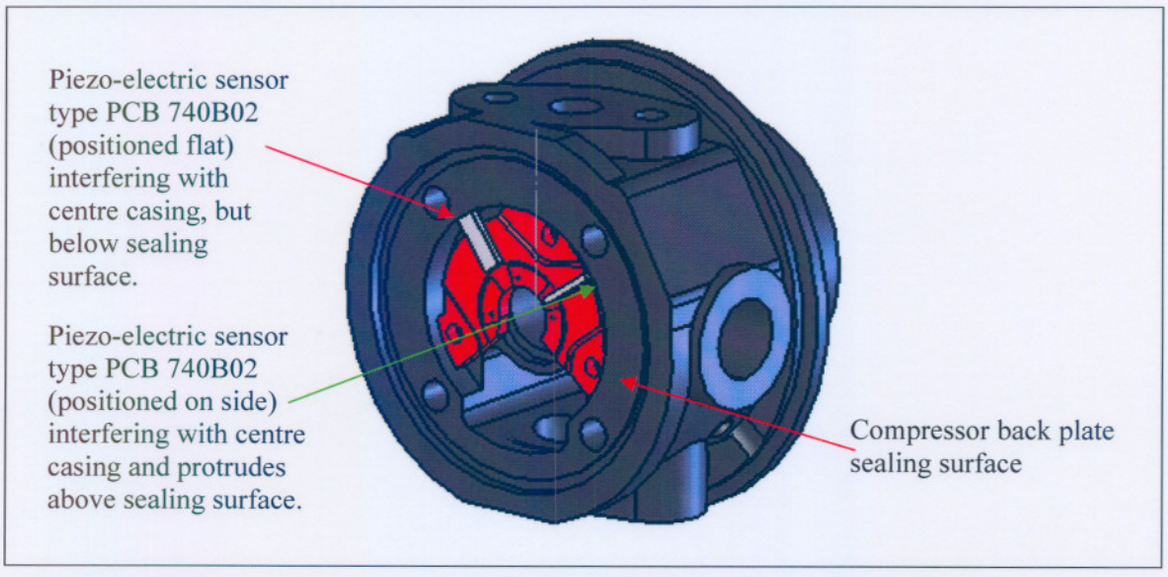


Figure 4.5: Turbocharger centre casing with thrust bearing and piezo-electric sensors.

4.2.4 Strain gauges:

In all of the methods or sensors of the preceding sections, the space constraint is the governing design parameter. Foil strain gauges offer a wide variety of sizes as small as a diameter of 4 to 5mm and only a few microns thick, therefore it will fit into the space available on the thrust bearing (Figures 4.1 and 4.3). The typical useful temperature range for strain gauges is in the order of -200 to +200˚C [15]. From PBMM test data, it was obtained that the return line oil temperature ranges between 70 and 80˚C. It was estimated that the thrust bearing operating temperature is less than 120˚C (assumption). Thus the

operating temperature of the thrust bearing falls well within the operating range of strain gauges and the second design criterion is met. A number of sealants are available to seal the strain gauges from the lubrication oil present in the turbocharger centre casing [14]. In Section 2.3.1 literature has been presented where strain gauges were wired in a Wheatstone bridge on a tilting pad thrust bearing of a pump.

The application of foil strain gauges meet all the design criteria as stated in the beginning of this chapter and poses probably the only feasible option to be implemented for thrust measurement on the HPTU of the PBMM.

4.3 Strain gauge measuring systems theory:

With the design of any strain gauge measuring system, a number of factors have to be taken into consideration such as [15]:

- the type of Wheatstone bridge to be used (full-, half- or quarter bridge),
- type of strain gauge to be used,
- type of adhesive to be used,
- type of covering agent to be used,
- type of strain field like homogeneous or non-homogeneous,
- ambient conditions like pressure and temperature.

All of the considerations above will now be treated in the design of a strain gauge thrust measuring system. The fundamental equation for any calculation when working with strain gauges is Equation 4.1. This equation gives the relationship between the electrical quantities namely voltage and resistance, and the mechanical quantity of strain. Each strain gauge can be modeled as an electrical resistance.

$$\frac{U_A}{U_E} = \frac{k}{4} \cdot B \cdot \left(\frac{\Delta R}{R} \right) = \frac{k}{4} \cdot B \cdot \varepsilon \qquad (4.1)$$

where

$U_A \equiv$ [V] Bridge output voltage

$U_E \equiv$ [V] Bridge excitation voltage

$\Delta R \equiv [\Omega]$ A change in resistance

$R \equiv [\Omega]$ Nominal resistance

$k \equiv [\frac{\Omega/\Omega}{m/m}]$ Gauge factor or sensitivity

$B \equiv$ [dimensionless] Bridge factor

$\varepsilon \equiv$ [m/m] Strain

4.3.1 Types of strain gauges:

Over the years, a few concepts of strain gauges developed like the semiconductor strain gauge, Vapour-deposited strain gauges, capacitive strain gauges, piezo-electric strain gauges, photo-elastic strain gauges and metal foil strain gauges. Today, the most widely used and developed type is metal foil strain gauges. This type of strain gauge consists of a base material or carrier, the metal grid and lead attachments. A very wide variety of strain gauges in terms of geometry, size and application are available and produced with high precision. Each manufacturer has their own classifications but in general metal strain gauges can be classified under the following applications: extreme temperature strain gauges (-200 to +250°C), strain gauges for transducer manufacturing, pre-wired strain gauges, strain gauges for high strain, weldable strain gauges and general purpose strain gauges for most stress analysis applications [15].

The choice of strain gauge would depend on the type of application, type of material, useful temperature range, strain range and a homogeneous or non-homogeneous strain field. If a long grid strain gauge is used in a non-homogeneous strain field, the strain gauge will measure the arithmetic mean strain across the grid. A different strain gauge selection will have to be made for each application according to manufacturer specifications.

4.3.2 Bridge configurations:

A quarter bridge with one active strain gauge (Figure 4.6) has an inherent linearity error. That is a difference in the signal between a compressive strain and a tension strain with the same magnitude. Thus in tension (positive) a certain strain value will result in a certain positive output signal while the same compressive (negative) strain of the same magnitude will result in a different negative output signal [8]. The term "active" strain gauge is used for a strain gauge that is positioned to measure a strain on a specimen. Half bridges (Figure 4.7) also generate linearity errors but the magnitude of the error is much smaller than with a quarter bridge. Eder gives an example where the linearity error for a half bridge is ten times smaller than the linearity error of a quarter bridge [8]. A half bridge configuration gives a further advantage that the output signal is larger than with a quarter bridge for the same excitation voltage. It should be noted to obtain a larger output signal R_1 and R_2 should have opposite polarity. One strain gauge must measure a positive strain and the other a negative signs. Mathematically this is obtained by Equation 4.2.

$$\frac{U_A}{U_E} = \frac{k}{4}\cdot B\cdot\left(\frac{\Delta R_1}{R_1} - \frac{(-\Delta R_2)}{R_2} + \frac{\Delta R_3 = 0}{R_3} - \frac{\Delta R_4 = 0}{R_4}\right) = \frac{k}{4}\cdot B\cdot\left(\varepsilon_1 - (-\varepsilon_2)\right)$$

$$\therefore \frac{U_A}{U_E} = \frac{k}{4}\cdot B\cdot\left(\frac{\Delta R_1}{R_1} + \frac{\Delta R_2}{R_2} + \frac{0}{R_3} - \frac{0}{R_4}\right) = \frac{k}{4}\cdot B\cdot\left(\varepsilon_1 + \varepsilon_2\right) \qquad (4.2)$$

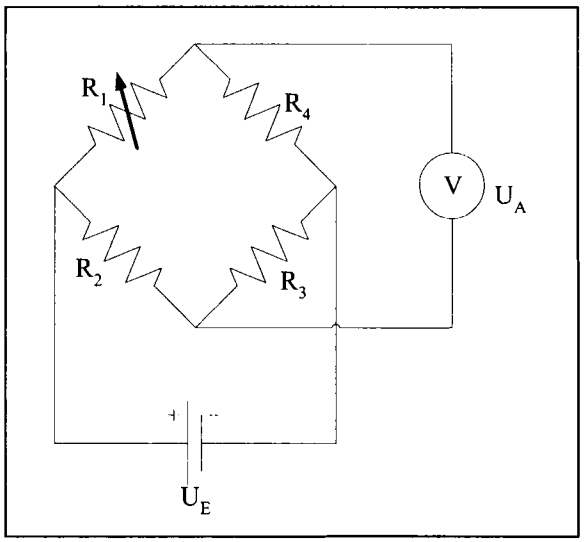


Figure 4.6: Quarter bridge circuit with one active gauge R_1.

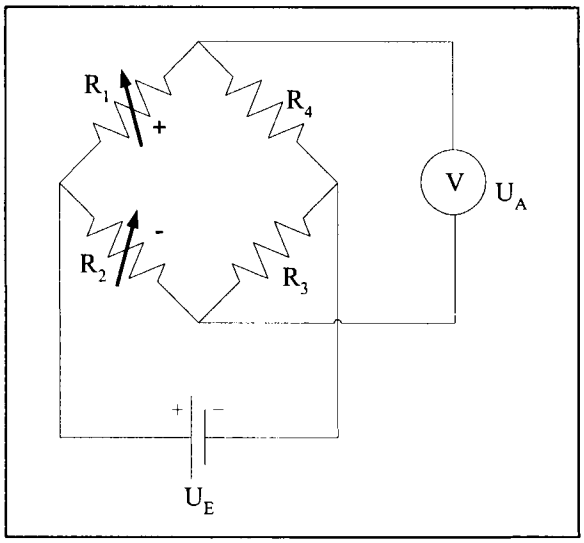


Figure 4.7: Half bridge circuit with two active gauges R_1 and R_2.

A full bridge incorporating four active strain gauges (Figure 4.8) has no linearity errors [8] and has the largest output signal of all the bridge configurations. This is only obtained if R_1 and R_3 has the same polarity; resistances R_2 and R_4 has the same polarity but opposite to that of R_1 and R_3. Mathematically it is expressed as:

$$\frac{U_A}{U_E} = \frac{k}{4} \cdot B \cdot \left(\frac{\Delta R_1}{R_1} - \frac{(-\Delta R_2)}{R_2} + \frac{\Delta R_3}{R_3} - \frac{(-\Delta R_4)}{R_4} \right) = \frac{k}{4} \cdot B \cdot \left(\varepsilon_1 - (-\varepsilon_2) + \varepsilon_3 - (-\varepsilon_4) \right)$$
$$\therefore \frac{U_A}{U_E} = \frac{k}{4} \cdot B \cdot \left(\frac{\Delta R_1}{R_1} + \frac{\Delta R_2}{R_2} + \frac{\Delta R_3}{R_3} + \frac{\Delta R_4}{R_4} \right) = \frac{k}{4} \cdot B \cdot \left(\varepsilon_1 + \varepsilon_2 + \varepsilon_3 + \varepsilon_4 \right) \quad (4.3)$$

The bridge factor B for a quarter-, half and full bridge is 1, 2 and 4 respectively.

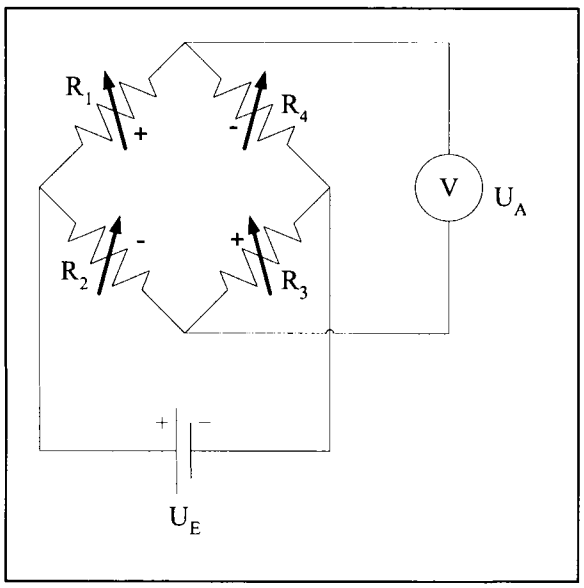


Figure 4.8: Full bridge circuit with all gauges active.

4.3.3 Cable errors:

A change in ambient temperature causes a change in the resistance of the lead wires. The effect of the lead wires is modelled with additional resistances in series with that of the strain gauge. For a quarter bridge circuit like in Figure 4.9, the lead wire resistances causes a resistance that is not cancelled in any of the other bridge arms.

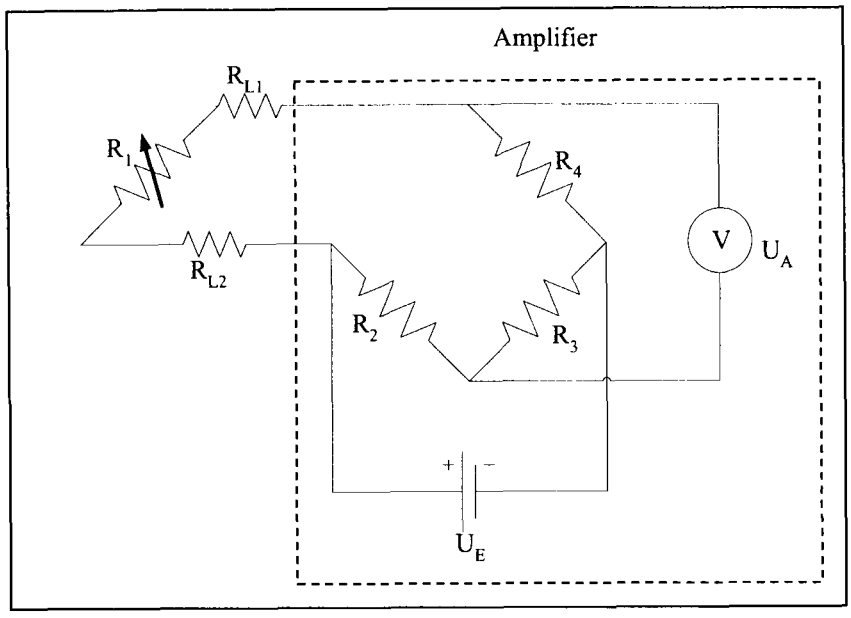


Figure 4.9: Quarter bridge with lead wire resistances.

The effect is that the output signal contains the strain gauge resistance as well as lead wire resistances caused by an ambient temperature change. Thus the lead wire resistances cause an error in the output signal as shown by Equation 4.4.

$$\frac{U_A}{U_E} = \frac{k}{4} \cdot B \cdot \left(\frac{R_1 + \Delta R_1 + \overbrace{R_{L1} + R_{L2}}^{\text{error}}}{R_1 + \Delta R_1 + R_2} - \frac{R_3}{R_3 + R_4} \right) = \frac{k}{4} \cdot B \cdot \varepsilon_1 \tag{4.4}$$

This error due to a change in ambient temperature can be overcome by using a three wire quarter bridge (Figure 4.10) but a smaller error remains in the measured strain value [8]. With a half bridge circuit as showed in Figure 4.11, the cable error is cancelled out as in Equation 4.5 because R_{L1}, R_{L2} and R_{L3} all have the same magnitude and appear in each bridge arm. It should be noted that cable errors causes a decrease in the sensitivity.

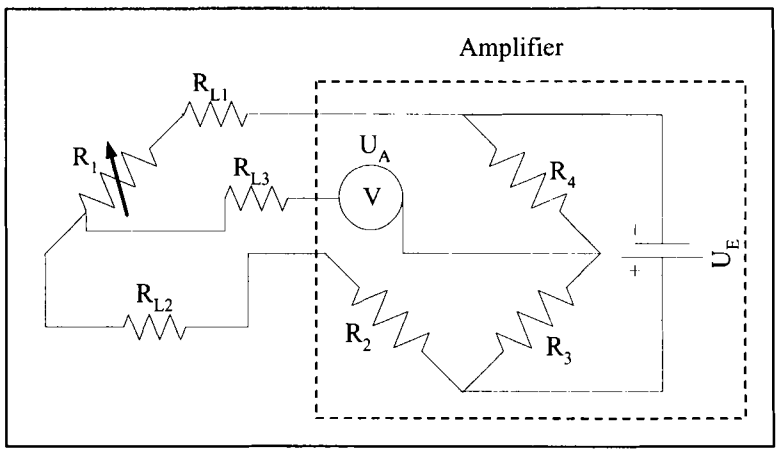


Figure 4.10: Three wire quarter bridge circuit

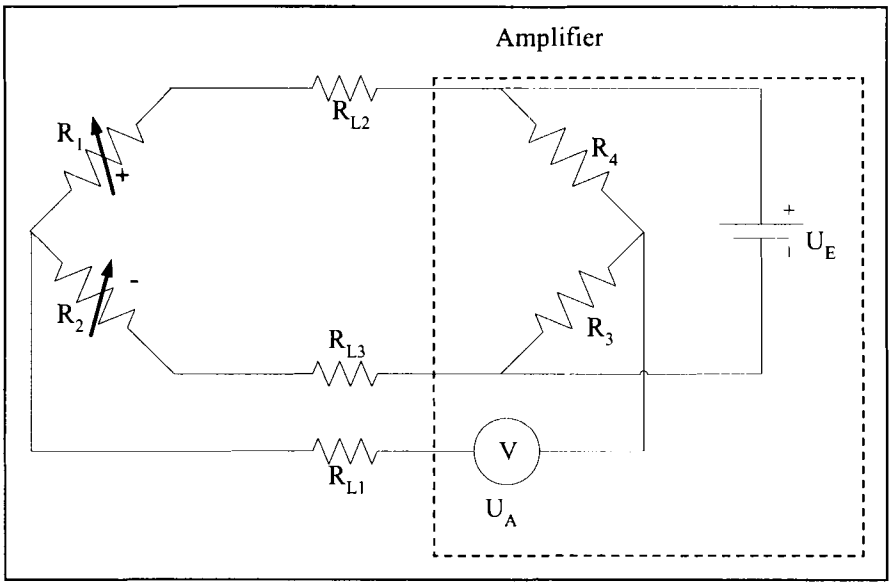


Figure 4.11: Half bridge with lead wire resistances.

$$\frac{U_A}{U_E} = \frac{k}{4} \cdot B \cdot \left(\frac{R_1 + \Delta R_1 + R_{L2}}{R_1} - \frac{R_2 + \Delta R_2 + R_{L3}}{R_2} + \frac{R_3 + R_{L3}}{R_3} - \frac{R_4 + R_{L2}}{R_4} \right)$$
$$= \frac{k}{4} \cdot B \cdot (\varepsilon_1 - \varepsilon_2) \tag{4.5}$$

Similar to the half bridge, cable errors are cancelled out in full bridge configurations as shown by Figure 4.12 and Equation 4.6 [16]. Cables R_{L1} and R_{L4} are connected in series with the high input impedance of the amplifier and therefore does not affect the measurement [16]. R_B is identified as the bridge shunt resistance or input resistance [15].

$$R_B = \frac{(R_1 + R_2) \cdot (R_3 + R_4)}{R_1 + R_2 + R_3 + R_4}$$
$$\frac{U_A}{U_E} = \frac{k}{4} \cdot B \cdot (\varepsilon_1 + \varepsilon_2 + \varepsilon_3 + \varepsilon_4) \cdot \underbrace{\frac{R_B}{R_B + R_{L2} + R_{L3}}}_{\text{Correction term}} \tag{4.6}$$

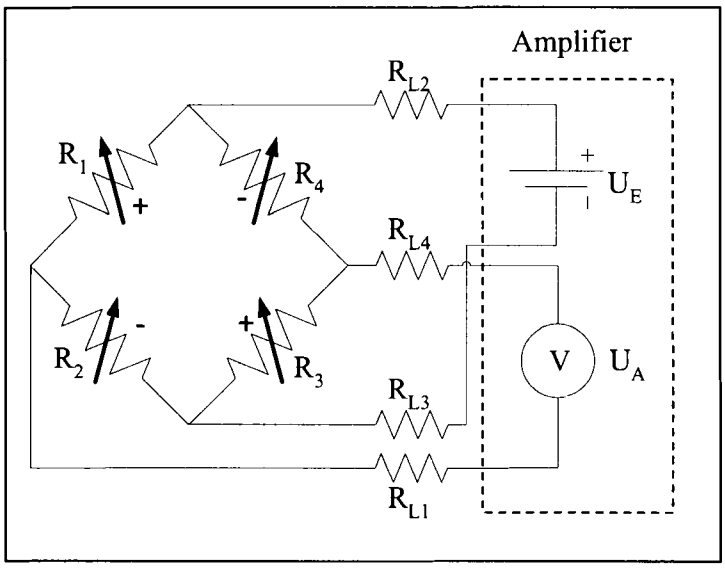


Figure 4.12: Full bridge with lead wire resistances.

4.3.4 Temperature effects:

Any change in temperature affects the measurement in the following ways: Thermal expansion of the gauges and test specimen, gauge sensitivity is dependent on temperature, the lead wire resistance changes and creep can occur. The strain gauge measurement reacts to each of these effects and therefore it should be compensated or cancelled by some means.

Strain gauges are ordered to match the thermal expansion of the test specimen and also the temperature range; it is called "self-temperature compensated strain gauges". By adding alloying elements to the grid material of the strain gauge, or heat treatment, the thermal expansion of the grid material is matched to the thermal expansion of the test specimen [15]. Then it is still found that anisotropic conditions in the material cause differences in thermal expansion. A temperature compensated strain gauge cannot compensate for such anisotropic effects.

A leaflet is enclosed with each strain gauge that gives a characteristic curve for the change in strain gauge sensitivity or gauge factor with temperature. Thus the corresponding gauge factor can be calculated for the specific test specimen temperature or ambient conditions.

The change of lead wire resistance due to temperature changes is compensated for by the bridge configuration and wiring as described in the preceding section concerned with cable errors.

If a strain gauge is subjected to a static strain, the resistance of the strain gauge changes with time. This phenomenon where a constant strain changes the resistance of the strain gauge is termed "creep" [15]. The strain gauge and bonding material under load reacts similar to a tensioned spring. Shear stresses are

generated in the region of the end loops of the grid on the contact surface of the carrier material and the grid. With time the reactive bonding force between the carrier and grid relax. This reduction in bonding force is perceived as a negative error and the output signal reduces [15]. As creep mainly occurs at the end loops of the grid, short strain gauges are more susceptible to creep than long strain gauges [15]. To counter the effect of creep in strain gauges, special gauges are manufactured with bigger end loops. Creep does not only occur in the strain gauge but also in the adhesive. Creep tests were performed in a range of temperatures with combinations of adhesives and strain gauges. A total effect of strain gauge and adhesive creep is then obtained. For one combination it was found that HBM's X60 adhesive shows poor creep characteristics at temperatures above room temperature and good results at 0°C. HBM's Z70 adhesive gave better results at a temperature of 50°C [15].

As mentioned before, the anisotropic properties of the test specimen cannot be cancelled by a self-temperature compensated strain gauge. To cancel such errors the compensating properties of the bridge is used. For a three-wire quarter bridge with a compensating strain gauge as given in [15], thermal errors are cancelled with Equation 4.7. The active strain gauge (ε_1) measures the sum of the mechanical strain and a thermal strain component. A second compensating gauge (ε_2) only measures the thermal strain component. Equation 4.7 then gives the measured strain [15].

$$\varepsilon = \underbrace{\left(\varepsilon_{mechanical} + \varepsilon_{thermal}\right)}_{\varepsilon_1} - \underbrace{\left(\varepsilon_{thermal}\right)}_{\varepsilon_2} \tag{4.7}$$

For a half bridge incorporating two active strain gauges (ε_1 and ε_2), the same thermal compensation can be accomplished if both strain gauges experience the same temperature variations. The mathematical relationship is given by Equation 4.8.

$$\begin{aligned} \varepsilon &= \underbrace{\left(+\varepsilon_{mechanical\,1} + \varepsilon_{thermal\,1}\right)}_{\varepsilon_1} - \underbrace{\left(-\varepsilon_{mechanical\,2} + \varepsilon_{thermal\,2}\right)}_{\varepsilon_2} = \varepsilon_{mechanical\,1} + \varepsilon_{mechanical\,2} \\ \varepsilon &= \underbrace{\left(+\varepsilon_{mechanical\,1} + \varepsilon_{thermal\,1}\right)}_{\varepsilon_1} - \underbrace{\left(+\varepsilon_{mechanical\,2} + \varepsilon_{thermal\,2}\right)}_{\varepsilon_2} = \varepsilon_{mechanical\,1} - \varepsilon_{mechanical\,2} \end{aligned} \tag{4.8}$$

For a full bridge, the same relation as for a half bridge holds as shown in Equation 4.9 if all four strain gauges experience the same temperature variations and strain gauges R_1 and R_3 has the same sign (Figure 4.12) and R_2 and R_4 has the same sign but opposite to R_1 and R_3.

$$\begin{aligned} \varepsilon &= \underbrace{\left(+\varepsilon_{mechanical\,1} + \varepsilon_{thermal\,1}\right)}_{\varepsilon_1} - \underbrace{\left(-\varepsilon_{mechanical\,2} + \varepsilon_{thermal\,2}\right)}_{\varepsilon_2} + \underbrace{\left(+\varepsilon_{mechanical\,3} + \varepsilon_{thermal\,3}\right)}_{\varepsilon_3} - \underbrace{\left(-\varepsilon_{mechanical\,4} + \varepsilon_{thermal\,4}\right)}_{\varepsilon_4} \\ &= \varepsilon_{mechanical\,1} + \varepsilon_{mechanical\,2} + \varepsilon_{mechanical\,3} + \varepsilon_{mechanical\,4} \\ \varepsilon &= \underbrace{\left(+\varepsilon_{mechanical\,1} + \varepsilon_{thermal\,1}\right)}_{\varepsilon_1} - \underbrace{\left(+\varepsilon_{mechanical\,2} + \varepsilon_{thermal\,2}\right)}_{\varepsilon_2} + \underbrace{\left(+\varepsilon_{mechanical\,3} + \varepsilon_{thermal\,3}\right)}_{\varepsilon_3} - \underbrace{\left(+\varepsilon_{mechanical\,4} + \varepsilon_{thermal\,4}\right)}_{\varepsilon_4} \\ &= \varepsilon_{mechanical\,1} - \varepsilon_{mechanical\,2} + \varepsilon_{mechanical\,3} - \varepsilon_{mechanical\,4} \end{aligned} \tag{4.9}$$

In [8] an example is given of a full bridge where resistances R_2 and R_4 in Figure 4.12 are replaced by dummy strain gauges installed on a test specimen that only experience the thermal strain component and

not a mechanical strain. A similar setup as a half bridge is obtained except that the bridge factor is 4 and R_1 and R_3 are the active gauges that have the same sign.

$$\varepsilon = \underbrace{\left(+\varepsilon_{mechanical\,1} + \varepsilon_{thermal\,1}\right)}_{\varepsilon_1} - \underbrace{\left(\varepsilon_{thermal\,2}\right)}_{\varepsilon_2} + \underbrace{\left(+\varepsilon_{mechanical\,3} + \varepsilon_{thermal\,3}\right)}_{\varepsilon_3} - \underbrace{\left(\varepsilon_{thermal\,4}\right)}_{\varepsilon_4} = \varepsilon_{mechanical\,1} + \varepsilon_{mechanical\,3} \quad (4.10)$$

4.3.5 Types of adhesives:

Adhesives are classified as hot curing at temperatures above room temperature or cold curing at room temperature and further as a single component or two components. The selection criteria for the appropriate epoxy to use for the application will be: Application temperature, test specimen material and structure like brittle or porous, strain gauge type and requirements for long term stability and reproducibility [14]. Each manufacturer's specifications will serve as guide to make the correct choice of adhesive for each application.

4.3.6 Types of covering agents:

Quality of the measurement is also affected by external effects such as humidity, mechanical damage and corrosion. A suitable covering agent is needed to protect the strain gauge and measuring point against such external effects. The selection criteria for a suitable covering agent consist of the test specimen's temperature and the surrounding media [14]. A variety of covering agents are offered by the different manufacturers to protect the strain gauge at various temperatures and against a number of possible surrounding media.

4.4 Installation of first thrust measurement system:

4.4.1 Installation of strain gauges on thrust bearing for Thrust Test 1:

Young's modulus and Poisson ratio is needed as input for a finite element analysis. These two parameters are material based. To determine the material of the thrust bearing a sample analysis was performed with an electron microscope. The material of the thrust bearing was identified as a grey cast iron with an assumed Young's modulus of 165GPa and a Poisson ratio of 0.27 [6].

A finite element analysis was performed to determine the most suitable position for the strain gauge installation. This is the same finite element analysis illustrated in Figure 4.4 to determine the position for the piezo-electric strain sensor. The circled areas in Figure 4.3 show the mounting bolt positions as well as the thrust collar area. Thus the strain gauges could not be installed inside these areas.

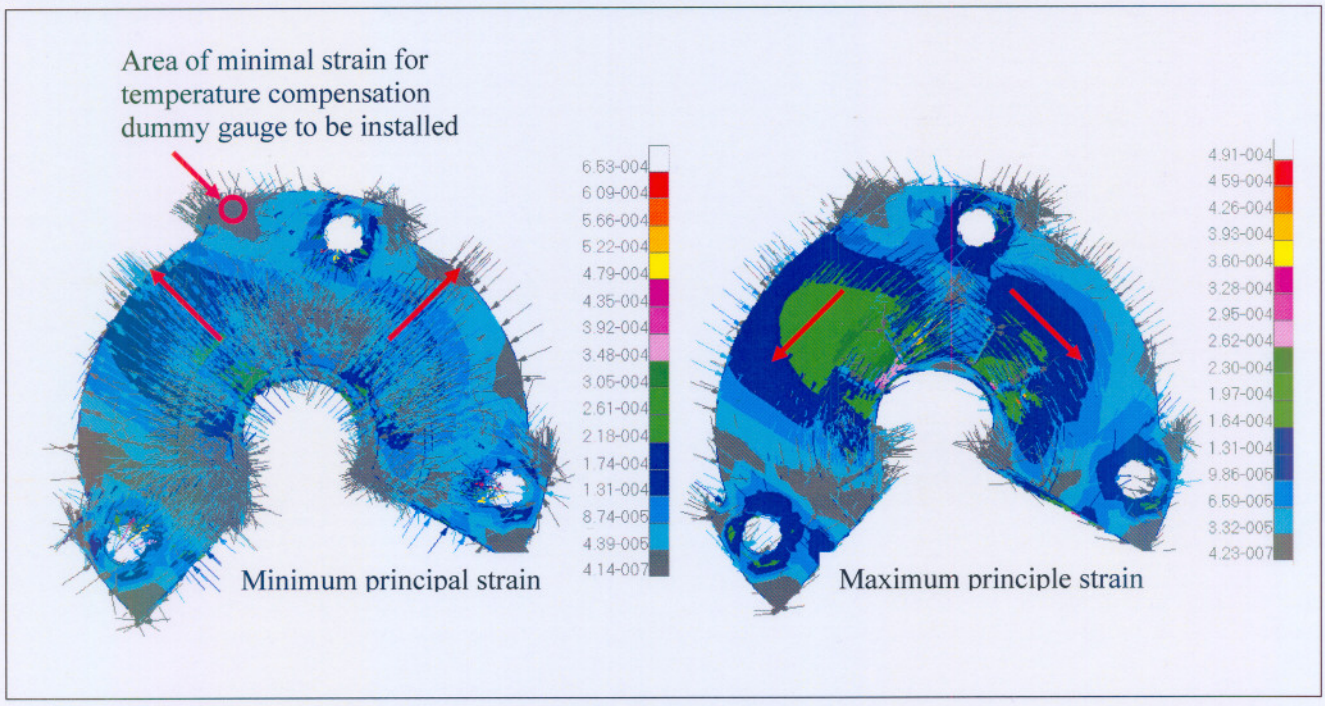


Figure 4.13: Finite element analysis vector plot of maximum and minimum principle strains for the thrust bearing for a thrust force of 400N in the "turbine to compressor" direction.

Figure 4.13 shows a vector plot of the maximum and minimum principle strains for a thrust force of 400N in the direction "turbine to compressor". As in Figure 4.4, the largest strains outside the circled areas of Figure 4.3 occur radially outward from the recess between the "thrust shoes". The red arrows of Figure 4.13 indicate the directions of the minimum and maximum strain direction at the areas where the strain gauges can be installed. Thus the grid of the strain gauge should be aligned in the radial direction to measure the minimum principal strain when the thrust is exerted in the direction "turbine to compressor" and the maximum strain when the thrust is exerted in the direction "compressor to turbine".

The strain gauge selected for this thrust test was the type KFC-2-D16-11; a self-temperature compensated strain gauge for steel from the manufacturer Kyowa. This type of strain gauge is a general use type of strain gauge, with two measuring grids aligned at an angle of 90° with respect to each other. It has a nominal resistance of 120Ω, a grid length of 2mm and a gauge factor of 2.12. The diameter of the carrier material is 4mm. This particular strain gauge was selected due to the small diameter of the carrier material. The small diameter facilitates the installation of the measuring grid as close as possible to the thrust collar circle, where the largest strain occur. The strain field is non-homogeneous; therefore the short measuring grid will be able to measure a point strain. The maximum operating temperature of this type of strain gauge is 150°C, which is higher than the expected 120°C operating temperature of the thrust bearing. The thermal expansion coefficient of grey cast iron is given as 12.1×10^{-6}/°C [5], while HBM uses 9.0×10^{-6}/°C [14]. The strain gauge used has a thermal expansion coefficient of 10.8×10^{-6}/°C for steel, which is considered suitable for this application on cast iron.

For this application, the operating temperature was estimated to be in the range of 80 to 120°C and lubrication oil is present at the thrust bearing. The maximum temperature range for HBM Z70 adhesive is 120°C [14], which is the top end of the estimated operating temperature range. HBM EP310S is a hot curing - two component epoxy resin adhesive, with a maximum operating temperature of 310°C for dynamic applications and can be applied in a very thin layer. Hot curing adhesives meet higher quality demands and EP310S adhesive is typically applied for transducer manufacturing due to its good long term stability even at high temperatures [14]. Due to the high temperature operation and stability, EP310S was selected as the adhesive for bonding of the strain gauges onto the thrust bearing.

From the finite element analysis, it was found that the strain has the same sign at the locations earmarked for the installation of the strain gauges (Figure 4.4). This cancels the output of a half bridge because two positive signals will subtract from each other according to Equation 4.8. A KWS 673.D8 amplifier (5 kHz carrier frequency amplifier) from HBM was used for signal conditioning in the strain gauge thrust measuring system. This amplifier has a bridge selection switch only for an inductive half bridge, a strain gauge half bridge and a strain gauge full bridge and not for a two- or three-wire strain gauge quarter bridge. This is also indicated by the circuit diagram of the amplifier [13]. Thus quarter bridge circuits cannot be used as input to this amplifier. Due to the errors encountered with the use of quarter bridges and the advantages of a full bridge circuit as discussed in Sections 4.3.2 to 4.3.4, the use of a full bridge was imperative. Again the two positive signs of the strain at the strain gauge positions mean that the active strain gauges cannot be connected in two adjacent bridge arms. Thus the configuration described by Equation 4.10, where R_1 and R_3 are the active strain gauges and R_2 and R_4 (Figure 4.15) are temperature compensation dummy gauges that experience only the thermal strain components, was implemented. The use of a full bridge also implicate that temperature compensation was obtained and cable errors were cancelled out.

To protect the strain gauge measurement system against the oil and mechanical damage by the oil flow at 80 to 120°C, HBM's SG250 silicone rubber was selected as a covering agent, since it is chemically resistant to oil. SG250 can be used in temperatures up to 250°C [14].

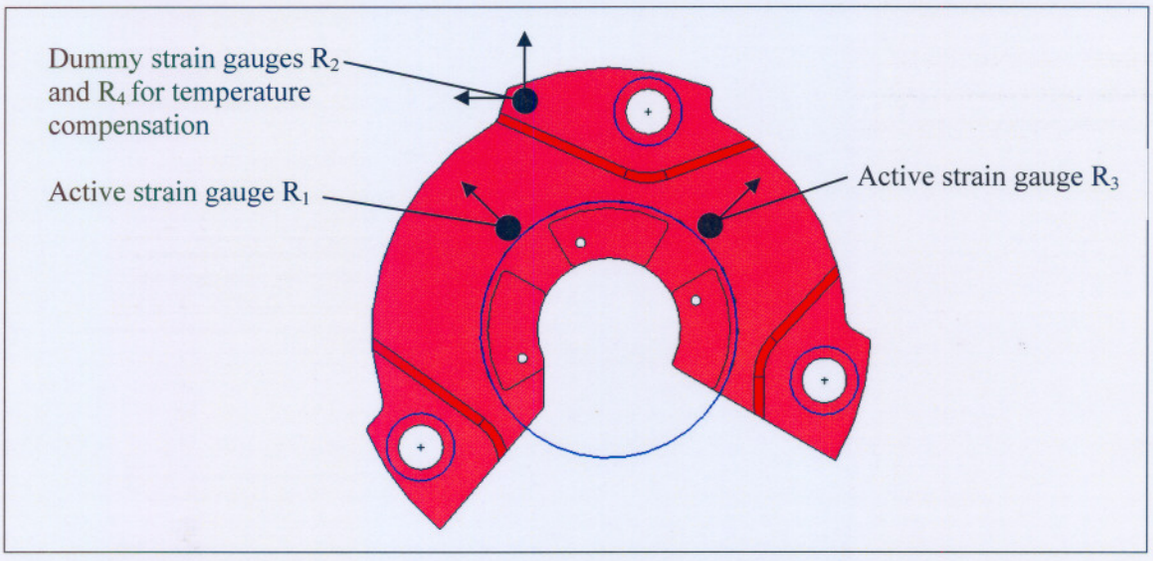


Figure 4.14: Installation positions for strain gauges with grid alignment markings.

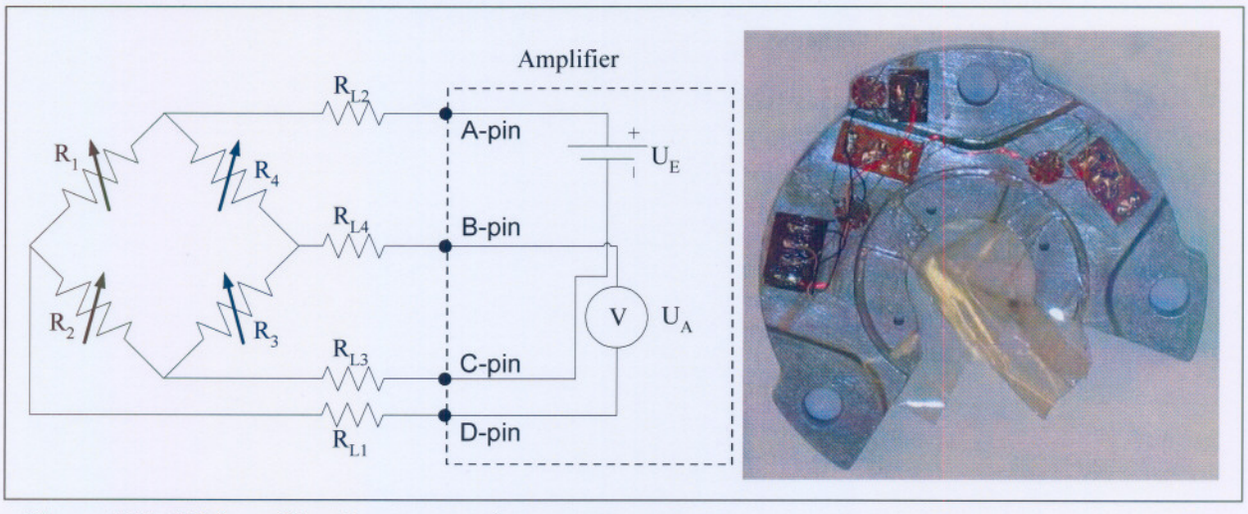


Figure 4.15: Wiring of the thrust measuring system.

After considering all of the design constraints and the theory of strain gauge measuring systems, the strain gauges were installed as illustrated in Figure 4.14 and according to the procedure given in Appendix B1. Upon completion of the installation of the strain gauges, the strain gauges were wired and connected to the amplifier as shown in Figure 4.15. For the jumper wires of the bridge, Teflon insulated wires were used and a four core shielded Teflon insulated cable was used to connect the bridge to the amplifier. By using a single cable with four cores the length of the four wires are kept the same; therefore the cable resistances are the same.

4.4.2 Calibration of the strain gauge thrust measuring system 1:

Once the strain gauges had been installed and wired, the strain gauge bridge was connected to the amplifier and adjusted for a no-load condition by following the procedure given in Appendix B2. The primary aim of the measurement with the strain gauges was not to measure strain but thrust. Therefore it was needed to calibrate the output of the strain gauges for force. The calibration was performed in both

directions "turbine to compressor" and "compressor to turbine". From preliminary calculations with the method of Liebner as discussed in Chapter 3, it was established from PBMM test data on 11 August 2005 that the thrust force ranged in the order of 650N. The calibration was performed by installing the thrust bearing inside the turbocharger centre casing (Figure 4.16) and applying a dead weight force from 0 to 676N (Figure 4.17). The centre casing was not mounted to the frame in Figure 4.17; this ensured that bending effects on the frame did not influence the calibration. From the graphs generated (Figure 4.18 and 4.19), a fairly linear relation between strain and force with a band of error was obtained. When the PBMM was operated, the recorded output from the strain gauges was adjusted with the calibration values to obtain the exerted thrust. When the calibration was performed in the direction "turbine to compressor", the thrust bearing needed to be dismounted to install an insert that exerts the dead weight force on the thrust bearing. To ensure that the thrust bearing was installed exactly the same as before, the thrust bearing was dismounted, the bolts were torqued to 2.9N.m (M4 grade 8.8 bolts) and the reading on the amplifier returned to zero without any adjustment.

After the load calibration had been finished, the turbocharger was assembled completely. The complete turbocharger was then put in a temper oven to perform a zero drift test without load at temperatures up to 120°C. A thermocouple was fitted onto the thrust bearing to measure the thrust bearing temperature for the thermal drift test. A third order curve was fitted to the results of the thermal drift test, as shown in Figure 4.20. This was a similar curve as supplied with strain gauges for the compensation of sensitivity at different temperatures. The aim of this curve was to make corrections to the output of the strain gauge thrust measuring system according to the operating temperature of the thrust bearing.



Figure 4.16: Thrust bearing installed inside the turbocharger centre casing.



Figure 4.17: Calibrating the thrust measuring system with dead weights.

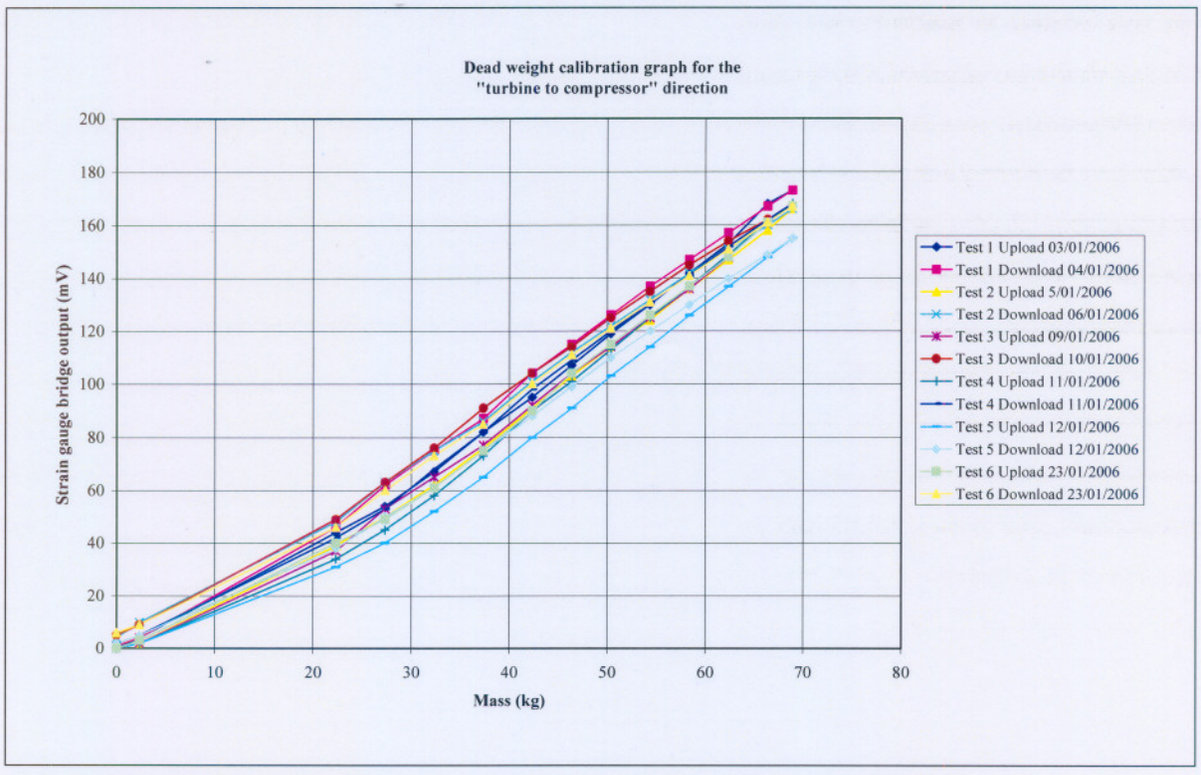


Figure 4.18: Dead weight calibration graph for "turbine to compressor" direction.

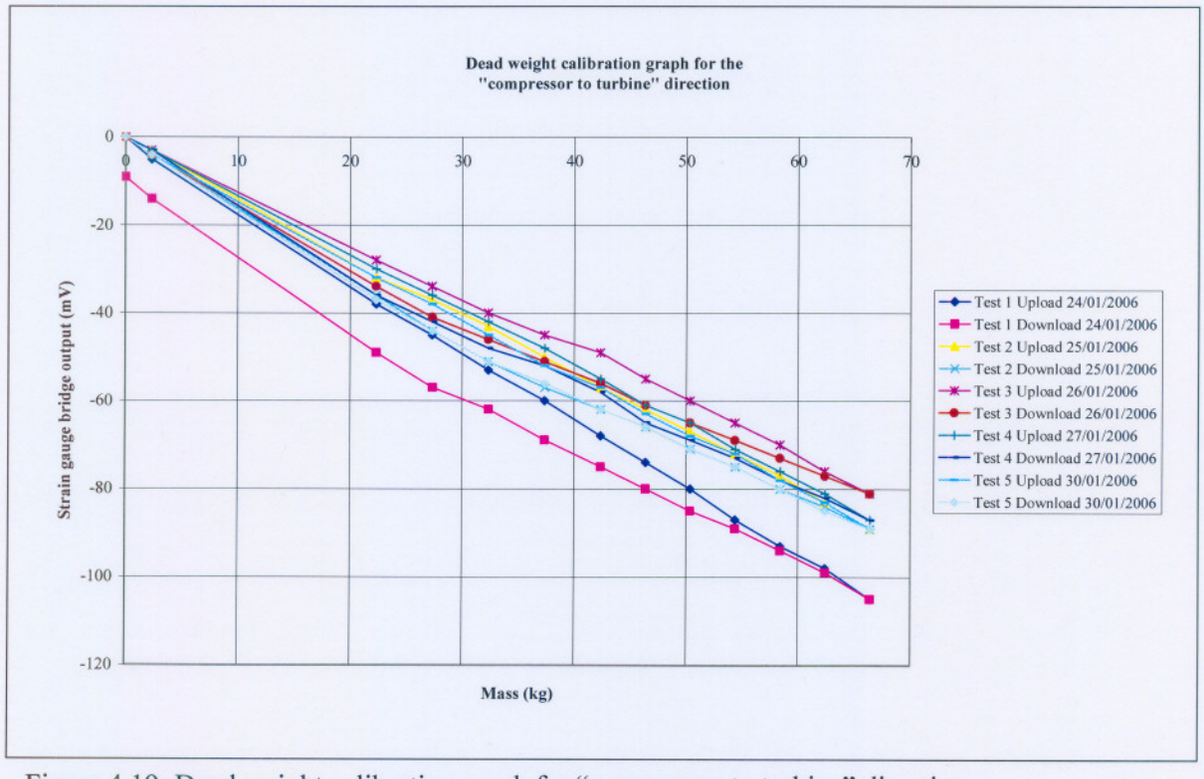


Figure 4.19: Dead weight calibration graph for "compressor to turbine" direction.

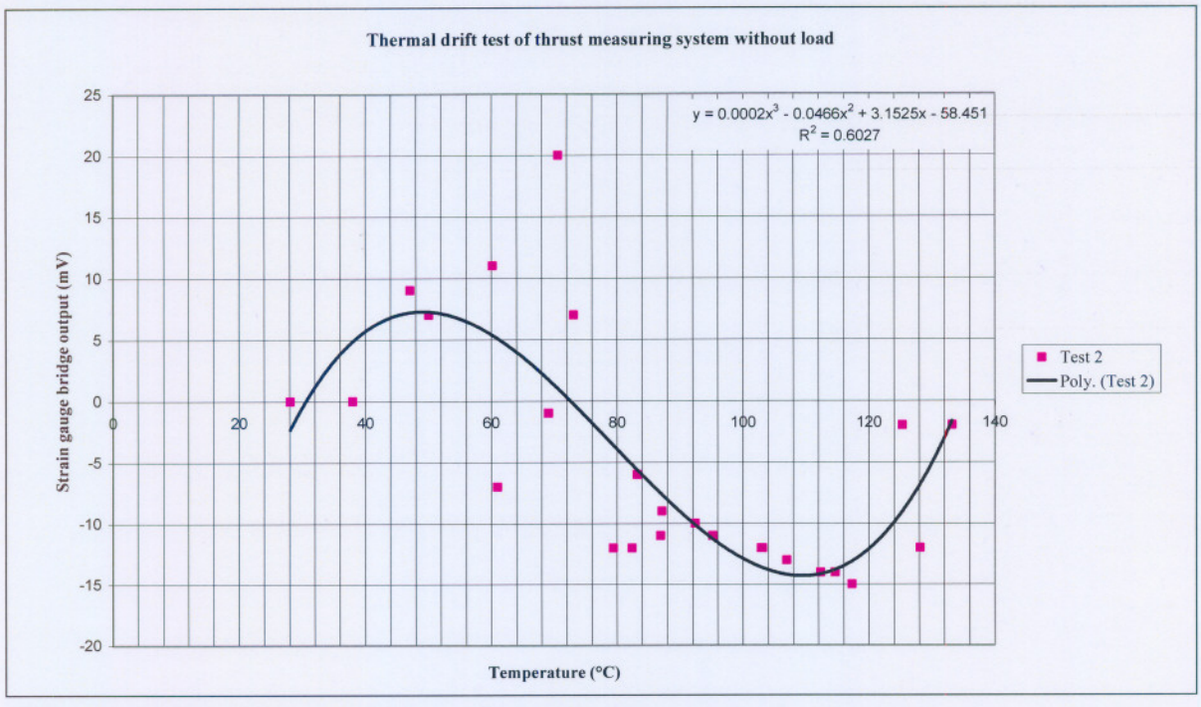


Figure 4.20: Thermal output of the strain gauge bridge.

The Y-axis values of Figures 4.18 to 4.20 are not micro strain but the reading on the digital readout of the amplifier. For the thrust measurement system the amplifier reading will suffice as the amplifier reading is calibrated for a certain thrust force. An additional verification of the thrust force was done by converting the amplifier reading to micro strain and comparing it with the finite element analysis results.

As mentioned before, the gauge factor of the strain gauges was 2.12. The strain gauges were wired in a full bridge configuration with two dummy gauges and two active gauges, which means that the bridge factor was four. A bridge excitation voltage of 1V was used to minimize the internal heating of the strain gauges. For some strain gauge amplifiers, the gauge factor can also be given as input. The amplifier used in this study cannot accommodate the gauge factor as input; therefore the reading on the digital readout had to be divided by the gauge factor to obtain a micro strain reading. By selecting a full bridge on the amplifier (step 5 in Appendix B2), the bridge factor B, is four (refer to Equation 4.11). Just for assurance that the reading on the amplifier had to be multiplied by the gauge factor only to obtain a micro strain reading, strain gauges were installed on a cantilever beam (Figure 4.21) that could be easily checked with a theoretical calculation.

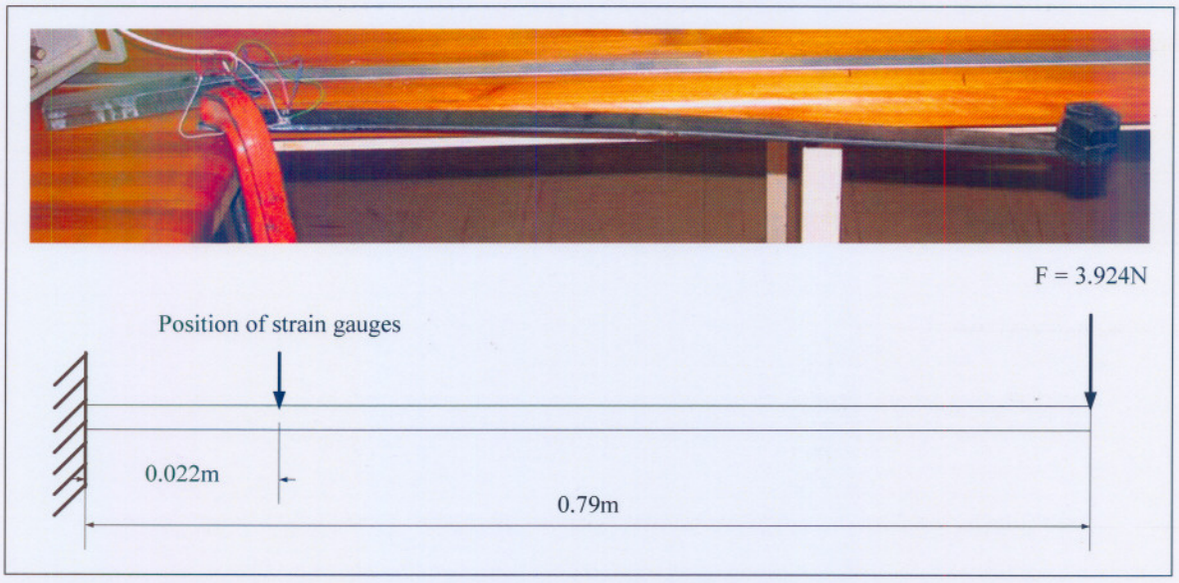


Figure 4.21: Cantilever beam for verification of amplifier reading.

Two active strain gauges were installed on the cantilever beam next to each other to have the same magnitude, and two dummy gauges on a separate piece of steel for temperature compensation. The four strain gages were wired in a full bridge configuration to obtain exactly the same setup as used on the thrust bearing. A load of 400g was applied to the end of the cantilever beam. The beam had the following dimensions: 0.79m in length, 0.03m wide and 0.005m high. The two active strain gauges were installed at a distance of 0.022m from the clamped side. A moment of 3.014Nm acted at the position of the active strain gauges for a force of 3.924N. The theoretical calculation for strain is performed as follows [26]:

$$\sigma = \frac{M \cdot c}{I}$$

where

$\sigma \equiv$ stress (Pa)

$M \equiv$ Moment (Nm)

$c \equiv$ maximum distance from neutral axis to outer edge (m)

$I \equiv$ moment of inertia (m^4)

and

$$I = \frac{b \cdot h^3}{12}$$ for a beam with rectangular cross section

with

b = width of beam

h = height of beam

$$\sigma = \frac{M \cdot c}{\frac{b \cdot h^3}{12}}$$

$$= \frac{3.014\text{Nm} \cdot 0.0025\text{m}}{\frac{0.03\text{m} \cdot 0.005^3\,\text{m}^3}{12}}$$

$$= 24.112\text{MPa}$$

but

$$\varepsilon = \frac{\sigma}{E}$$

with

$\varepsilon \equiv$ strain

$E \equiv$ Young's modulus = 207GPa for mild steel

$$\varepsilon = \frac{24.114 \times 10^6\ \text{Pa}}{207 \times 10^9\ \text{Pa}}$$

$$= 0.0001164 \frac{\text{m}}{\text{m}}\text{: theoretical strain at the position of the strain gauges}$$

For the measured strain Equation 4.1 is used with U_A measured as 233mV (readout of amplifier) and U_E is 1000mV (1V excitation voltage).

$$\frac{U_A}{U_E} = \frac{k}{4} \cdot B \cdot \varepsilon$$

$$\frac{233\text{mV}}{1000\text{mV}} = 2.12 \cdot \varepsilon \qquad (4.11)$$

$$\varepsilon = 0.000109905 \frac{\text{m}}{\text{m}}\text{ measured strain}$$

This gave an error of 5.6% between the measured strain and calculated strain. Thus the reading from the amplifier should be divided by the gauge factor only. The amplifier takes the bridge factor, B and the denominator of four into account.

4.4.3 Preparation for Thrust test 1 with thrust measuring system 1 installed in PBMM:

After the calibration had been completed for the thrust measurement system of the HPTU, the HPTU was ready to be installed inside the PBMM for a test. An extension piece was added to the outlet port of the HPTU centre casing to facilitate sealed protrusions out of the lubrication port for the cable of the thrust measurement system as well as the thermocouple that measures the thrust bearing temperature (Figure 4.22). The thermocouple measuring the thrust bearing temperature was connected to the control system of the PBMM and automatically logged by the data capturing system. A computer with Labview 7.1® data capturing software was connected to the output of the amplifier to log the voltage output signal from the strain gauge thrust measurement system, HPTU rotor speed and HPTU vibration.

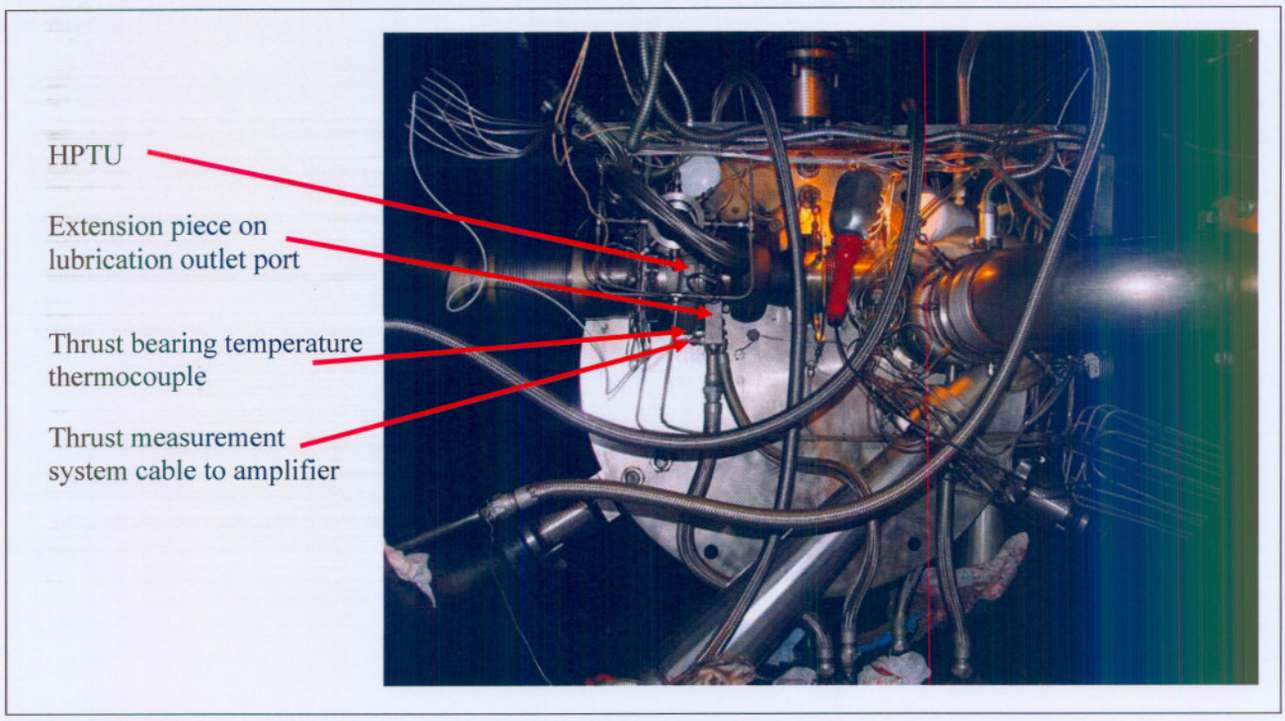


Figure 4.22: HPTU installed inside PBMM with thrust measurement system.

4.4.4 Thrust Test 1:

The PBMM operates on the principle that the nitrogen is cycled with a blower while the heater heats the gas until the process becomes self-sustainable and the turbines produce enough power to drive the compressors. This process is termed "bootstrap". From experience it is found that the system bootstraps at an inlet temperature of 580°C to the high pressure turbine (HPT), when the inlet pressure to the low pressure compressor (LPC) is at 95kPa (absolute). Thus the test plan was to set the amplifier to zero (no-load condition) before the blower was started because once the blower had been started, the turbochargers start to turn and thrust was exerted on the thrust bearing until the process became self-sustainable. Once the process was self-sustainable, the LPC pressure was set to 95kPa absolute and the HPT inlet temperature to 580°C if not already reached when bootstrapped. A low pressure (inventory) and low temperature operating point was established (Figure 4.23, Point 1). Then the LPC pressure was increased (gas inventory increased) to 105kPa absolute and further to 115kPa absolute (Figure 4.23, Point 2). A high pressure, low temperature operating point was reached. The HPT temperature was then increased to 650°C to obtain a high pressure and high temperature operating point that should give the maximum thrust (Figure 4.23, Point 3). Pressure to the LPC was then decreased but the inlet temperature to the HPT was kept constant at 650°C to reach a high temperature, low pressure scenario (Figure 4.23, Point 4). The inlet temperature to the HPT was then decreased to 580°C to reach the start of the cycle (Figure 4.23, Point 1). The strain gauge amplifier reading should be the same as when the cycle started.

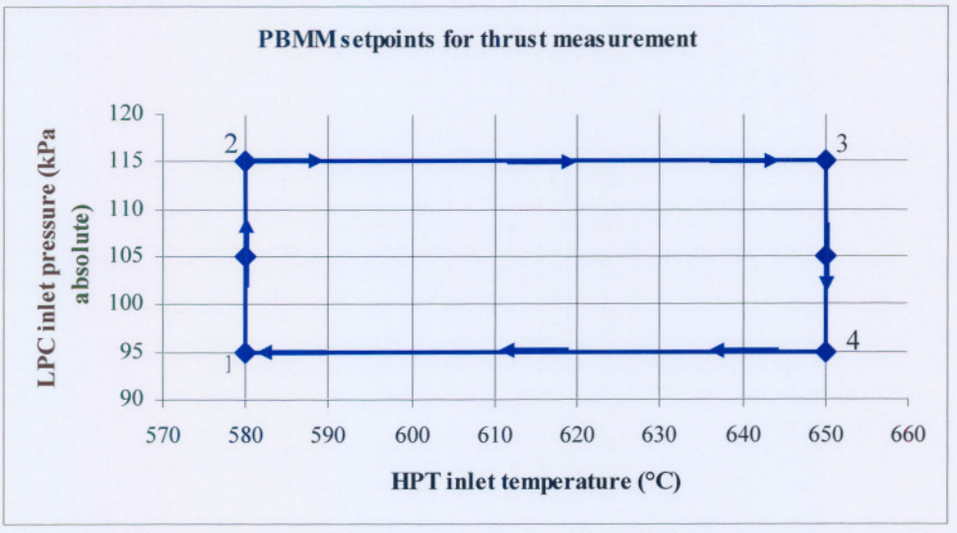


Figure 4.23: PBMM HPT inlet temperature- and LPC inlet pressure set points for thrust measurement test.

The following parameters were recorded for theoretical thrust calculation purposes: inlet- and outlet temperature of the high pressure turbine (HPT), inlet- and outlet pressure of the HPT, inlet- and outlet temperature of the high pressure compressor (HPC), inlet- and outlet pressure of the HPC, mass flow rate of the primary cycle, rotor speed of the high pressure turbo unit (HPTU). For the experimental thrust measurement, the thrust bearing temperature was recorded for temperature compensation and the strain gauge thrust force reading.

4.4.5 Thrust Test 1 results:

Results of the first thrust test are illustrated in Figure 4.24. The measured thrust is compared with the results of the different thrust calculation methodologies as calculated in Chapter 3. The minimum and maximum measured thrust lines were calculated from the uncertainty ranges of Figures 4.18 and 4.19 The numbers in Figure 4.24 correspond to the set points of the test plan given in Figure 4.23. From the test results, it was found that thermal drift caused the experimental thrust reading to drift unpredictably (not predictable by Figure 4.20). No correlation could be made between the thermal correction graph of Figure 4.20 and the experimental measured thrust of Figure 4.24. Thus this thrust test proved to be unsuccessful due to unreliable thrust measurements. All the theoretical thrust calculation methodologies showed the same trend; when pressure or temperature was increased, the thrust also increased and vice versa. The predicted thrust values obtained from the different thrust calculation methodologies differed considerably as was expected from the analyses in Chapter 3.

From this particular test, it was learned that the thrust bearing operating temperature ranged between 70 to 90˚C, which was lower than the maximum of 120˚C estimated previously. Now that the thrust bearing operating temperature was known, insight had been gained into the conditions that the thrust measurement system had to be able to sustain.

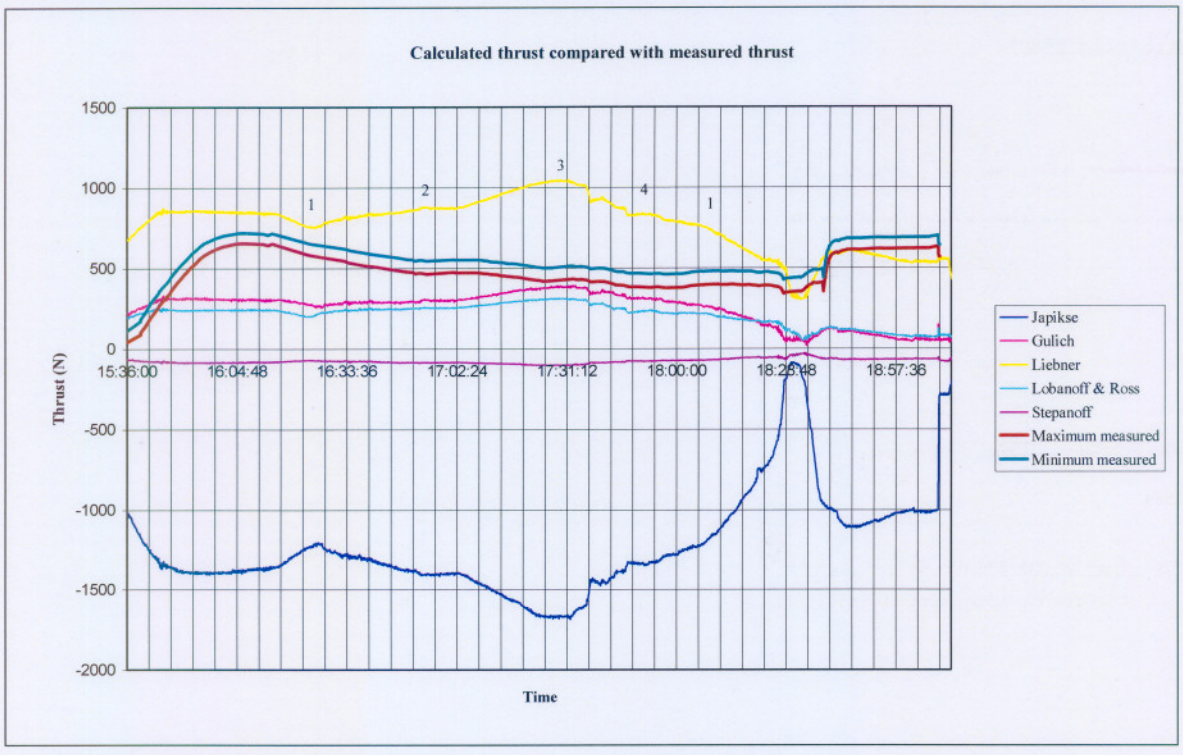


Figure 4.24: Thrust test 1 results.

When the turbocharger was disassembled after the test it was confirmed that the strain gauges did not came loose during the test. The thermal drift that occured with this thrust test was attributed to factors such as metallurgical changes in the strain gauges or the adhesive [15] or creep between the strain gauges, adhesive and thrust bearing metal. A new thrust measurement system had to be designed to address the factors given above for the thermal drift that occurred.

4.5 Installation of thrust measurement system 2:

4.5.1 Installation of strain gauges on thrust bearing for Test 2:

As explained in Section 4.4.1, the position for installation of the active strain gauges was limited. Therefore, the active gauges for this installation were positioned at the same locations as the previous test. It should be noted that the position of the strain gauges in the previous test did not cause problems. Thus two active unidirectional strain gauges (R_1 and R_3 in Figure 4.25) were installed in a radial direction.

It could be possible that the temperature compensating strain gauges (R_2 and R_4) of the previous installation did not cancel the thermal strains entirely as the two grids were aligned at an angle of 90°. Thus for the second installation, two temperature compensating strain gauges were installed on a separate metal piece of the same material as the thrust bearing. The aim of the separate metal piece was to have a section that definitely only experience the thermal strains and not any mechanical strains. On the thrust bearing itself, there was no space available for the installation of two strain gauges that will experience thermal strains only with certainty. During the first test, the highest rotational speed of the HPTU was

recorded as 67000 r/min or 1117Hz. Thus the natural frequency or resonance frequency should at least be more than 1500Hz. By performing a modal finite element analysis, the natural frequency of a piece of metal (Young's modulus of 165GPa, density of 6900kg/m^3 and a Poisson ratio of 0.27) as shown in Figure 4.25, was predicted to be 2712Hz. Thus the metal insert would not experience too much amplification from excitation by the rotor.

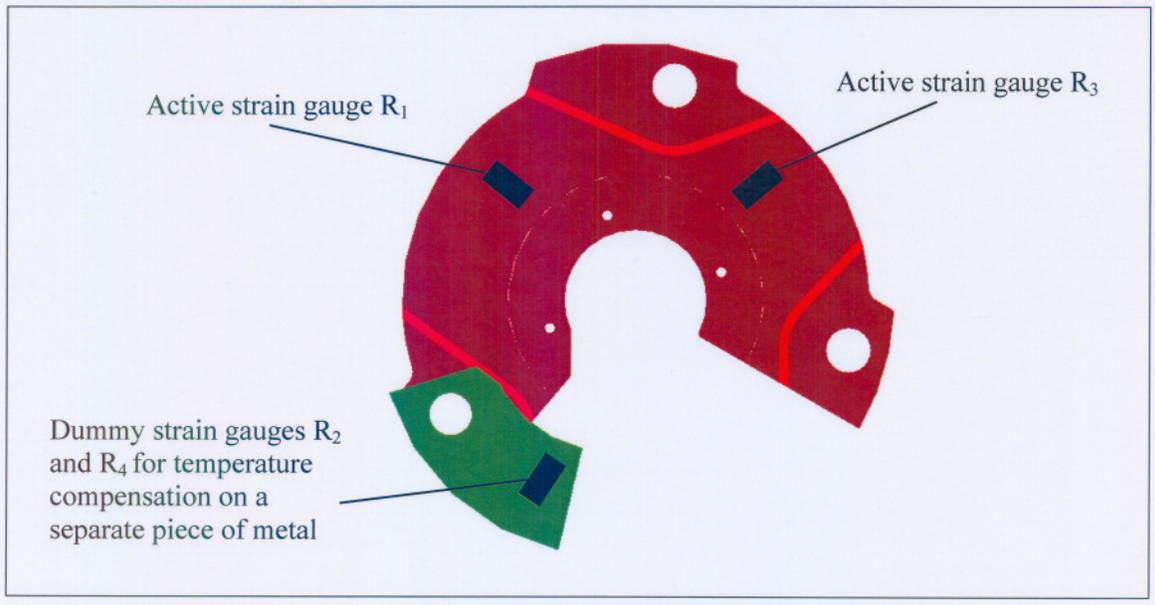


Figure 4.25: Installation positions for strain gauges with grid alignment markings.

To cancel the effect of vibration, one strain gauge was installed on the top and the other on the bottom side of the plate. Thus one strain gauge would experience a positive strain and the other a negative strain that would cancel each other.

In the selection of strain gauges for the second thrust measurement system, attention was given to the maximum operating temperature of the strain gauges, creep compensation (Section 4.3.4) and self-temperature compensation as this could have caused the problems with the first setup. The strain gauge selected for the second thrust test was the type 1-LK11K-3/350; a self-temperature compensated strain gauge for steel with a thermal expansion coefficient of 10.8×10^{-6} /°C from the manufacturer HBM. This type of strain gauge is a transducer class strain gauge with a nominal resistance of 350Ω, a grid length of 3mm and has a gauge factor of 2.07. The size of the carrier material is 9.5mm long and 5mm wide. This particular strain gauge was selected for its small size with creep compensation. The size had to be kept as small as possible to fit onto the thrust bearing's available area. The larger size of the strain gauges for the second setup than the previous gauges implicated that the measurement would be taken over a larger area and the output would be the arithmetic mean of the larger area. The maximum operating temperature of this type of strain gauge is 200°C, which is much higher than the measured 80°C operating temperature of the thrust bearing.

EP 310S, a two component, hot curing adhesive from HBM, was selected again as the adhesive for the second thrust measurement system as it is the best adhesive for transducer applications and it can be used at temperatures up to 310°C.

For this installation, the strain gauges and adhesive were from one manufacturer namely HBM, thus the strain gauges and adhesive were matched to be used together. In the previous installation, the strain gauges were from Kyowa and the adhesive from HBM. For the installation of the strain gauges on the thrust bearing, the procedure given in Appendix B1 was followed.

The same wiring scheme was used as shown in Figure 4.15 for the second thrust measurement system. Two active gauges were wired in the opposing legs of a full bridge and two temperature compensating gauges in the two other opposing legs.

The bridge was wired according to Figure 4.15 by using Teflon flexible stranded wire (cross section of $0.24mm^2$ and resistance of $0.0741\Omega/m$) to complete the bridge. A four core shielded Teflon insulated cable was used to connect the bridge to the amplifier. The length of the four cores was the same to keep the cable resistances equal.

SG 250 silicone rubber sealant from HBM was used to protect the strain gauges against the oil present at the measuring points.

4.5.2 Calibration of the strain gauge thrust measuring system 2:

As before, the thrust force exerted on the thrust bearing during the operation of the PBMM needed to be measured with a strain gauge thrust measuring system. Thus the output of the strain gauges needed to be recorded for a range of known thrust forces exerted on the thrust bearing. When the PBMM was operated, the reverse process was followed by recording the output from the strain gauges and converting it according to the calibration graphs to obtain the thrust force. The strain gauge bridge had a certain thermal output which was a function of the temperature that the bridge was exposed to. This thermal output needed to be characterized. In Section 4.4.2 the load calibration was performed first and then the characterization of the thermal output. As the previous test was unsuccessful due to thermal drift that occurred, the thermal characterization was performed first for the second thrust measurement system, after which the load calibration followed.

Upon completion of the strain gauge installation on the thrust bearing and the wiring, the strain gauge bridge was connected to the KWS 673.D8 amplifier (5 kHz carrier frequency amplifier) from HBM, the same as in the previous thrust test. The amplifier was then balanced (set to null for a no-load condition) for this specific strain gauge bridge according to the procedure given in Appendix B2. If the excitation

voltage for the strain gauges was set above 1V, self heating of the strain gauges occured and the output started to drift. Thus the excitation voltage for this strain gauge bridge was set at 1V. The HPTU with the installed thrust measurement system was placed in the temper oven to do the thermal output characterization. The temperature was raised from room temperature to 80°C, which had been established as the operating temperature of the thrust bearing from the previous thrust test. The reading on the amplifier rose steadily as the temperature increased until the temperature reached 41°C. Then the reading started to drift extremely. When the turbocharger was cooled down to room temperature again, the reading on the amplifier did not return to null. No load was exerted on the thrust bearing during this test. The sudden drift of the reading implicated that the amplifier received some signal that is not a true strain signal. It was decided to use a different amplifier to determine if the output drifted the same.

A Vishay 2200 strain gauge amplifier was connected according to the wiring diagram of Figure 4.26 to the thrust measurement system. The amplifier was tared according to the procedure given in Appendix B3. This amplifier did not have a display module of the output, as was the case with the HBM amplifier. A multi-meter was used to display the output of the strain gauge bridge in millivolt.

With the Vishay amplifier, the reading on the multimeter shifted negatively as the temperature of the thrust bearing on the HPTU increased. The temperature was raised up to 80°C and the output on the multi-meter stabilized. As the HPTU cooled down to ambient temperature, the output on the multi-meter returned to null. Some hysteresis was observed between the heating and cooling curves. The heating curve reflected transient behaviour while the cooling curve represented steady-state behaviour. The rate at which heating and cooling happens also affected the amount of hysteresis that was obtained. Figure 4.27 gives the thermal output of the strain gauge bridge without an applied thrust force.

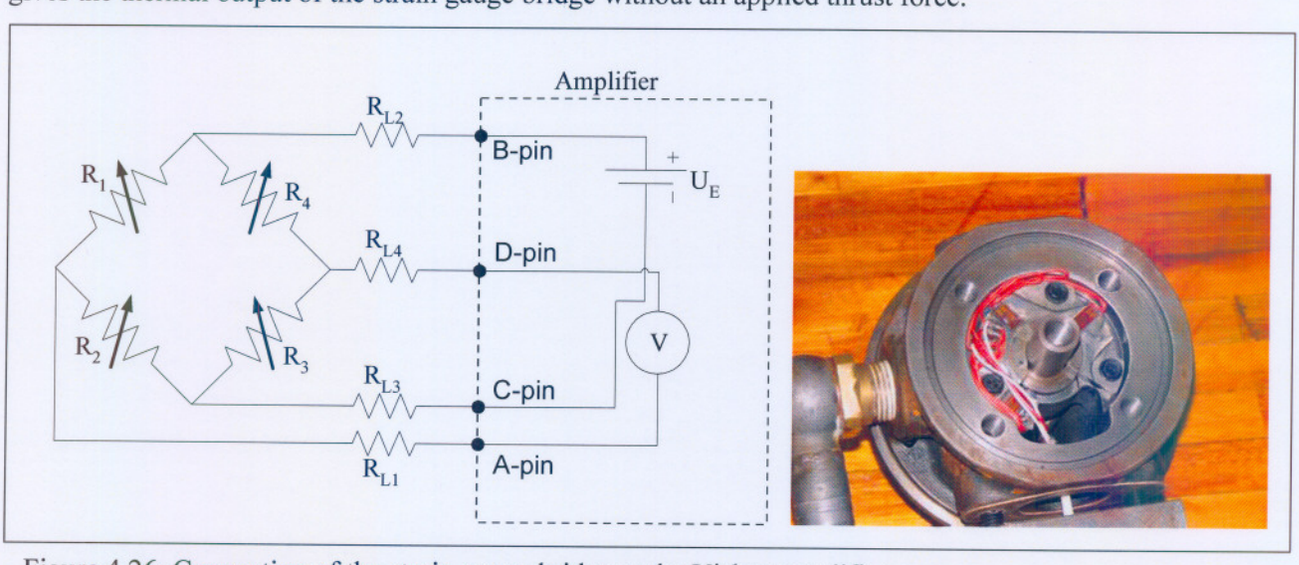


Figure 4.26: Connection of the strain gauge bridge to the Vishay amplifier.

If the function of thermal output enclosed on the packaging of the strain gauges is plot, then the bridge output of Figure 4.27 is much lower per degree Celsius than that of the function on the packaging. This is because the full bridge configuration cancelled some of the thermal output, but not everything.

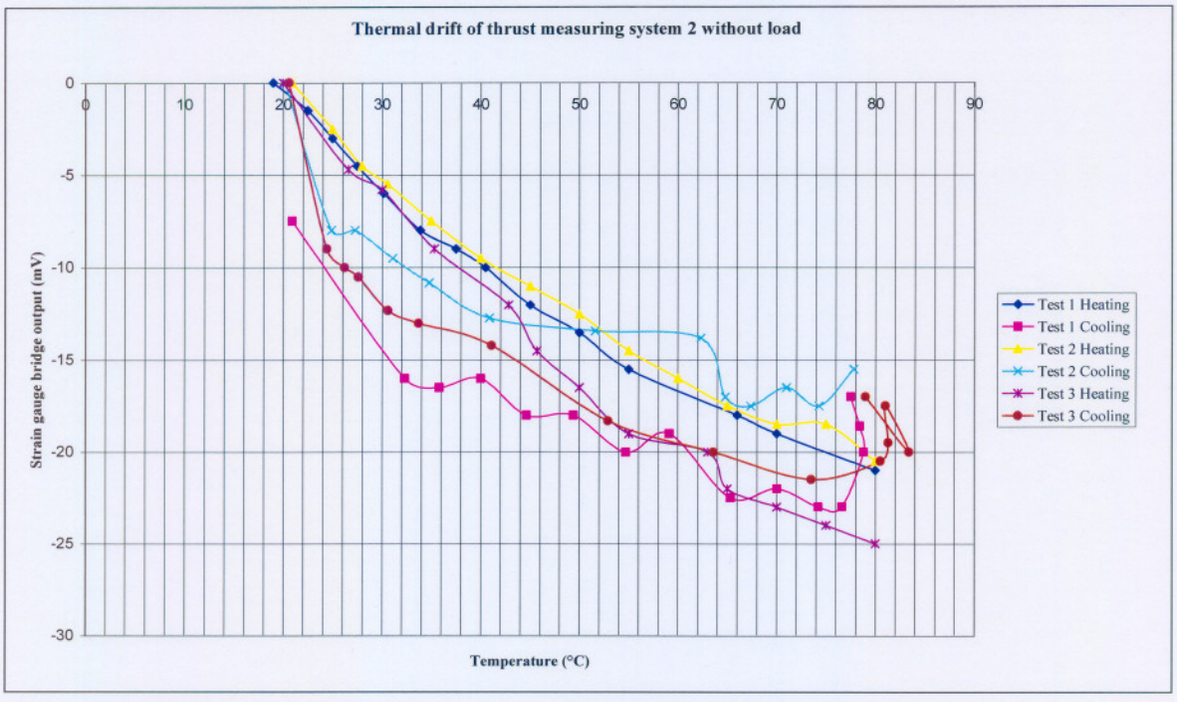


Figure 4.27: Thermal output of the strain gauge bridge without load.

Figure 4.20 and Figure 4.27 are the thermal output graphs for the two thrust measuring systems respectively. Figure 4.20 follows the pattern of the function given on the packaging of the Kyowa strain gauges while Figure 4.27 does not follow the same pattern. When thrust measuring system 1 was operated inside the PBMM under load, thermal drift occurred under the thrust load. To ensure that thrust measurement system 2 did not show the same behaviour, the HPTU was placed in the temper oven with a dead weight thrust load of 202.5N in the direction "compressor to turbine". The temperature was then raised from room temperature to 80°C and cooled down again to determine if the same trend as in Figure 4.27 was obtained, except for an offset of the load component. This was indeed the case as shown in (Figure 4.28). Thus if thrust measurement system 2 was operated inside the PBMM, the thermal output component, calculated from Figure 4.27, could be deducted from the total output signal and the remainder would be the exerted thrust load. For the direction "turbine to compressor" the thermal output would lower the reading (shifted positive) as the thermal output was a negative value, while for the direction "compressor to turbine" the thermal output added to the thrust component (shifted negative).

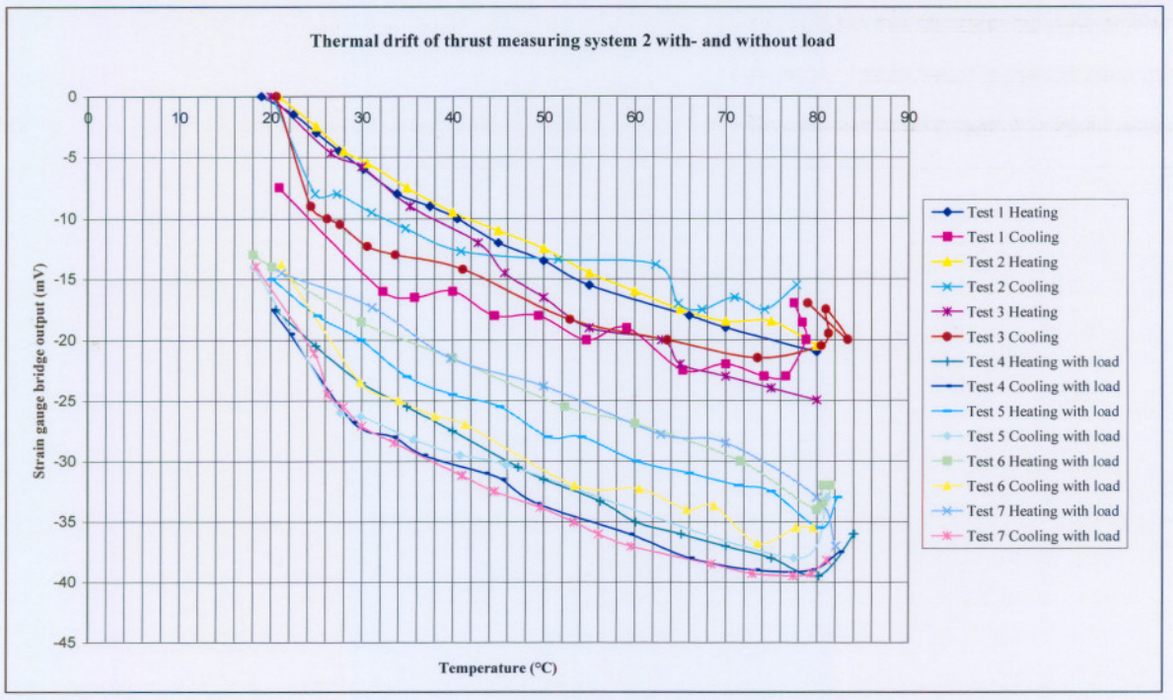


Figure 4.28: Thermal output of the strain gauge bridge with and without load.

Now that the thermal output of the strain gauge bridge was predictable without load and with load, the load calibration could proceed. Thrust measurement system 1 was load calibrated with dead weights as shown in Figure 4.17. The size of the frame limited the number of weights that could be used. A bigger range for the load calibration was desirable, as the amplifier reading reached the top end of the calibrated range during Thrust test 1. Thus for the load calibration of thrust measurement system 2, a pre-calibrated load cell was used along with a screw rod to apply the thrust force. The calibration range was extended from 676N to 1079N. Figures 4.30 and 4.31 show the calibration graphs obtained for both directions "compressor to turbine" and "turbine to compressor".

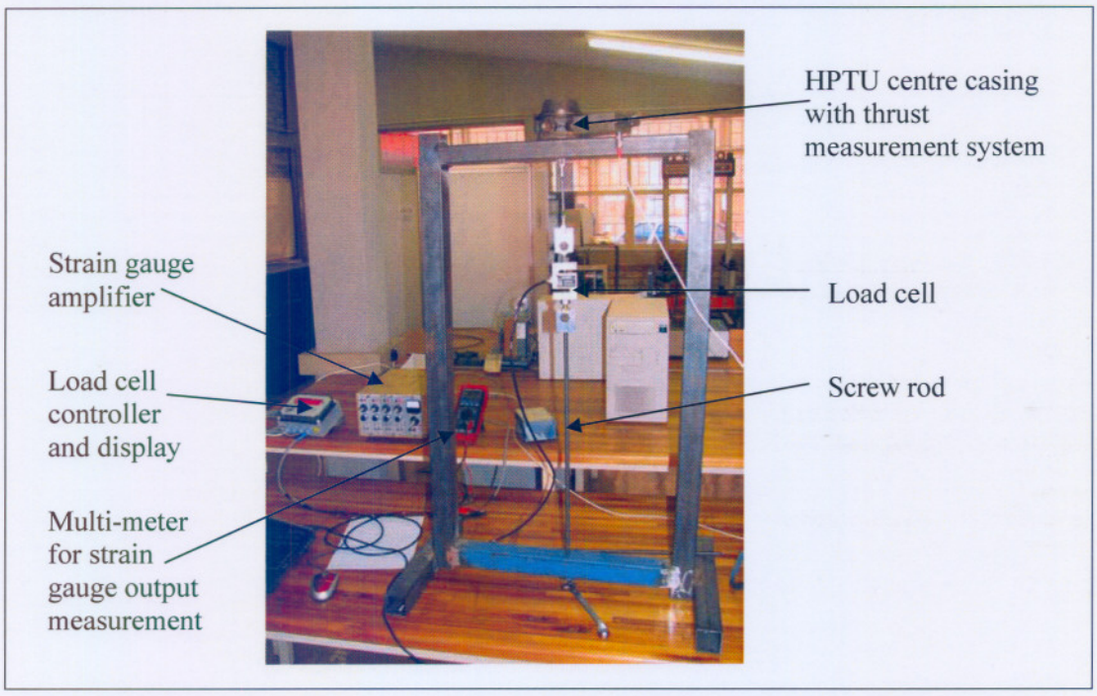


Figure 4.29: Load calibration of the thrust measurement system with a load cell.



Figure 4.30: Load calibration for the direction "turbine to compressor".

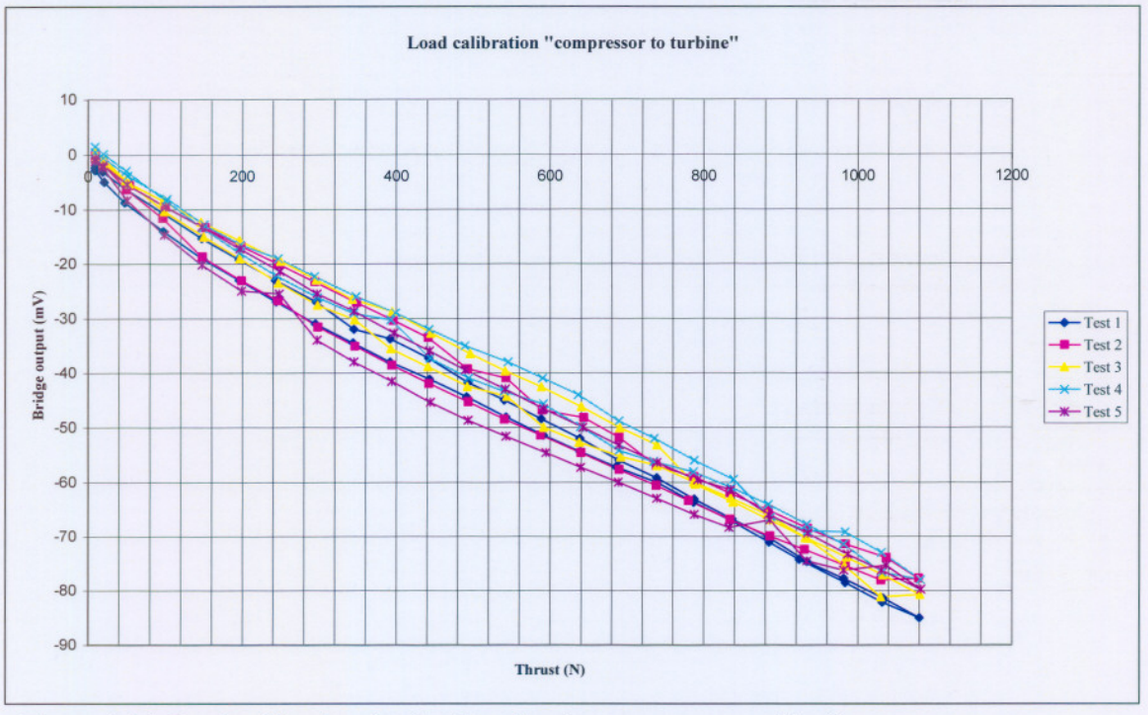


Figure 4.31: Load calibration for the direction "compressor to turbine".

4.5.3 Preparation for Thrust test 2 with thrust measuring system 2 installed in PBMM:

After the load and thermal output of Thrust measuring system 2 had been calibrated, the HPTU with the thrust measurement system was installed inside the PBMM as before.

4.5.4 Thrust test 2:

The plan for Thrust test 2 was the same as the plan set out in Figure 4.23 for Thrust test 1. This was to balance (set null load condition) the strain gauge amplifier before the lubrication oil was circulated to the bearings and the thrust bearing temperature was still at ambient temperature. After the amplifier had been balanced, the lubrication oil was circulated through the bearings and the blower and heater were started to reach self-sustaining conditions. Circulation of the lubrication oil caused the thrust bearing temperature to rise and the strain gauge measurement system gave an output signal due to the thermal strain. As the turbines and compressors started turning, thrust was exerted on the thrust bearing. Thus there was no chance to balance the amplifier again once the lubrication oil was circulated and the blower started to drive the turbo units. Once the process was self-sustaining, the inlet pressure at the LPC and inlet temperature to the HPT was adjusted according to the set points of Figure 4.23. Additionally two steady state tests and two transient tests were conducted. Thrust measurements were logged during these four tests as well to have more measured thrust data. From Thrust Test 1 it was learned to control the cooling water flow rate to control the thrust bearing temperature at 80°C. The same parameters were recorded as for Thrust test 1.

The results of Thrust test 2 are discussed in detail in the next chapter because the thrust test data was considered successful.

4.6 Summary:

The aim of this chapter is to describe the design process of a thrust measurement system for the HPTU of the PBMM to verify the theoretical thrust calculations of Chapter 3 experimentally. In the beginning of this chapter several possible thrust measurement systems are considered like electro-magnetic, force washers, piezo-electric strain sensors and strain gauges. Due to cost implications and size constraints, a strain gauge thrust measurement system presented to be the only viable option.

Literature on strain gauge measurement systems is presented and the theory is applied to develop a strain gauge thrust measurement system. Thrust measurement system 1 was developed by configuring two active strain gauges for thrust measurement and two temperature compensating strain gauges in a full bridge. Self-temperature compensated strain gauges from the manufacturer Kyowa were used along with HBM's EP310S two-component hot curing adhesive. The thrust measurement system was then load calibrated and the thermal output was characterized. A KWS 673.D8 amplifier from HBM was used for strain gauge signal conditioning. After the load calibration of the strain gauge thrust measurement system, the HPTU containing the thrust measurement system was installed inside the PBMM for experimental testing. Thrust test 1 was conducted and it was found that unpredictable thermal drift occurred. This implicated that the thermal strain component could not be deducted from the total strain gauge output signal to obtain a reliable thrust load component. The thermal drift that occurred was attributed to some form of creep between the strain gauges, adhesive and thrust bearing metal. It was established that the operating temperature of the thrust bearing could be controlled at 80°C. Upon dismantling of the HPTU after the test, it was found that the strain gauges were still bound to the thrust bearing. Thus Thrust test 1 was unsuccessful with regard to thrust measurement.

A second attempt was made to construct a strain gauge thrust measurement system. This time, special self-temperature and creep compensated strain gauges were used from HBM with EP310S adhesive. It was found to be important to use the same brand strain gauges and adhesive as the materials are matched to be used together. When thrust measurement system 2 was connected to the KWS 673.D8 amplifier from HBM and placed in the oven for thermal response characterization, the null balance of the amplifier started to drift again from 40°C upward. A Vishay amplifier was connected to thrust measurement system 2 to determine if the same drift behaviour was obtained. It was then found that the null balance drifted as the thrust bearing temperature rose but the output stabilized at 80°C. Once the HPTU cooled to ambient temperature the amplifier output returned to zero. The thermal output of the strain gauge system was then characterised as it was found to be repeatable. The thrust measurement system was also load calibrated to

be able to measure the thrust. Again the HPTU was installed inside the PBMM to conduct a second thrust test. This time the thermal response could be predicted and subtracted from the total strain gauge signal to obtain the load component of the output signal. The output signal was converted to thrust according to the load calibration. A series of measured thrust data was obtained from Thrust test 2 and the results are presented in the next chapter.

5. Thrust Test 2 results & comparison

5.1 Introduction:

In this chapter a discussion follows regarding the thrust test data that was obtained with Thrust Test 2. Chapter 4 contains the load and thermal output calibration data. When the thrust measurement system was load calibrated, a known thrust force was exerted on the thrust bearing and the strain gauge measurement system's millivolt output signal was recorded. With the thermal calibration, the strain gauge measurement system was subjected to a range of temperatures and zero load. The strain gauge measurement system then gave a millivolt thermal output signal that was recorded. The thrust measurements recorded with Labview during Thrust Test 2 was the total output signal that was made up by two components namely: The thrust load strain component and the thermal strain component. The aim of the thrust test was to determine the thrust load; therefore it was needed to separate the total output signal into the two components and obtain the thrust load component that was of interest. A thermal strain component was calculated by taking the thrust bearing temperature and fit it to the calibration data to obtain a millivolt signal for each temperature. This millivolt signal was then subtracted from the total signal to obtain the load component only. This load component was a value in millivolt and was then converted to a thrust in Newton by fitting this load signal to the load calibration data.

Once the experimental measured thrust load data was obtained, it could be compared with the theoretical thrust calculation methodologies discussed in Chapter 3. Thus the experimentally measured thrust data and the comparison with theoretical data are presented in this chapter.

5.2 Determination of measured thrust load data:

In Figures 4.27 and 4.28 the ambient temperature was 20°C, thus the reference temperature, where the amplifier was balanced, was 20°C. On the day when Thrust Test 2 was performed, the thrust bearing temperature at ambient temperature was 13°C. Thus the amplifier was balanced (set to zero) at 13°C, which was 7 degrees lower than the thermal calibration data. This also implied that an offset of 7°C needed to be applied to the thermal calibration data. It should be noted that no thrust should be exerted on the thrust bearing to determine the thermal output of the strain gauge system. On the day that Thrust Test 2 was performed, there were five occasions where no thrust was exerted on the thrust bearing across a range of thrust bearing temperatures (See Figure 5.1). The first occasion was at ambient temperature (13°C) before the PBMM is started, the second at the first trip of the plant (70 to 81°C), the second plant trip (61 to 80°C), when the Brayton cycle (self-sustaining process) was shut down and the blower was started (70 to 80°C) and lastly at the end when the blower was shut down (30 to 60°C). Thus a new

thermal calibration graph (Figure 5.2) could be compiled that could be applied specifically for the data of Thrust Test 2.

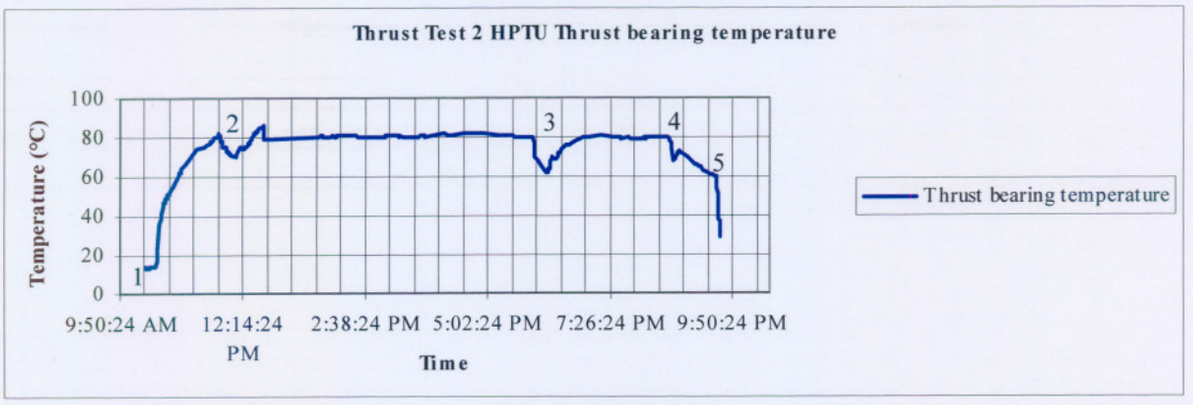


Figure 5.1: Thrust bearing temperature during Thrust Test 2.

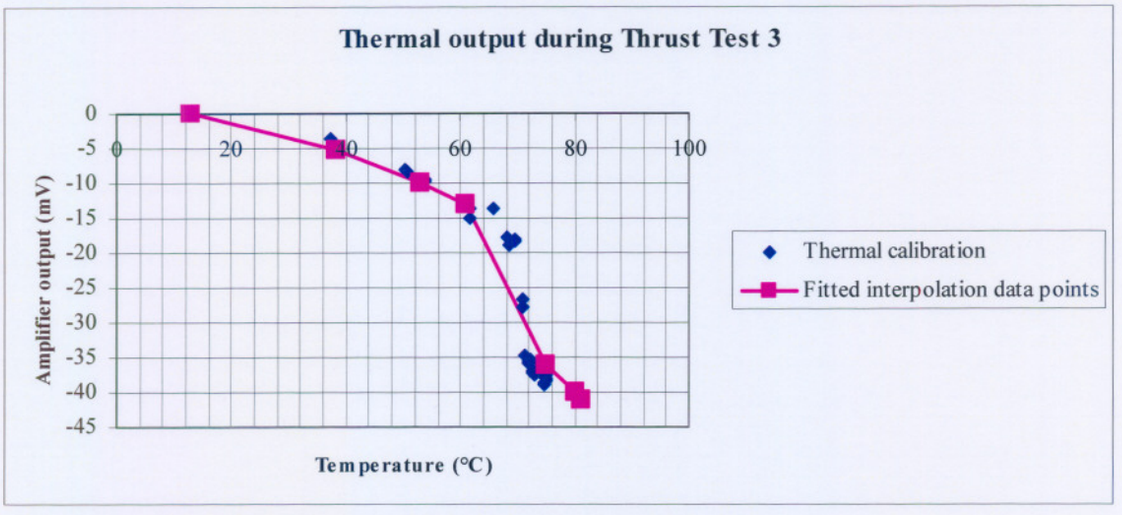


Figure 5.2: Thermal calibration data during Thrust Test 2.

With the thermal calibration data of Figure 5.2, the thermal component and the load component of the total recorded amplifier output could be calculated. Figure 5.3 shows this calculation for the total duration of Thrust Test 2. The millivolt signal needed to be converted to a force value. With the load calibration of Figures 4.30 and 4.31, a maximum and minimum boundary could be determined from the lower- and upper bound curves for both directions. Thus four curves were identified to define the upper and lower boundaries for the two directions namely: "turbine to compressor" and "compressor to turbine". For the direction "turbine to compressor" the upload data from "Test 1" was used as the lower boundary and the download data from "Test 5" as the upper boundary. Similarly for the direction "compressor to turbine", the upload data of "Test 4" was used as the lower boundary and the download data of "Test 5" as the upper boundary. A conversion program was programmed in EES to convert the millivolt signal to a force value. For each data point, a check was done to determine the sign of the thrust force. For a negative value, the two curves for the direction "compressor to turbine" were used and for a positive value, the two curves for the direction "turbine to compressor" were used. Then by interpolation of the appropriate set of

curves applicable to the sign of the signal, the millivolt signal was converted to a force. A minimum- and maximum thrust force curve was generated from this process as shown in Figure 5.4.

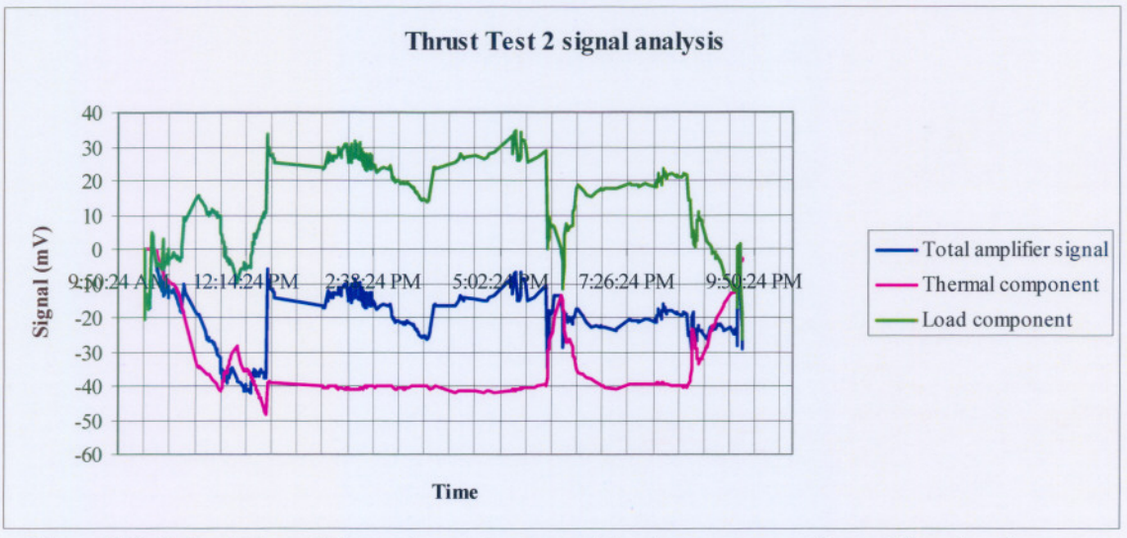


Figure 5.3: Calculation of thermal component and load component of amplifier signal.

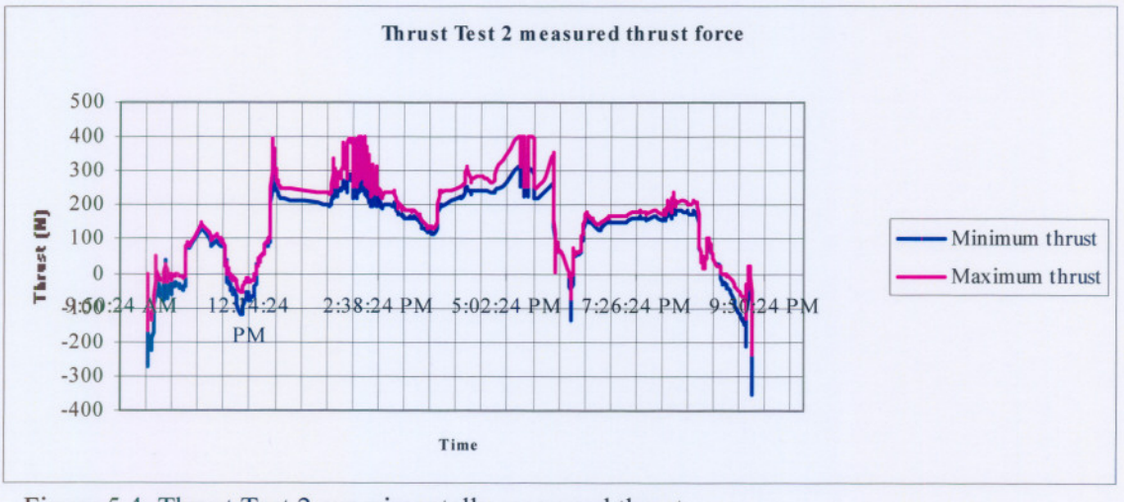


Figure 5.4: Thrust Test 2 experimentally measured thrust.

5.3 Theoretical thrust calculation parameter graphs for Thrust Test 2:

To perform the theoretical thrust calculations, the parameters as stated in Section 4.4.4 were logged. For Thrust Test 2 the graphs of these parameters are illustrated in Figures 5.5 to 5.9. The graphs show all data from the moment that the blower was started to drive the compressors until the end of the test when the cooling cycle was finished and the blower was stopped again.

The numbers one to four (1 to 4) above the graph line corresponds to the temperature and pressure set points of Figure 4.23. Number five (5) corresponds to the time when a steady-state condition was reached in the recuperator at an inlet pressure of 105kPa (gauge) to the LPC and at an inlet temperature of 635°C to the HPT. At the time interval of number six (6), two transient tests were executed by opening the

injection control valve to 15 and 20% respectively. A second steady state condition was reached at number seven (7); this time the LPC inlet pressure was set at 115kPa (gauge).

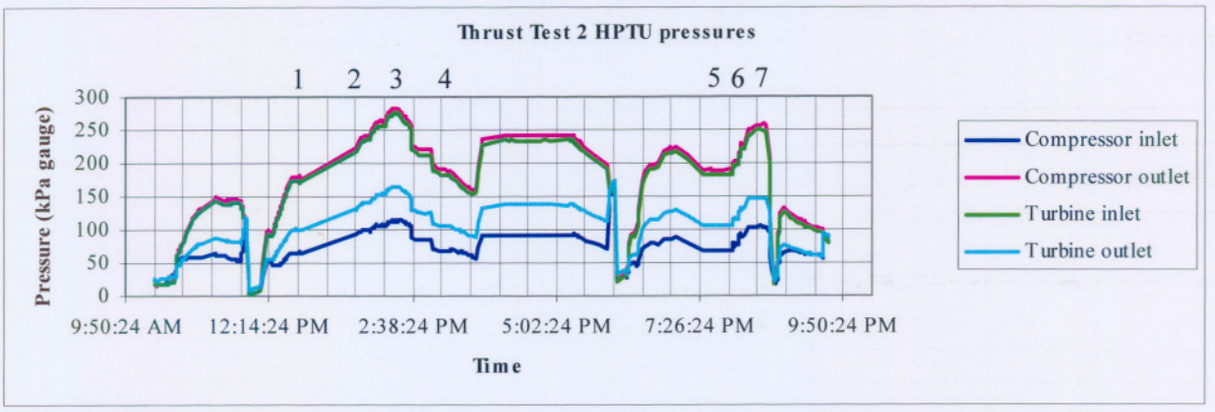


Figure 5.5: Thrust Test 2 HPTU pressures.

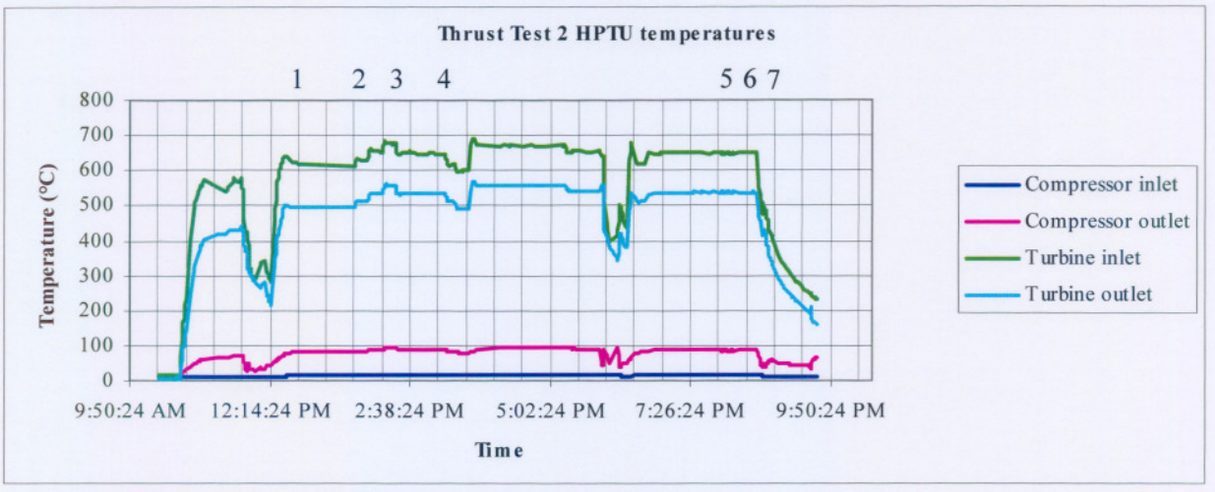


Figure 5.6: Thrust Test 2 HPTU temperatures.

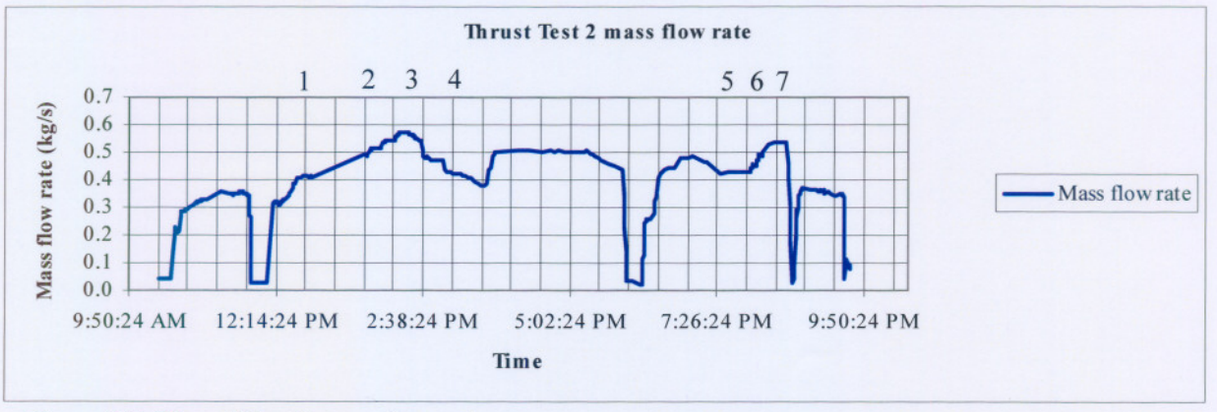


Figure 5.7: Thrust Test 2 mass flow rate.

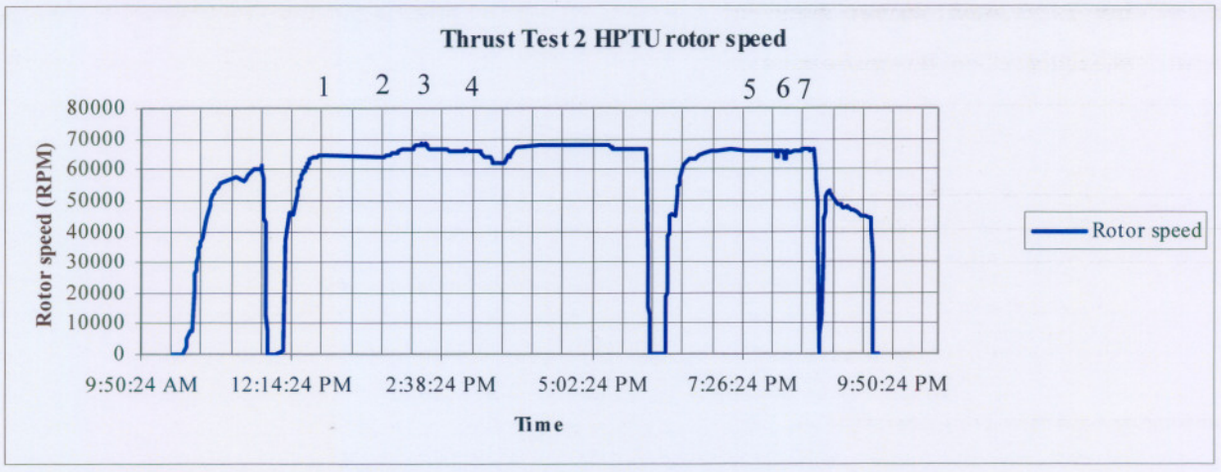


Figure 5.8: Thrust Test 2 HPTU rotor speed.

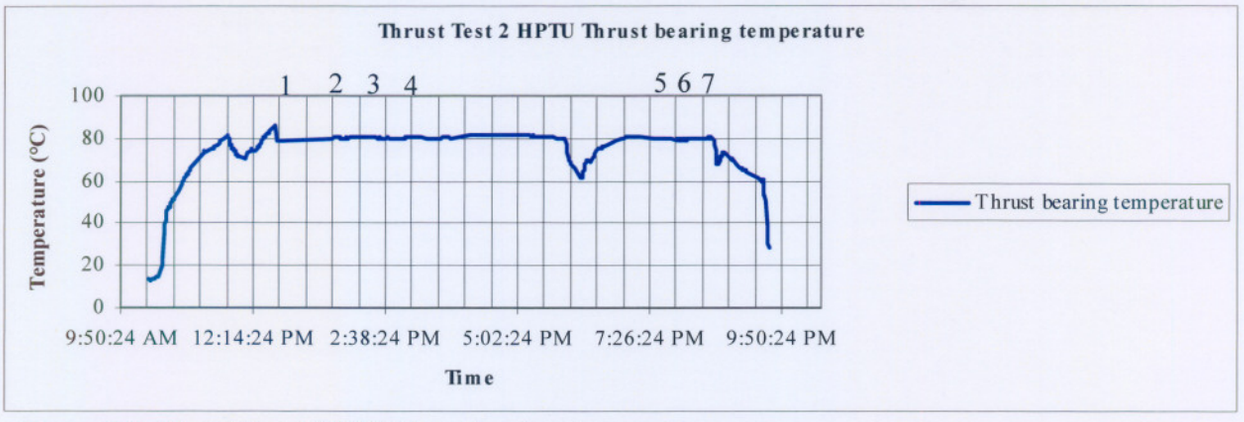


Figure 5.9: Thrust Test 2 HPTU thrust bearing temperature.

The thrust bearing temperature was controlled by an increase or decrease in the HPTU cooling water flow rate. Figure 5.9 shows that the thrust bearing temperature was controlled between 79 and 81°C during the thrust test. The deviations before number one and between number four and five, corresponds to the two plant trips; the heater was tripped resulting in a decrease in heat input to the HPTU center casing but the cooling water still cools the center casing, therefore a decrease in thrust bearing temperature was observed. By controlling the thrust bearing temperature nearly constant at 80°C, the thermal output of the strain gauge bridge was constant. Thus the error due to the thermal output of the strain gauge bridge could be considered as constant.

5.4 Comparison of experimental thrust and thrust calculation methodologies:

Experimental data from the previous section is substituted in all of the thrust calculation methodologies discussed in Chapter 3. In Chapter 3, the five different thrust calculation methodologies gave radical different results and can now be verified against experimentally measured thrust data.

5.4.1 Method 1 by Lobanoff and Ross [19]:

When the applicable parameter data from Figures 5.5 to 5.8 is substituted in the equations of the thrust calculation method of Lobanoff and Ross (Appendix A1), the theoretical thrust calculation illustrated in Figure 5.10 is obtained. The theoretical thrust is compared with the experimentally measured thrust during Thrust Test 2.

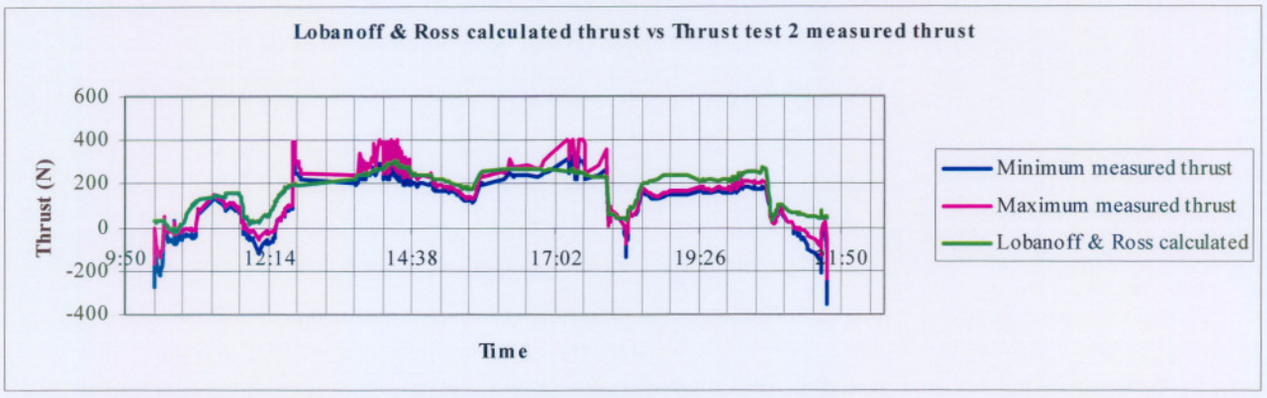


Figure 5.10: Lobanoff & Ross methodology compared with experimentally measured thrust.

Figure 5.10 shows that the thrust calculation method of Lobanoff and Ross gives good correlation with the measured thrust data but tends to over-estimate the measured thrust slightly. In the calculation of $T_{A,c}$ and $T_{A,t}$ the frontal area corresponding to the inlet blade height and outlet blade height respectively, is left out of the equation that results in a reduction of the thrust force. This method of Lobanoff and Ross is a thrust calculation method applied to pumps. In this study, the method of Lobanoff and Ross is applied to a centrifugal compressor and turbine with compressible flow. Thus the method of Lobanoff and Ross can be used to predict the thrust of the HPTU.

5.4.2 Method 2 by Stepanoff [27]:

The thrust parameter data of Thrust Test 2 is also substituted in the equations of the thrust calculation method of Stepanoff (Appendix A2). A graphical comparison between the experimentally measured thrust and the theoretical calculation is given in Figure 5.11.

In Chapter 3 the assumption was made that the specific weight of the fluid for the rear shrouds of the compressor and turbine impellers are calculated with a weighted density. The weighted density is calculated by assuming that the density varies with the square of the radius. Under these two assumptions the "Stepanoff calculated" line in Figure 5.11 is obtained when the thrust calculation parameter data of Thrust Test 2 is substituted in the equations of Appendix A2. The calculated thrust under-estimates the measured thrust enormously and is insensitive to changes in pressure or temperature. The net direction is calculated as "compressor to turbine" but is measured in the direction "turbine to compressor".

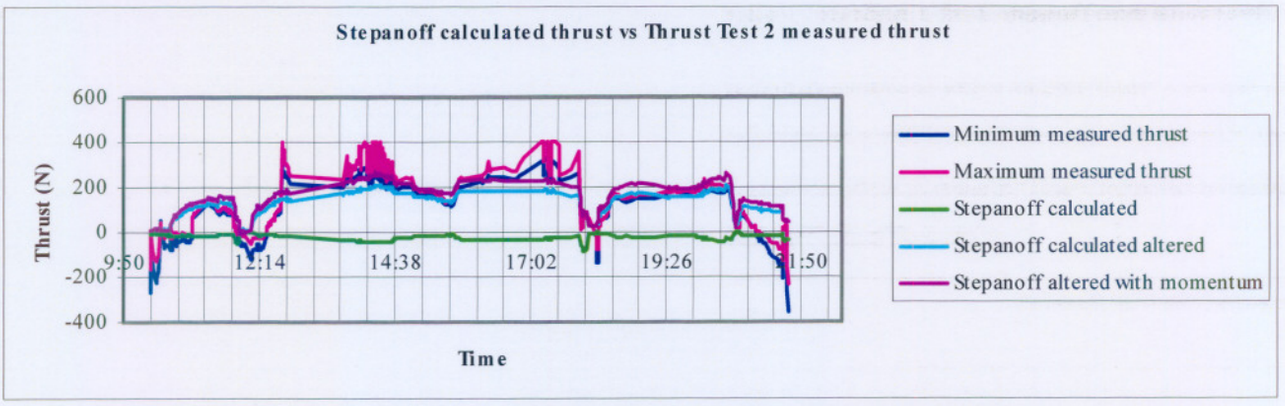


Figure 5.11: Stepanoff methodology compared with experimentally measured thrust.

If the specific weight of the fluid at the outlet of the compressor and at the inlet of the turbine is calculated with the outlet density and inlet density respectively instead of the weighted density, a much better correlation is obtained between the calculated thrust and the measured thrust ("Stepanoff calculated altered" line in Figure 5.11). By making this change of calculating the specific weight with the inlet and outlet density of the compressor and turbine respectively, it can be considered to predict the thrust with the method of Stepanoff by incorporating a factor of safety to the calculated value.

It should be noted that the method of Stepanoff does not take the change of fluid momentum into account under the assumption that the fluid enters an open pump impeller radially. But if momentum is included (Figure 5.12) in the thrust calculation for the HPTU an even better correlation is obtained than in Figure 5.11 (The HPTU compressor and turbine are not entirely open impellers as the definition for a pump).

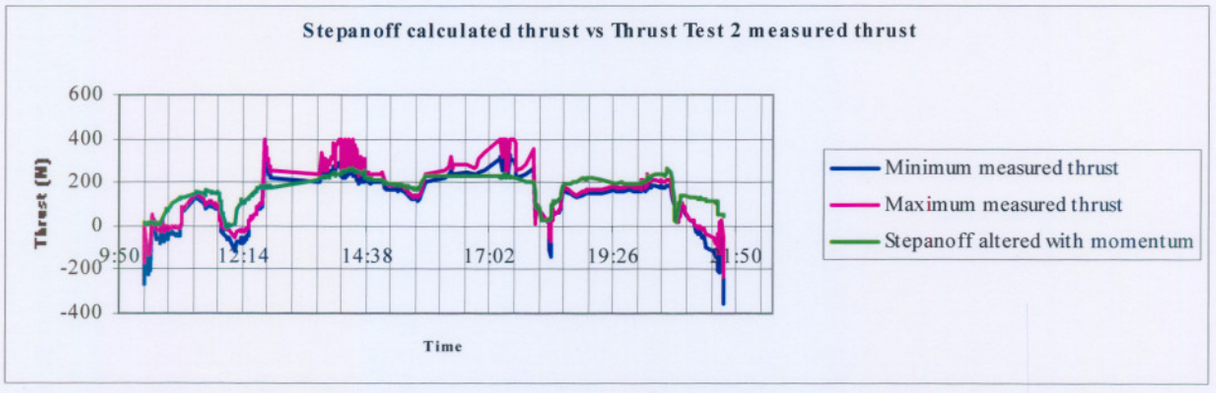


Figure 5.12: Stepanoff methodology with momentum included compared with experimentally measured thrust.

5.4.3 Method 3 by Japikse [17]:

Thrust calculation parameter data of Thrust Test 2 is also substituted in the equations given in Appendix A3 for the thrust calculation method of Japikse. A graphical comparison between the measured thrust and the calculated thrust is illustrated in Figure 5.13. The direction in which the net thrust acts is predicted incorrectly. It is calculated that the thrust acts in the direction "compressor to turbine" but the measured

thrust shows that the thrust force acts in the direction "turbine to compressor". With regard to the magnitude, the measured thrust is over-estimated by the thrust calculation.

The inlet- and outlet cavity speed ratios of both the compressor and turbine are assigned a value of 0.75 because it is cited that 0.75 is a good starting value for the thrust calculation. It is found that the solution of this thrust calculation method is very sensitive to the values assigned to the cavity speed ratios. By setting the compressor front cavity speed ratio to 0.525, the compressor rear cavity speed ratio equal to 0.3, the turbine front cavity speed ratio to 0.75 and the turbine rear cavity speed ratio equal to 0.53, the net thrust direction is predicted as 'turbine to compressor" and the magnitude is in the order of the measured thrust, but still does not correlate well (Figure 5.14). It is also obtained with other combinations of speed cavity ratios that the calculated thrust under-estimates the measured thrust. Thus the cavity speed ratios must be known exactly to use this thrust calculation methodology. The thrust calculation method of Japikse is much more advanced than the method of Stepanoff, but the method of Stepanoff gives reasonable good results. Thus for first order thrust calculations, the use of the method of Japikse is not advised. When designing turbo machines and the cavity speed ratios are determined during the design phase, Japikse's thrust calculation method might deliver better results.

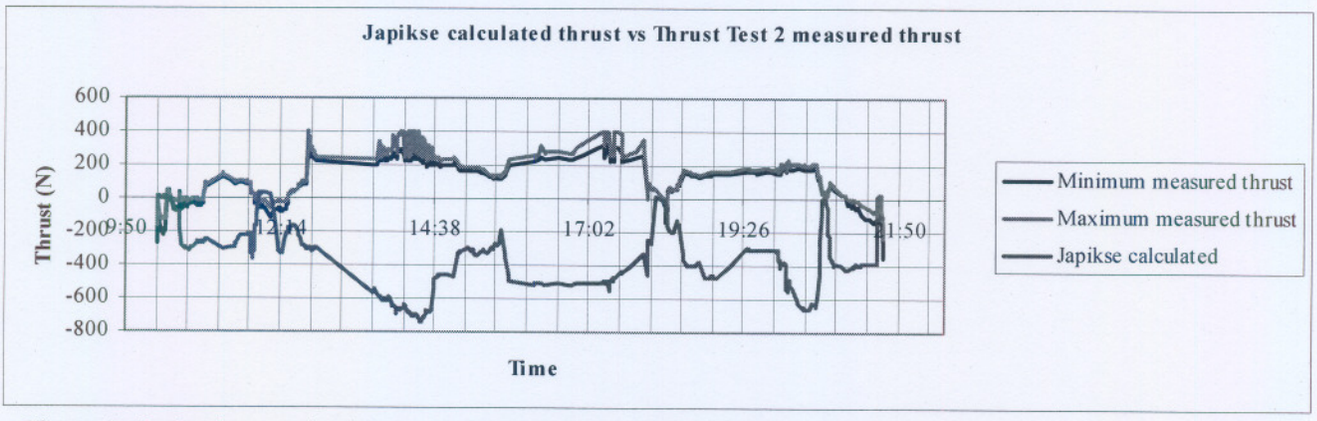


Figure 5.13: Japikse methodology compared with experimentally measured thrust.

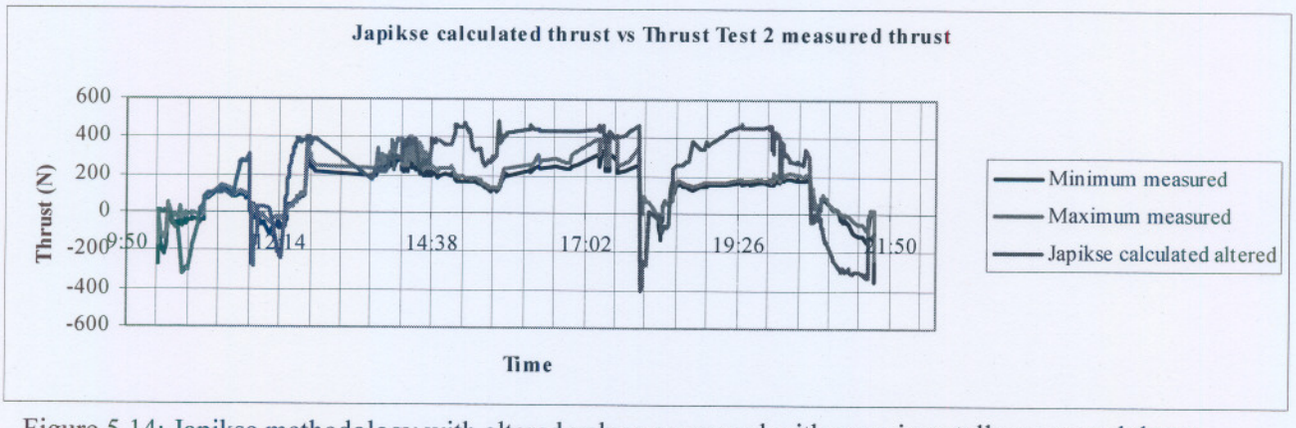


Figure 5.14: Japikse methodology with altered values compared with experimentally measured thrust.

5.4.4 Method 4 by Gülich [11]:

A theoretical thrust calculation is performed by substitution of the thrust calculation parameter data of Thrust Test 2 in the equations of the thrust calculation method of Gülich (Appendix A5). After the thrust due to pressure is calculated with the equations in Appendix A5, the thrust due to a change in the fluid momentum must be added (Refer to Chapter 3). If the fluid momentum is not added in the thrust calculation, the "Gülich without momentum incl." line of Figure 5.15 is obtained. Then if the fluid momentum is added to the thrust calculation, the "Gülich calculated with momentum incl." line in Figure 5.15 is obtained which shows good correlation with the measured thrust.

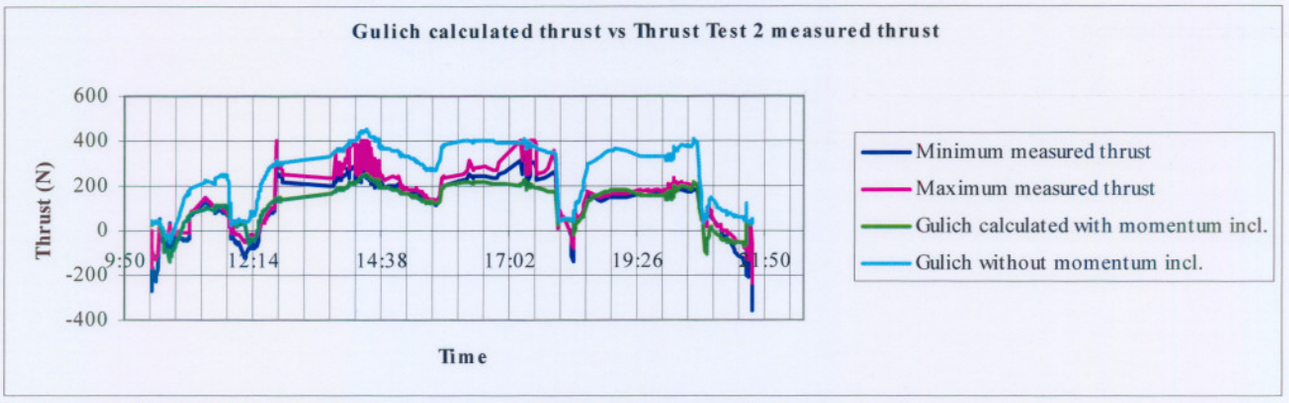


Figure 5.15: Gülich methodology compared with experimentally measured thrust.

Before the thrust calculation can be performed with the thrust calculation method of Gülich, the middle rotation factors must be calculated (Appendix A4). The middle rotation factors are calculated as 0.3606 for the compressor and 0.4377 for the turbine. With these values the thrust is calculated as given in Figure 5.15. If the value of the middle rotation factor for both the turbine and compressor is changed to 0.5, then a good correlation with the measured thrust is still obtained. Thus the thrust calculation method of Gülich is not as sensitive to the middle rotation factor values as Japikse's method. Thus for first order thrust calculations and design purposes, the method of Gülich is well suited.

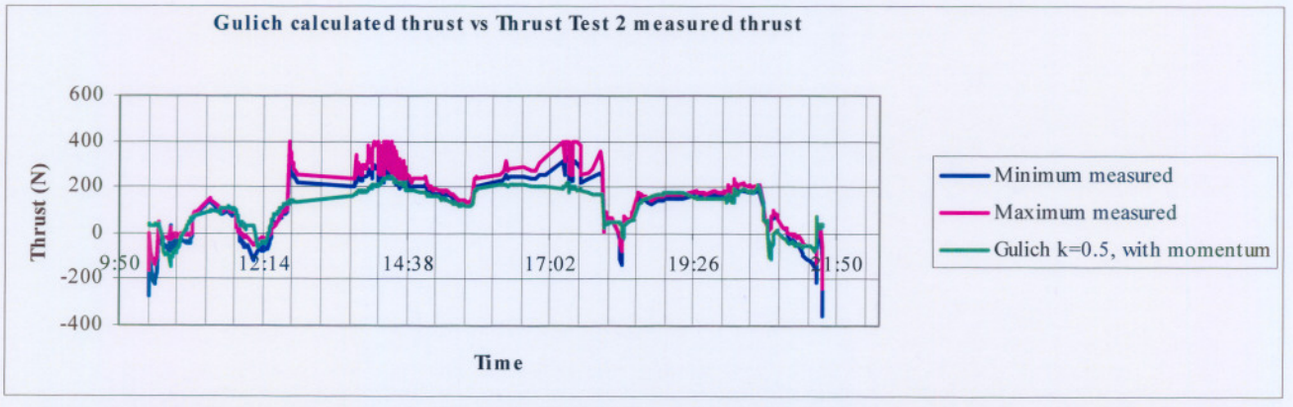


Figure 5.16: Gülich methodology with altered values compared to experimentally measured thrust.

5.4.5 Method 5 by Liebner [18]:

Figure 5.17 shows the comparison between the measured thrust of Thrust Test 2 and the calculated thrust with the method by Liebner. If the thrust due to the pressures acting on the impellers and the thrust due to fluid momentum change is added, a very conservative over-estimated thrust value is obtained with a factor of safety. If the thrust due to fluid momentum is ignored, the measured thrust is over-estimated even further. This thrust calculation method of Liebner tends to be ideal for design purposes as the measured thrust is over-estimated by a factor of 1.6 to 3, which is very conservative. A great advantage of this thrust calculation method is that there are no multiplication factors that can change the solution drastically as with the method of Japikse.

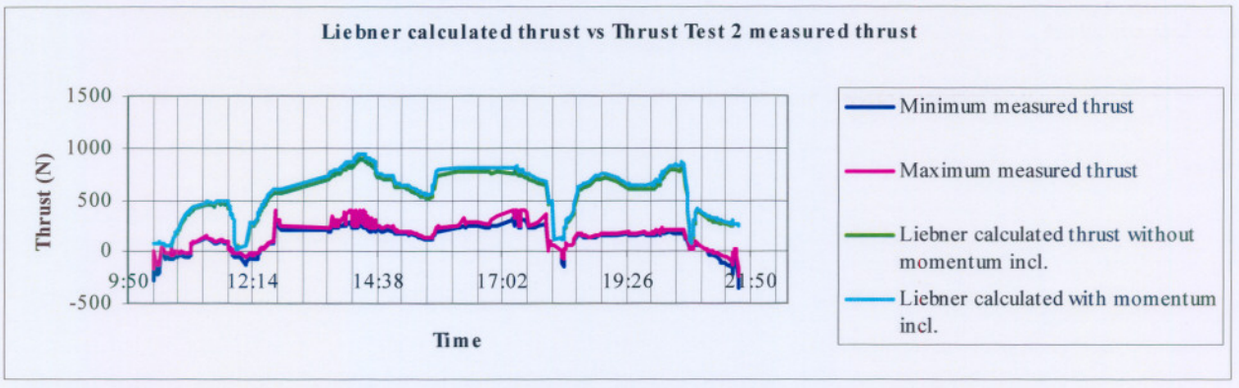


Figure 5.17: Liebner methodology compared with experimentally measured thrust.

5.5 Summary:

The strain gauge thrust measurement system 2 designed in Chapter 4, was used to measure the thrust exerted on the thrust bearing during Thrust Test 2. A millivolt amplifier signal was the measured output of the strain gauge thrust measurement system. This millivolt signal was then divided into a thermal output component that represents an error due to temperature variations and a thrust load component. With the thermal output calibration and load calibration data, the load component of the millivolt amplifier signal was converted to a thrust in Newton that gave an experimentally measured thrust value.

All of the five thrust calculation methodologies that are discussed in Chapter 3 were compared with the experimentally measured thrust data of Thrust Test 2. It was found that the thrust calculation methodologies of Lobanoff & Ross, Stepanoff (if the specific weight is calculated with the compressor outlet density and turbine inlet density) and Gülich give good correlation with the experimental thrust. Japikse's thrust calculation method is sensitive to the values substituted for the cavity speed ratios and therefore gives radical different thrust values for different cavity speed ratios. Liebner's thrust calculation method seems to be a good method when performing design calculations as it over-estimates the measured thrust with a factor varying between 1.6 and 3. Thus for future theoretical thrust calculations pertaining to the HPTU of the PBMM it is suggested that the method of Gülich is used as a first choice, as

it fits the measured data best, or as a second choice, the simpler methods of Lobanoff & Ross and Stepanoff. Figure 5.18 plots the methods of Gülich (one with the middle rotation factors set to 0.3606 for the compressor and 0.4377 for the turbine and the other for both middle rotation factors set to 0.5), Lobanoff & Ross and Stepanoff against each other. It is found that the different middle rotation factor values yield almost the same graph. Stepanoff's thrust calculation methodology under-estimates the thrust when the rotor is stationary but correlates well with the method of Gülich when the rotor is running. The method of Lobanoff & Ross over-estimates the thrust at some stages.

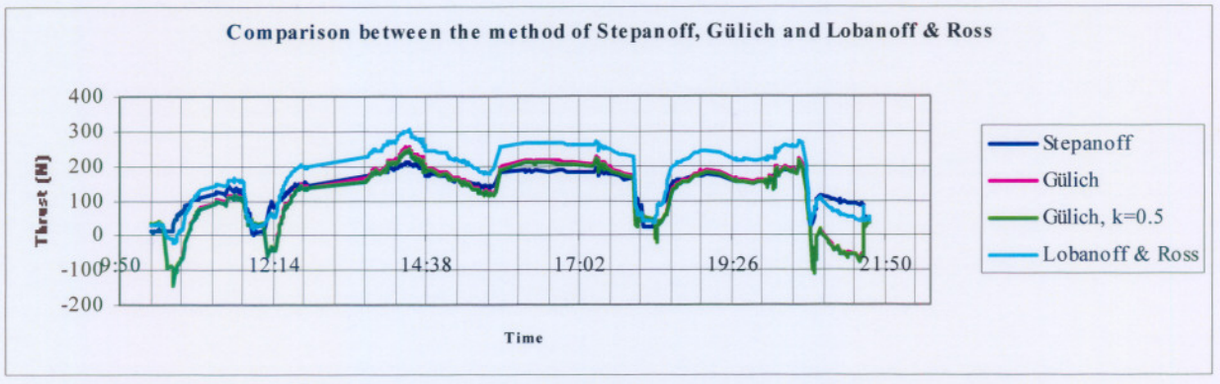


Figure 5.18: Comparison between the methods of Gülich, Stepanoff and Lobanoff & Ross.

Now that the thrust of the HPTU is reasonably known from experimental measurements, the probable cause of the thrust bearing failure, mentioned in the introduction of this dissertation, can be re-evaluated.

In Chapter 1 it was cited that the manufacturer of the HPTU specified that the pressure difference between the compressor outlet and the turbine inlet should not exceed 84.6kPa [23]. This is when the turbocharger is operated in earthmoving equipment. For the HPTU, where the inlet of the compressor and the outlet of the turbine are not at atmospheric conditions, this condition can possibly be evaluated by subtracting the differential pressure across the compressor from the differential pressure across the turbine (Equation 5.1).

$$\Delta P_{HPTU} = (P_{inlet,t} - P_{outlet,t}) - (P_{outlet,c} - P_{inlet,c}) \quad (5.1)$$

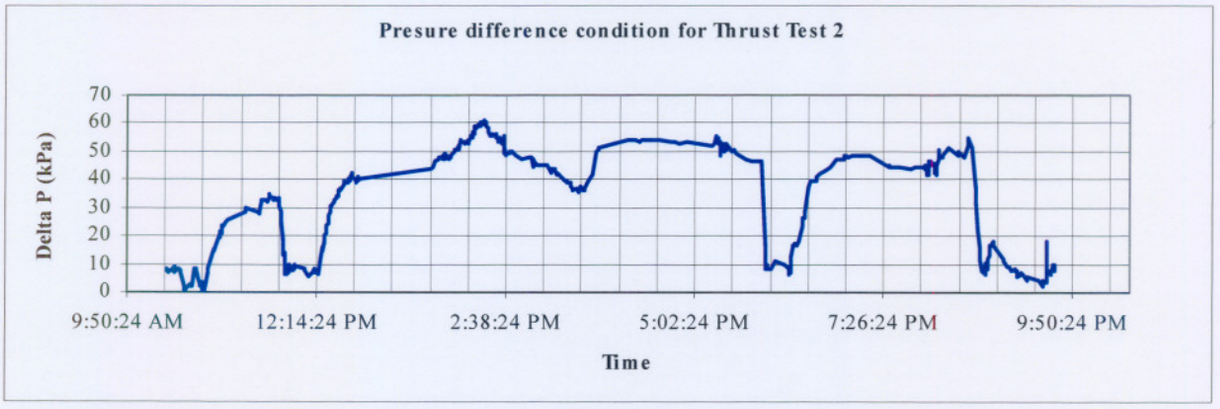


Figure 5.19: Pressure difference condition for HPTU during Thrust Test 2.

Figure 5.19 plots the pressure difference condition for the duration of Thrust Test 2. The highest value reached is 60kPa which is still lower than 84.6kPa. According to the mentioned criterion, the thrust bearing could not have failed due to overloading.

A more scientific approach would be to compare the predicted thrust load of this machine in its design application to the measured thrust load in the PBMM application. The design application is turbo boosting of a diesel engine of earth-moving equipment.

The assumptions made for this thrust prediction are:

- Inlet pressure to the compressor is 86.5kPa (atmospheric), the same as the measured pressure during Thrust Test 2.
- Atmospheric inlet temperature to the compressor is 25°C.
- The exhaust gas temperature at the inlet of the turbine, ranges in the order of 200 to 500°C [26].
- The compression and expansion processes in the compressor and turbine respectively, are isentropic.
- Pressure ratios as given in Table 5.1 are used to calculate the static pressures at the outlet and inlet of the compressor and turbine respectively.
- Shaft speeds listed in Table 5.1 is used in the thrust calculation.
- The inlet pressure to the turbine is 84.6kPa higher than the compressor outlet pressure (turbo manufacturer specifications).

With the assumptions stated above, thrust is calculated for a range of operating parameters, with the method of Gülich. The results are tabulated in Table 5.1.

The maximum measured thrust exerted during Thrust Test 2 was 254.19N. From Table 5.1 it can be seen that the thrust on the HPTU of the PBMM is at least 1.3 to 1.6 times larger than in a turbo diesel engine of earth-moving equipment. This "overload" factor does not seem large enough to contribute the thrust bearing failure of the HPTU solely to overload. It could however be a contributing factor to the failure.

Compressor pressure ratio (static/static)	Turbine pressure ratio (static/static)	Turbine inlet temperature	Shaft rotation speed	Thrust exerted on thrust bearing
1.8	1.5	350˚C	65000RPM	6.971N
2.2	1.5	350˚C	65000RPM	156.7N
2.2	2	350˚C	65000RPM	-69.2N
1.8	2	350˚C	65000RPM	-190.5N
1.8	1.5	500˚C	65000RPM	5.382N
2.2	1.5	500˚C	65000RPM	154.9N
2.2	2	500˚C	65000RPM	-71.01N
1.8	2	500˚C	65000RPM	-192.1N
1.8	1.5	500˚C	55000RPM	10.54N
1.8	1.5	500˚C	70000RPM	2.479N

Table 5.1: Turbo thrust calculated for a turbo diesel engine arrangement.

6. Conclusion & recommendations

6.1 Conclusions:

Five different thrust calculation methodologies are described that are used in centrifugal pump- and centrifugal compressor design. The methods of Lobanoff and Ross, Stepanoff and Gülich are all applied to pumps while the method of Japikse is applied to centrifugal compressors. Liebner gave a method that can be applied in general to any centrifugal turbo machine. Some changes and assumptions had to be made to apply the thrust calculation techniques for pumps (where fluids with constant density are pumped) on a centrifugal compressor and turbine where a compressible fluid (Nitrogen gas) is present. To compare the solution of all the thrust calculation methodologies with each other, a single data point from a previous PBMM test run was substituted in the equations. The solutions varied from 1.7N with the method of Lobanoff and Ross up to 349.1N with the method of Liebner. Due to the large variation in solutions the methods could only be verified against experimentally measured thrust data.

This study entailed the design and implementation of a thrust measurement system that could measure the thrust during the operation of the PBMM. Limited space inside the center casing of the HPTU was the largest constraint on the method to be used for thrust measurement. The thrust bearing temperature variations and presence of lubrication oil placed additional constraints on the design of the thrust measurement system. Metal foil strain gauges were configured in a full Wheatstone bridge with two active strain gauges and two temperature compensating strain gauges for thrust measurement. The strain gauge measurement system was connected as input to an amplifier for signal conditioning, and the amplifier output was connected to a computer with Labview 7.1® for data capturing. Successful thrust measurements on the HPTU were recorded during Thrust Test 2 while the PBMM was operated.

Thrust parameter data of the HPTU like pressures, temperatures, mass flow rate and rotor speed from Thrust Test 2 were substituted in the equations of the five thrust calculation methodologies to obtain the calculated thrust of Thrust Test 2. The measured thrust of thrust Test 2 was compared with each of the five thrust calculation methodologies. It was found that the methods of Lobanoff & Ross, Stepanoff and Gülich correlated best with the measured thrust. Thus it is recommended that these methods are used in future for theoretical thrust calculations on the HPTU. The method of Japikse was sensitive to the cavity speed ratio values and gave radically different solutions for slight changes in the cavity speed ratio values. To use the method of Japikse, the exact values of the cavity speed ratios must be known. Liebner's thrust calculation methodology over-estimated the measured thrust and is therefore ideal for thrust calculations when performing a conservative thrust bearing design.

From the estimation of the thrust in a turbo diesel engine with the method of Gülich it can be concluded that the thrust in the PBMM application is exceeding the thrust exerted in a turbo diesel engine application.

After the thrust bearing failure had occurred, the problem with the aeration of the lubricating oil was solved. Since then, a number of test runs have been conducted on the PBMM, at the conditions of Thrust Test 2 without any thrust bearing failures. Thus it can be concluded that the combination of the aerated oil and larger thrust than the normal application must have caused the thrust bearing failure. Although the pressure difference condition of the manufacturer was met as calculated for the closed cycle of the PBMM, the thrust exerted in the PBMM application is larger than with a turbo diesel engine.

6.2 Recommendations for further work:

The predicted thrust of the HPTU, using the method of Gülich, can be programmed as a virtual channel on the data acquisition system of the PBMM, and related to an estimated allowable thrust capacity of its thrust bearing. This can be extended to the thrust of the other two turbochargers of the PBMM, the Low Pressure Turbo unit (LPTU) and the Electric Load Compressor (ELC). This can be a very useful tool in the Equipment Protection System (EPS) of the PBMM.

It is impractical with the standard centre casing of the HPTU to install a pressure measurement point at the rear of both the compressor and turbine. Such a measurement would facilitate a better estimation of the cavity speed ratios for application of the method of Japikse and the middle rotation factors for the method of Gülich. If a total new centre casing is designed and manufactured to facilitate pressure measurements at the rear and front of both the compressor and turbine, a detailed study can be conducted on the pressure distribution that surrounds the impeller.

Comparison between a CFD model for thrust prediction and the experimental thrust measurements could provide an interesting field of study.

An experimental strain measurement at temperatures above ambient temperature is no trivial task, especially with small strain gauges. It may be much easier to measure strain at elevated temperatures using weldable strain gauges, provided there is enough space. An even more daunting task is to measure strain at elevated temperatures if it is not possible to have two or four active strain gauges that measure strains with opposing signs. The accurate measurement of strain using resistance gauges at elevated temperatures is therefore a topic for further research.

The topic of strain measurement with piezo-electric strain sensors is still relatively novel. No articles on measurement with piezo-electric sensors at elevated temperatures could be found. Several studies have

been conducted in strain gauge measurement with piezo-electric sensors but at ambient temperature. Then also these studies were aimed more at the materials testing of such sensors. Commercialized sensors are available but cover a small range of applications and sizes. Thus the field of strain measurements with piezo-electric sensors is open for further studies.

Appendix A1: Lobanoff & Ross thrust calculation

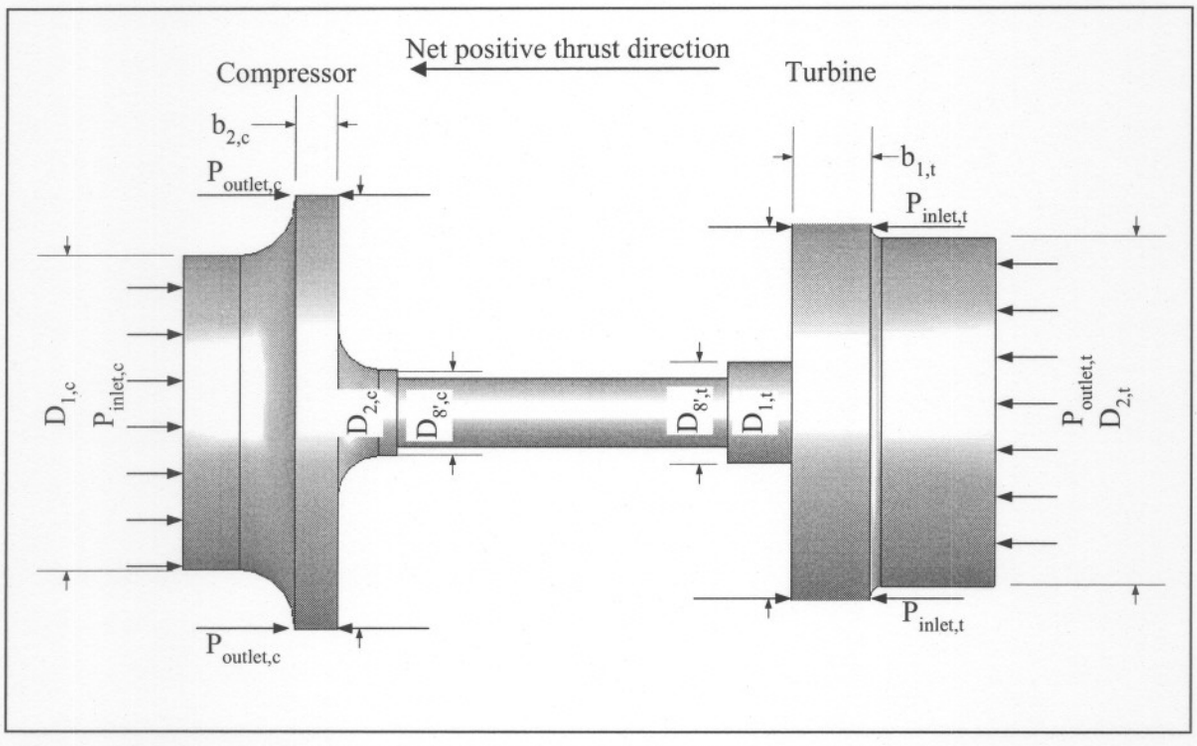


Figure A1.1: Nomenclature applied to complete turbocharger for the thrust calculation by Lobanoff and Ross.

Input parameters :

Fluid parameters :

$\dot{m} = 0.302$: [kg/s] Gas massflow rate through compressor and turbine

Compressor shaft:

$D_{8',c} = 0.0134$: [m] Shaft diameter at the compressor side

Compressor inlet:

$D_{1,c} = 0.0678$: [m] Compressor inlet diameter

$\phi_{1,c} = 0$: [degrees] Inclination angle of meridional streamline to impeller axis at inlet

$P_{inlet,c} = 43060$: [Pa] Compressor inlet pressure

$T_{inlet,c} = 287.15$: [K] Compressor inlet gas temperature

Compressor outlet:

$D_{2,c} = 0.094$: [m] Compressor outlet diameter

$\phi_{2,c} = 90$: [degrees] Inclination angle of meridional streamline to impeller axis at outlet

$b_{2,c} = 0.0065$: [m] Compressor outlet blade height

$P_{outlet,c} = 113834$: [Pa] Compressor outlet pressure

$T_{outlet,c} = 337.849$: [K] Compressor outlet temperature

Turbine shaft:

$D_{8',t} = 0.02$: [m] Shaft diameter on turbine side

Turbine inlet:

$D_{1,t} = 0.082$: [m] Turbine inlet diameter

$\phi_{1,t} = 90$: [degrees] Inclination angle of meridional streamline to impeller axis at inlet

$b_{1,t} = 0.0155$: [m] Turbine inlet blade height

$P_{inlet,t} = 109195$: [Pa] Turbine inlet pressure

$T_{inlet,t} = 792.135$: [K] Turbine inlet temperature

Turbine outlet:

$D_{2,t} = 0.075$: [m] Turbine outlet diameter

$\phi_{2,t} = 0$: [degrees] Inclination angle of meridional streamline to impeller axis at outlet

$P_{outlet,t} = 65645$: [Pa] Turbine outlet pressure

$T_{outlet,t} = 706$: [K] Turbine outlet temperature

Calculations

Compressor shaft

$A_{8',c} = \frac{\pi}{4} \cdot D_{8',c}^2 : [m^2]$ Compressor shaft area

Compressor inlet

$A_{1,c} = \frac{\pi}{4} \cdot D_{1,c}^2 : [m^2]$ Compressor inlet area

$\rho_{1,c} = \rho\left[\text{'Nitrogen'}, T = T_{inlet,c}, P = P_{inlet,c}\right] : [kg/m^3]$ Compressor inlet gas density

Compressor outlet

$A_{2,c} = \frac{\pi}{4} \cdot D_{2,c}^2 : [m^2]$ Compressor rear shroud area

$\rho_{2,c} = \rho\left[\text{'Nitrogen'}, T = T_{outlet,c}, P = P_{outlet,c}\right] : [kg/m^3]$ Compressor outlet gas density

Turbine shaft

$A_{8',t} = \frac{\pi}{4} \cdot D_{8',t}^2 : [m^2]$ Turbine shaft area

Turbine inlet

$A_{1,t} = \frac{\pi}{4} \cdot D_{1,t}^2 : [m^2]$ Turbine rear area

$\rho_{1,t} = \rho\left[\text{'Nitrogen'}, T = T_{3,t}, P = P_{3,t}\right] : [kg/m^3]$ Turbine inlet gas density

Turbine outlet

$A_{2,t} = \frac{\pi}{4} \cdot D_{2,t}^2 : [m^2]$ Turbine outlet area

$\rho_{2,t} = \rho\left[\text{'Nitrogen'}, T = T_{outlet,t}, P = P_{outlet,t}\right] : [kg/m^3]$ Turbine outlet gas density

Compressor thrust calculation

$\Delta P_c = \left[P_{outlet,c} - P_{inlet,c} \right]$: [Pa] Differential pressure across compressor

$C_{1,c} = \dfrac{\dot{m}}{\rho_{1,c} \cdot A_{1,c}}$: [m/s] Compressor inlet absolute velocity

$C_{2,c} = \dfrac{\dot{m}}{\rho_{2,c} \cdot b_{2,c} \cdot 2 \cdot \pi \cdot \dfrac{D_{2,c}}{2}}$: [m/s] Compressor outlet absolute velocity

$F_{momentum,c} = \dot{m} \cdot C_{1,c} \cdot \cos(\Phi_{1,c}) - \dot{m} \cdot C_{2,c} \cdot \cos(\Phi_{2,c})$: [N] Thrust force due to change in fluid momentum

$T_{A,c} = \left(P_{inlet,c} \cdot A_{8',c} \right) + \left[\left(A_{2,c} - A_{1,c} \right) \cdot \dfrac{\Delta P_c}{2} \right] + F_{momentum,c}$: [N] Thrust in direction A for the compressor

$T_{B,c} = \dfrac{3 \cdot \Delta P_c}{4} \cdot \left[A_{2,c} - A_{8',c} \right]$: [N] Thrust in direction B for the compressor

$T_{net,c} = T_{A,c} - T_{B,c}$: [N] Net thrust exerted by the compressor

Turbine thrust calculation

$\Delta P_t = \left[P_{inlet,t} - P_{outlet,t} \right]$: [Pa] Differential pressure across turbine

$C_{1,t} = \dfrac{\dot{m}}{\rho_{1,t} \cdot b_{1,t} \cdot 2 \cdot \pi \cdot \dfrac{D_{1,t}}{2}}$: [m/s] Turbine inlet absolute velocity

$C_{2,t} = \dfrac{\dot{m}}{\rho_{2,t} \cdot A_{2,t}}$: [m/s] Turbine outlet absolute velocity

$F_{momentum,t} = -\dot{m} \cdot C_{1,t} \cdot \cos(\Phi_{1,t}) - \dot{m} \cdot C_{2,t} \cdot \cos(\Phi_{2,t})$: [N] Thrust force due to change in fluid momentum

$T_{A,t} = \left(P_{outlet,t} \cdot A_{8',t} \right) + \left[\left(A_{1,t} - A_{2,t} \right) \cdot \dfrac{\Delta P_t}{2} \right] - F_{momentum,t}$: [N] Thrust in direction A for the turbine

$T_{B,t} = \dfrac{3 \cdot \Delta P_t}{4} \cdot \left[A_{1,t} - A_{8',t} \right]$: [N] Thrust in direction B for the turbine

$T_{net,t} = T_{A,t} - T_{B,t}$: [N] Net thrust exerted by the turbine

Net thrust exerted by compressor and turbine on thrust bearing

$Net_{turbo,thrust} = T_{net,t} - T_{net,c}$: [N]

Compressor	Turbine	
$D_{1,c} = 0.0678$ [m]	$D_{1,t} = 0.082$ [m]	$\dot{m} = 0.302$ [kg/s]
$D_{2,c} = 0.094$ [m]	$D_{2,t} = 0.075$ [m]	$Net_{turbo,thrust} = 130.1$ [N]
$D_{8',c} = 0.0134$ [m]	$D_{8',t} = 0.02$ [m]	
$b_{2,c} = 0.0065$ [m]	$b_{1,t} = 0.0155$ [m]	
$\Phi_{1,c} = 0$ [degrees]	$\Phi_{1,t} = 90$ [degrees]	
$\Phi_{2,c} = 90$ [degrees]	$\Phi_{2,t} = 0$ [degrees]	
$P_{inlet,c} = 43060$ [Pa]	$P_{inlet,t} = 109195$ [Pa]	
$P_{outlet,c} = 113834$ [Pa]	$P_{outlet,t} = 65645$ [Pa]	
$T_{inlet,c} = 287.2$ [K]	$T_{inlet,t} = 792.1$ [K]	
$T_{outlet,c} = 337.8$ [K]	$T_{outlet,t} = 706$ [K]	
$A_{1,c} = 0.00361$ [m^2]	$A_{1,t} = 0.005281$ [m^2]	
$A_{2,c} = 0.00694$ [m^2]	$A_{2,t} = 0.004418$ [m^2]	
$A_{8',c} = 0.000141$ [m^2]	$A_{8',t} = 0.0003142$ [m^2]	
$\Delta P_c = 70774$ [Pa]	$\Delta P_t = 43550$ [Pa]	
$\rho_{1,c} = 0.5053$ [kg/m^3]	$\rho_{1,t} = 0.4643$ [kg/m^3]	
$\rho_{2,c} = 1.135$ [kg/m^3]	$\rho_{2,t} = 0.3132$ [kg/m^3]	
$C_{1,c} = 165.5$ [m/s]	$C_{1,t} = 162.9$ [m/s]	
$C_{2,c} = 138.6$ [m/s]	$C_{2,t} = 218.3$ [m/s]	
$F_{momentum,c} = 49.99$ [N]	$F_{momentum,t} = -65.91$ [N]	
$T_{A,c} = 173.9$ [N]	$T_{A,t} = 105.3$ [N]	
$T_{B,c} = 360.9$ [N]	$T_{B,t} = 162.2$ [N]	
$T_{net,c} = -187$ [N]	$T_{net,t} = -56.9$ [N]	

Table A1.1: Lobaoff & Ross thrust calculation solution.

$$Net_{turbo,thrust} = \left[\left(P_{outlet,t} \cdot A_{8',t}\right) + \left[\left(A_{1,t} - A_{2,t}\right) \cdot \frac{\Delta P_t}{2}\right] - F_{momentum,t}\right] - \left[\frac{3 \cdot \Delta P_t}{4} \cdot \left(A_{1,t} - A_{8',t}\right)\right]$$

$$- \left[\left(P_{inlet,c} \cdot A_{8',c}\right) + \left[\left(A_{2,c} - A_{1,c}\right) \cdot \frac{\Delta P_c}{2}\right] + F_{momentum,c}\right] + \left[\frac{3 \cdot \Delta P_c}{4} \cdot \left(A_{2,c} - A_{8',c}\right)\right]$$

$$= \left[\left(65645 \cdot 0.0003142\right) + \left[\left(0.005281 - 0.004418\right) \cdot \frac{43550}{2}\right] - (-)65.91\right] - \left[\frac{3 \cdot 43550}{4} \cdot \left(0.005281 - 0.0003142\right)\right]$$

$$- \left[\left(43060 \cdot 0.000141\right) + \left[\left(0.00694 - 0.00361\right) \cdot \frac{70774}{2}\right] + 49.99\right] + \left[\frac{3 \cdot 70774}{4} \cdot \left(0.00694 - 0.000141\right)\right]$$

$$= \left[20.625 + 18.791 + 65.91\right] - \left[162.228\right] - \left[6.071 + 117.839 + 49.99\right] + \left[360.894\right]$$

$$= 130.1\text{N}$$

Appendix A2: Stepanoff thrust calculation

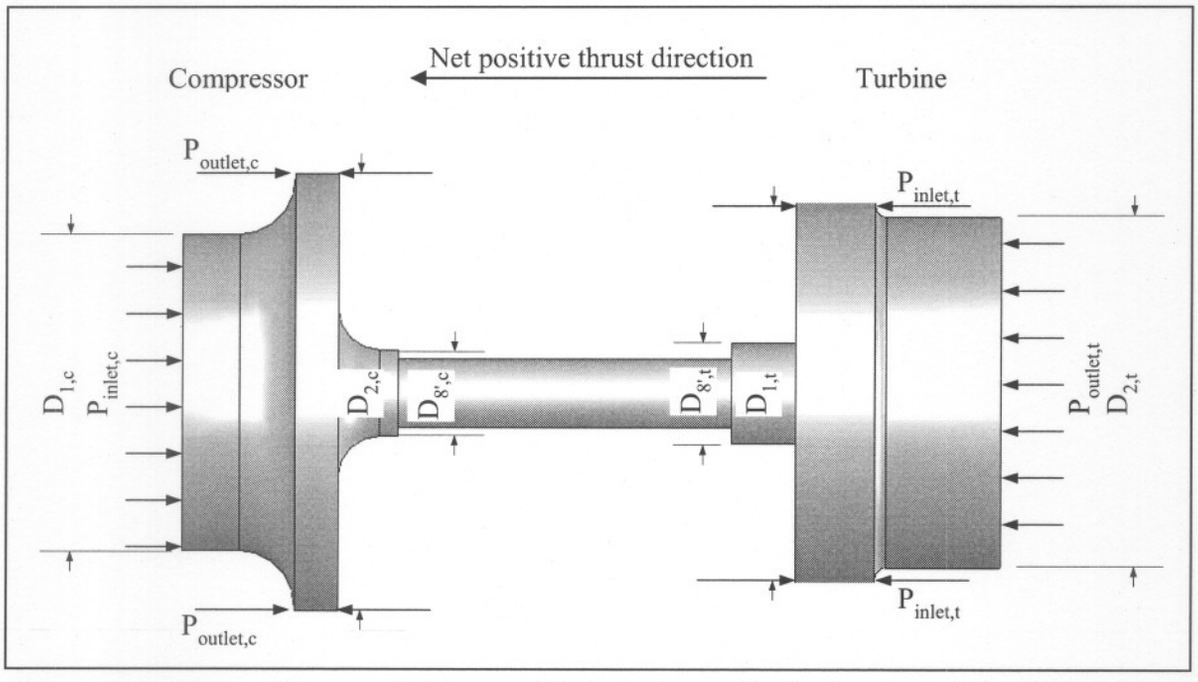


Figure A2.1: Nomenclature applied to complete turbocharger for the thrust calculation by Stepanoff.

Input parameters :

Compressor shaft :

$D_{8',c} = 0.0134$: [m] Shaft diameter at the compressor side

Compressor inlet:

$D_{1,c} = 0.0678$: [m] Compressor inlet diameter

$P_{inlet,c} = 43060$: [Pa] Compressor inlet pressure

$T_{inlet,c} = 287.15$: [K] Compressor inlet gas temperature

Compressor outlet:

$D_{2,c} = 0.094$: [m] Compressor outlet diameter

$P_{exit,c} = 113834$: [Pa] Compressor outlet pressure

$T_{exit,c} = 337.849$: [K] Compressor outlet temperature

Turbine shaft:

$D_{8',t} = 0.02$:[m] Shaft diameter on turbine side

Turbine inlet:

$D_{1,t} = 0.082$: [m] Turbine inlet diameter

$P_{inlet,t} = 109195$: [Pa] Turbine inlet pressure

$T_{inlet,t} = 792.135$: [K] Turbine inlet temperature

Turbine outlet:

$D_{2,t} = 0.075$: [m] Turbine outlet diameter

$P_{outlet,t} = 65645$: [Pa] Turbine outlet pressure

$T_{outlet,t} = 706$: [K] Turbine outlet temperature

Other :

$N = 56122.6$: [rpm] Rotational speed of rotor

$g = 9.81$: [m/s^2] Gravitational acceleration

Calculations

$$\omega = \frac{2 \cdot \pi \cdot N}{60} : [rad/s]$$ Rotational speed of rotor converted to radians/second

Compressor :

$$A_{8',c} = \frac{\pi \cdot D_{8',c}^2}{4} : [m^2]$$ Compressor side shaft area

$$A_{1,c} = \frac{\pi \cdot D_{1,c}^2}{4} : [m^2]$$ Compressor inlet area

$$A_{2,c} = \frac{\pi \cdot D_{2,c}^2}{4} : [m^2]$$ Compressor rear shroud area

$$r_{2,t,c} = \frac{D_{2,c}}{2} : [m]$$ Compressor outlet radius

$$r_{8',c} = \frac{D_{8',c}}{2} : [m]$$ Compressor shaft radius

$u_{2,c} = \omega \cdot r_{2,c} : [m/s]$ Compressor outlet peripheral velocity

$u_{8',c} = \omega \cdot r_{8',c} : [m/s]$ Compressor shaft peripheral velocity

$\rho_{1,c} = \rho\left['Nitrogen', T = T_{inlet,c}, P = P_{inlet,c}\right] : [kg/m^3]$ Compressor inlet gas density

$\rho_{2,c} = \rho\left['Nitrogen', T = T_{outlet,c}, P = P_{outlet,c}\right] : [kg/m^3]$ Compressor outlet gas density

$$\rho_{avg,c} = \frac{\left(\rho_{1,c} + \rho_{2,c}\right)}{2} : [kg/m^3]$$ Average compressor density

$$\rho_{weighted,c} = \frac{\rho_{2,c}\left[\left(\frac{D_{8',c}}{D_{2,c}}\right)^2 + 1\right]}{2} : [kg/m^3]$$ Weighted average density on rear shroud of compressor

$$Hv_c = \frac{P_{outlet,c}}{\rho_{2,c} \cdot g} : [m]$$ Compressor outlet pressure height

$\gamma_{front,c} = \rho_{avg,c} \cdot g : [kg/m^2s^2]$ Specific weight of fluid at the inlet of the compressor

$\gamma_{rear,c} = \rho_{weighted,c} \cdot g : [kg/m^2s^2]$ Specific weight of fluid at the outlet of the compressor

Turbine :

$$A_{8',t} = \frac{\pi \cdot D_{8',t}^2}{4} : [m^2]$$ Turbine side shaft area

$$A_{1,t} = \frac{\pi \cdot D_{1,t}^2}{4} : [m^2]$$ Turbine inlet area

$$A_{2,t} = \frac{\pi \cdot D_{2,t}^2}{4} : [m^2]$$ Turbine rear shroud area

$r_{1,t} = \frac{D_{1,t}}{2}$: [m] Turbine outlet radius

$r_{8',t} = \frac{D_{8',t}}{2}$: [m] Turbine shaft radius

$u_{1,t} = \omega \cdot r_{1,t}$: [m/s] Turbine inlet peripheral velocity

$u_{8',t} = \omega \cdot r_{8',t}$: [m/s] Turbine shaft peripheral velocity

$\rho_{1,t} = \rho\left['Nitrogen', T = T_{inlet,t}, P = P_{inlet,t}\right]$: [kg/m^3] Turbine inlet gas density

$\rho_{2,t} = \rho\left['Nitrogen', T = T_{outlet,t}, P = P_{outlet,t}\right]$: [kg/m^3] Turbine outlet gas density

$\rho_{avg,t} = \frac{\left(\rho_{1,t} + \rho_{2,t}\right)}{2}$: [kg/m^3] Average turbine density

$\rho_{weighted,t} = \frac{\rho_{1,t}\left[\left(\frac{D_{8',t}}{D_{1,t}}\right)^2 + 1\right]}{2}$: [kg/m^3] Weighted average density at the rear of turbine

$Hv_t = \frac{P_{inlet,t}}{\rho_{inlet,t} \cdot g}$: [m] Turbine inlet pressure height

$\gamma_{front,t} = \rho_{avg,t} \cdot g$: [kg/m^{2}s^2] Specific weight of fluid at the inlet of the turbine

$\gamma_{rear,t} = \rho_{weighted,t} \cdot g$: [kg/m^{2}s^2] Specific weight of fluid at the outlet of the turbine

Compressor thrust calculation :

$T_{B,c} = \left[\left(A_{2,c} - A_{8',c}\right) \cdot \left(Hv_c - \frac{1}{8} \cdot \left[\frac{u_{2,c}^2 - u_{8',c}^2}{2 \cdot g}\right]\right)\right] \cdot \gamma_{rear,c}$: [N] Thrust on back shroud of compressor

$T_{A,c} = \left[A_{2,c} - A_{1,c}\right] \cdot \frac{Hv_c}{2} \cdot \gamma_{front,c}$: [N] Thrust on eye side of the compressor

$T_{net,c} = T_{A,c} - T_{B,c}$: [N] Net thrust on compressor

Turbine thrust calculation :

$T_{B,t} = \left[\left(A_{1,t} - A_{8',t}\right) \cdot \left(Hv_t - \frac{1}{8} \cdot \left[\frac{u_{1,t}^2 - u_{8',t}^2}{2 \cdot g}\right]\right)\right] \cdot \gamma_{rear,t}$: [N] Thrust at back of turbine

$T_{A,t} = \left[A_{1,t} - A_{2,t}\right] \cdot \frac{Hv_t}{2} \cdot \gamma_{front,t}$: [N] Thrust on inside of the turbine

$T_{net,t} = T_{A,t} - T_{B,t}$: [N] Net thrust on turbine

Net thrust exerted on thrust bearing :

$Net_{turbo,thrust} = T_{net,t} - T_{net,c}$: [N]

Compressor	Turbine	
$D_{1,c} = 0.0678$ [m]	$D_{1,t} = 0.082$ [m]	$g = 9.81$ [m/s^2]
$D_{2,c} = 0.094$ [m]	$D_{2,t} = 0.075$ [m]	$N = 56123$ [rpm]
$D_{8',c} = 0.0134$ [m]	$D_{8',t} = 0.02$ [m]	$\omega = 5877$ [rad/s]
$r_{2,c} = 0.047$ [m]	$r_{1,t} = 0.041$ [m]	$Net_{turbo,thrust} = -4.176$ [N]
$r_{8',c} = 0.0067$ [m]	$r_{8',t} = 0.01$ [m]	
$A_{1,c} = 0.00361$ [m^2]	$A_{1,t} = 0.005281$ [m^2]	
$A_{2,c} = 0.00694$ [m^2]	$A_{2,t} = 0.004418$ [m^2]	
$A_{8',c} = 0.000141$ [m^2]	$A_{8',t} = 0.0003142$ [m^2]	
$P_{inlet,c} = 43060$ [Pa]	$P_{inlet,t} = 109195$ [Pa]	
$P_{outlet,c} = 113834$ [Pa]	$P_{outlet,t} = 65645$ [Pa]	
$T_{inlet,c} = 287.2$ [K]	$T_{inlet,t} = 792.1$ [K]	
$T_{outlet,c} = 337.8$ [K]	$T_{outlet,t} = 706$ [K]	
$\rho_{1,c} = 0.5053$ [kg/m^3]	$\rho_{1,t} = 0.4643$ [kg/m^3]	
$\rho_{2,c} = 1.135$ [kg/m^3]	$\rho_{2,t} = 0.3132$ [kg/m^3]	
$\rho_{avg,c} = 0.8202$ [kg/m^3]	$\rho_{avg,t} = 0.3887$ [kg/m^3]	
$\rho_{weighted,c} = 0.5791$ [kg/m^3]	$\rho_{weighted,t} = 0.2459$ [kg/m^3]	
$u_{2,c} = 276.2$ [m/s]	$u_{1,t} = 241$ [m/s]	
$u_{8',c} = 39.38$ [m/s]	$u_{8',t} = 58.77$ [m/s]	
$\gamma_{front,c} = 8.047$ [kg/m^{2}s^2]	$\gamma_{front,t} = 3.813$ [kg/m^{2}s^2]	
$\gamma_{rear,c} = 5.681$ [kg/m^{2}s^2]	$\gamma_{rear,t} = 2.413$ [kg/m^{2}s^2]	
$Hv_c = 10222$ [m]	$Hv_t = 23976$ [m]	
$T_{A,c} = 136.9$ [N]	$T_{A,t} = 39.46$ [N]	
$T_{B,c} = 376.4$ [N]	$T_{B,t} = 283.1$ [N]	
$T_{net,c} = -239.5$ [N]	$T_{net,t} = -243.7$ [N]	

Table A2.1: Stepanoff thrust calculation solution.

$$Net_{turbo,thrust} = \left[\left(A_{1,t} - A_{2,t}\right)\cdot\frac{Hv_t}{2}\cdot\gamma_{front,t}\right] - \left[\left(A_{1,t} - A_{8',t}\right)\cdot\left(Hv_t - \frac{1}{8}\cdot\left[\frac{u_{1,t}^2 - u_{8',t}^2}{2\cdot g}\right]\right)\right]\cdot\gamma_{rear,t}$$

$$-\left[\left(A_{2,c} - A_{1,c}\right)\cdot\frac{Hv_c}{2}\cdot\gamma_{front,c}\right] + \left[\left(A_{2,c} - A_{8',c}\right)\cdot\left(Hv_c - \frac{1}{8}\cdot\left[\frac{u_{2,c}^2 - u_{8',c}^2}{2\cdot g}\right]\right)\right]\cdot\gamma_{rear,c}$$

$$= \left[(0.005281 - 0.004418)\cdot\frac{23976}{2}\cdot 3.813\right] - \left[(0.005281 - 0.0003142)\cdot\left(23976 - \frac{1}{8}\cdot\left[\frac{241^2 - 58.77^2}{2\times 9.81}\right]\right)\cdot 2.413\right]$$

$$-\left[(0.00694 - 0.00361)\cdot\frac{10222}{2}\cdot 8.047\right] + \left[(0.00694 - 0.000141)\cdot\left(10222 - \frac{1}{8}\cdot\left[\frac{276.2^2 - 39.38^2}{2\times 9.81}\right]\right)\cdot 5.681\right]$$

$$= -4.176\text{N}$$

Appendix A3: Japikse thrust calculation

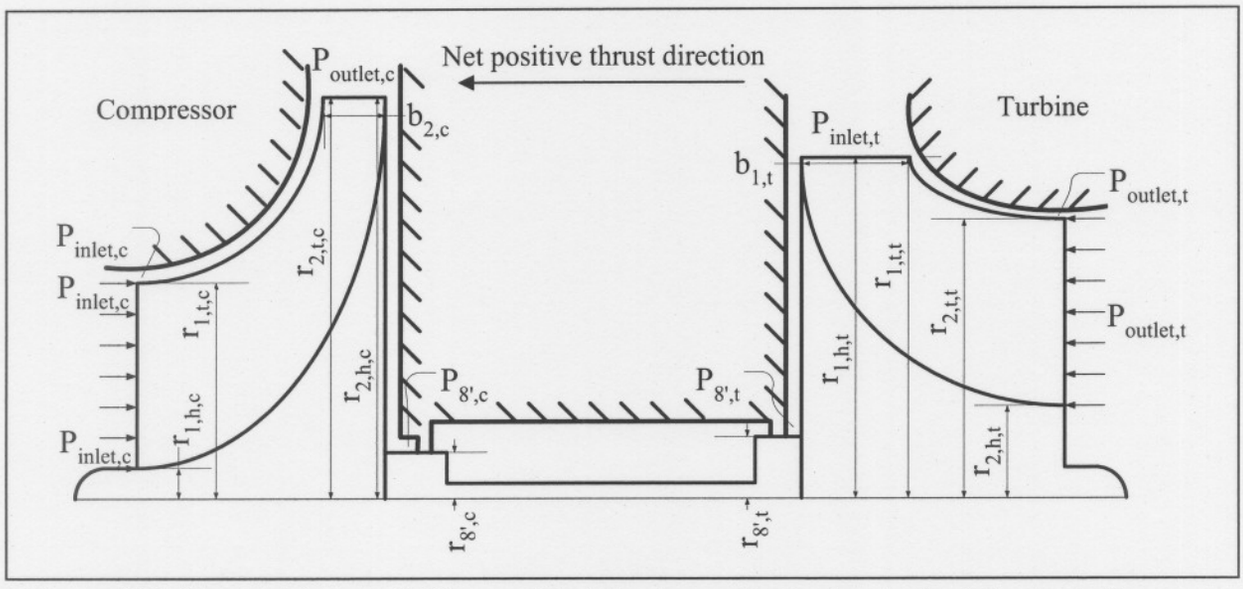


Figure A3.1: Nomenclature applied to complete turbocharger for the thrust calculation by Japikse

Input parameters :

Compressor inlet :

$r_{1,h,c} = 0.007$:[m] Compressor inlet hub radius

$r_{1,t,c} = 0.0339$:[m] Compressor inlet tip radius

$\Phi_{1,c} = 0$:[degrees] Inclination angle of meridional streamline to impeller axis at inlet

$P_{inlet,c} = 43060$:[Pa] Compressor inlet hub pressure

$T_{inlet,c} = 287.15$:[K] Compressor inlet gas temperature

Compressor outlet :

$r_{2,h,c} = 0.047$:[m] Compressor outlet hub radius

$r_{2,t,c} = 0.047$:[m] Compressor outlet tip radius

$b_{2,c} = 0.0065$:[m] Compressor outlet blade height

$\Phi_{2,c} = 90$:[degrees] Inclination angle of meridional streamline to impeller axis at outlet

$P_{outlet,c} = 113834$:[Pa] Compressor outlet pressure

$T_{outlet,c} = 337.849$:[K] Compressor outlet temperature

Compressor shaft :

$r_{8',c} = 0.0067$:[m] Shaft radius at the compressor side

$P_{8',c} = P_{outlet,c}\left[\left(\frac{r_{8',c}}{r_{2,h,c}}\right)^2\right]$:[Pa] Compressor shaft seal pressure

Compressor thrust parameters :

$F_{f,c} = 0.75$:[dimensionless] Compressor front cavity speed ratio

$F_{r,c} = 0.75$:[dimensionless] Compressor rear cavity speed ratio

Turbine inlet :

$r_{1,h,t} = 0.041$:[m] Turbine inlet hub radius

$r_{1,t,t} = 0.041$:[m] Turbine inlet tip radius

$\Phi_{1,t} = 90$:[degrees] Inclination angle of meridional streamline to impeller axis at inlet

$b_{1,t} = 0.0155$:[m] Turbine inlet blade height

$P_{inlet,t} = 109195$:[Pa] Turbine inlet hub pressure

$T_{inlet,t} = 792.135$:[K] Turbine inlet temperature

Turbine outlet :

$r_{2,h,t} = 0.0122$:[m] Turbine outlet hub radius

$r_{2,t,t} = 0.03755$:[m] Turbine outlet tip radius

$\Phi_{2,t} = 0$:[degrees] Inclination angle of meridional streamline to impeller axis at outlet

$P_{outlet,t} = 65645$:[Pa] Turbine outlet pressure

$T_{outlet,t} = 706$: [K] Turbine outlet temperature

Turbine shaft :

$r_{8',t} = 0.01$:[m] Shaft radius on turbine side

$$P_{8,acsent,t} = P_{inlet,t}\left[\left(\frac{r_{8',t}}{r_{1,h,t}}\right)^2\right] : [Pa] \text{ Turbine shaft seal pressure}$$

Turbine thrust parameters :

$F_{f,t} = 0.75$:[dimensionless] Turbine front cavity speed ratio

$F_{r,t} = 0.75$:[dimensionless] Turbine rear cavity speed ratio

Other :

$N = 935.37$: [rev/s] Rotational speed of rotor

$\dot{m} = 0.302$: [kg/s] Massflow rate

Calculations

Compressor fluid density calculation

$\rho_{1,c} = \rho\left('Nitrogen', P = P_{inlet,c}, T = T_{inlet,c}\right) : [kg/m^3]$ Compressor inlet gas density

$\rho_{2,c} = \rho\left('Nitrogen', P = P_{outlet,c}, T = T_{outlet,c}\right) : [kg/m^3]$ Compressor outlet gas density

$\rho_{avg,c} = \left(\frac{\rho_{1,c} + \rho_{2,c}}{2}\right) : [kg/m^3]$ Average compressor density

$\rho_{weighted,c} = \frac{\rho_{2,c}\left[\left(\frac{r_{8',c}}{r_{2,h,c}}\right)^2 + 1\right]}{2} : [kg/m^3]$ Weighted average density on rear shroud of compressor

Compressor velocity calculations

$\omega = 2 \cdot \pi \cdot N : [rad/s]$ Rotor speed converted to rad/s

$A_{1,c} = \pi \cdot \left(r_{1,t,c}^2 - r_{1,h,c}^2\right) : [m^2]$ Compressor inlet area

$C_{1,c} = \frac{\dot{m}}{\rho_{1,c} \cdot A_{1,c}} : [m/s]$ Compressor inlet absolute velocity

$U_{1,c} = \omega \cdot r_{1,t,c} : [m/s]$ Compressor inlet peripheral velocity

$U_{8',c} = \omega \cdot r_{8',c} : [m/s]$ Compressor shaft peripheral velocity

$C_{2,c} = \frac{\dot{m}}{\rho_{2,c} \cdot b_{2,c} \cdot 2 \cdot \pi \cdot r_{2,h,c}} : [m/s]$ Compressor outlet absolute velocity

Turbine fluid density calculation

$\rho_{1,t} = \rho\left('Nitrogen', P = P_{inlet,t}, T = T_{inlet,t}\right) : [kg/m^3]$ Turbine inlet gas density

$\rho_{2,t} = \rho\left('Nitrogen', P = P_{outlet,t}, T = T_{outlet,t}\right) : [kg/m^3]$ Turbine outlet gas density

$\rho_{avg,t} = \left(\frac{\rho_{1,t} + \rho_{2,t}}{2}\right) : [kg/m^3]$ Average turbine density

$\rho_{weighted,t} = \frac{\rho_{1,t}\left[\left(\frac{r_{8',t}}{r_{1,h,t}}\right)^2 + 1\right]}{2} : [kg/m^3]$ Weighted average density at the rear of turbine

Turbine velocity calculations

$U_{2,t} = \omega \cdot r_{2,t,t} : [m/s]$ Turbine outlet peripheral velocity

$C_{1,t} = \frac{\dot{m}}{\rho_{1,t} \cdot b_{1,t} \cdot 2 \cdot \pi \cdot r_{1,h,t}} : [m/s]$ Turbine inlet absolute velocity

$U_{8',t} = \omega \cdot r_{8',t} : [m/s]$ Turbine shaft peripheral velocity

$A_{2,t} = \pi \cdot \left(r_{2,t,t}^2 - r_{2,h,t}^2\right)$:[m^2] Turbine outlet area

$C_{2,t} = \frac{\dot{m}}{\rho_{2,t} A_{2,t}}$:[m/s] Turbine outlet absolute velocity

Compressor thrust calculation

$F_{momentum,c} = \dot{m} \cdot C_{1,c} \cdot \cos(\Phi_{1,c}) - \dot{m} \cdot C_{2,c} \cdot \cos(\Phi_{2,c})$:[N] Axial component of momentum

$Pressure_{1,c} = P_{inlet,c} \cdot \pi \cdot r_{1,h,c}^2$:[N] Inlet pressure acting on compressor shaft area

$Pressure_{2,c} = \frac{\left(P_{inlet,c} + P_{inlet,c}\right)}{2} \cdot \pi \cdot \left(r_{1,t,c}^2 - r_{1,h,c}^2\right)$:[N] Average inlet pressure acting on compressor inlet blade area

$A_{f,c} = \frac{\rho_{avg,c}}{2} \cdot \left(1 - F_{f,c}^2\right) \cdot (2\pi\omega)^2$:[kg/m^{3}s^2] Front A - factor

$Pressure_{3,c} = \frac{\pi}{2} \cdot A_{f,c} \cdot \left(r_{2,t,c}^4 - r_{1,t,c}^4\right)$:[N] Force on front cavity from inlet tip to outlet tip

$B_{f,c} = P_{inlet,c} - \frac{\rho_{avg,c}}{2} \cdot \left(1 - F_{f,c}^2\right) \cdot U_{1,c}^2$:[Pa] Front B - factor

$Pressure_{4,c} = \pi \cdot B_{f,c} \cdot \left(r_{2,t,c}^2 - r_{1,t,c}^2\right)$:[N] Force on front cavity from inlet tip to outlet tip

$A_{r,c} = \frac{\rho_{weighted,c}}{2} \cdot \left(1 - F_{r,c}^2\right) \cdot (2\pi\omega)^2$:[kg/m^{3}s^2] Rear A - factor

$Pressure_{5,c} = \frac{-\pi}{2} A_{r,c} \left(r_{2,h,c}^4 - r_{8',c}^4\right)$:[N] Force on rear cavity from outlet tip to shaft

$B_{r,c} = P_{8',c} - \frac{\rho_{weighted,c}}{2} \cdot \left(1 - F_{r,c}^2\right) \cdot U_{8',c}^2$:[Pa] Rear B - factor

$Pressure_{6,c} = -\pi \cdot B_{r,c} \cdot \left(r_{2,h,c}^2 - r_{8',c}^2\right)$:[N] Force on rear cavity from outlet tip to shaft

$Pressure_{7,c} = -P_{outlet,c} \cdot \pi \cdot \left(r_{2,t,c}^2 - r_{2,h,c}^2\right)$:[N] Outlet pressure acting on rear disk area

$T_{net,c} = F_{momentum,c} + Pressure_{1,c} + Pressure_{2,c} + Pressure_{3,c} + Pressure_{4,c} + Pressure_{5,c} + Pressure_{6,e} + Pressure_{7,c}$:[N] Total compressor thrust

Turbine thrust calculation

$F_{momentum,t} = -\dot{m} \cdot C_{1,t} \cdot \cos(\Phi_{1,t}) - \dot{m} \cdot C_{2,t} \cdot \cos(\Phi_{2,t})$:[N] Axial component of momentum

$Pressure_{1,t} = P_{outlet,t} \cdot \pi \cdot r_{2,h,t}^2$:[N] Outlet pressure acting on turbine shaft area

$Pressure_{2,t} = P_{outlet,t} \cdot \pi \cdot \left(r_{2,t,t}^2 - r_{2,h,t}^2\right)$:[N] Outlet pressure acting on turbine outlet blade area

$A_{f,t} = \frac{\rho_{avg,t}}{2} \cdot \left(1 - F_{f,t}^2\right) \cdot (2\pi\omega)^2$:[kg/m^{3}s^2] Front A - factor

$Pressure_{3,t} = \frac{\pi}{2} \cdot A_{f,t} \cdot \left(r_{1,t,t}^4 - r_{2,t,t}^4\right)$:[N] Force on front cavity from inlet tip to outlet tip

$B_{f,t} = P_{outlet,t} - \frac{\rho_{avg,t}}{2} \cdot \left(1 - F_{f,t}^2\right) \cdot U_{2,t}^2$:[Pa] Front B - factor

$$Pressure_{4,t} = \pi \cdot B_{f,t} \cdot \left(r_{1,t,t}^2 - r_{2,t,t}^2\right) : [N] \text{ Force on front cavity from inlet tip to outlet tip}$$

$$A_{r,t} = \frac{\rho_{weighted,t}}{2} \cdot \left(1 - F_{r,t}^2\right) \cdot \left(2\pi\omega\right)^2 : [kg/m^3s^2] \text{ Rear A - factor}$$

$$Pressure_{5,t} = \frac{-\pi}{2} A_{r,t} \left(r_{1,h,t}^4 - r_{8',t}^4\right) : [N] \text{ Force on rear cavity from inlet tip to shaft}$$

$$B_{r,t} = P_{8',t} - \frac{\rho_{weighted,t}}{2} \cdot \left(1 - F_{r,t}^2\right) \cdot U_{8',t}^2 : [Pa] \text{ Rear B - factor}$$

$$Pressure_{6,t} = -\pi \cdot B_{r,t} \cdot \left(r_{1,h,t}^2 - r_{8',t}^2\right) : [N] \text{ Force on rear cavity from inlet tip to shaft}$$

$$Pressure_{7,t} = -P_{inlet,t} \cdot \pi \cdot \left(r_{1,t,t}^2 - r_{1,h,t}^2\right) : [N] \text{ Intlet pressure acting on rear area}$$

$$T_{net,t} = -F_{momentum,t} + Pressure_{1,t} + Pressure_{2,t} + Pressure_{3,t} + Pressure_{4,t} + Pressure_{5,t} + Pressure_{6,t} + Pressure_{7,t} : [N] \text{ Total turbine thrust}$$

Total axial thrust on turbocharger thrust bearing

$$Net_{turbo,thrust} = T_{net,t} - T_{net,c} : [N]$$

Compressor	Turbine	
$r_{1,h,c}$ = 0.007 [m]	$r_{1,h,t}$ = 0.041 [m]	$\dot{m}$ = 0.302 [kg/s]
$r_{1,t,c}$ = 0.0339 [m]	$r_{1,t,t}$ = 0.041 [m]	N = 935.37 [rev/s]
$r_{2,h,c}$ = 0.047 [m]	$r_{2,h,t}$ = 0.0122 [m]	ω = 5877 [rad/s]
$r_{2,t,c}$ = 0.047 [m]	$r_{2,t,t}$ = 0.03755 [m]	$Net_{turbo,thrust}$ = -146.1 [N]
$r_{8',c}$ = 0.0067 [m]	$r_{8',t}$ = 0.01025 [m]	
$b_{2,c}$ = 0.0065 [m]	$b_{1,t}$ = 0.0155 [m]	
$A_{1,c}$ = 0.003456 [m^2]	$A_{2,t}$ = 0.003962 [m^2]	
$\Phi_{1,c}$ = 0 [degrees]	$\Phi_{1,t}$ = 90 [degrees]	
$\Phi_{2,c}$ = 90 [degrees]	$\Phi_{2,t}$ = 0 [degrees]	
$F_{f,c}$ = 0.75 [dimensionless]	$F_{f,t}$ = 0.75 [dimensionless]	
$F_{r,c}$ = 0.75 [dimensionless]	$F_{r,t}$ = 0.75 [dimensionless]	
$P_{inlet,c}$ = 43060 [Pa]	$P_{inlet,t}$ = 109195 [Pa]	
$P_{outlet,c}$ = 113834 [Pa]	$P_{outlet,t}$ = 65645 [Pa]	
$P_{8',c}$ = 2313 [Pa]	$P_{8',t}$ = 6825 [Pa]	
$T_{inlet,c}$ = 287.2 [K]	$T_{inlet,t}$ = 792.1 [K]	
$T_{outlet,c}$ = 337.8 [K]	$T_{outlet,t}$ = 706 [K]	
$\rho_{1,c}$ = 0.5053 [kg/m^3]	$\rho_{1,t}$ = 0.4643 [kg/m^3]	
$\rho_{2,c}$ = 1.135 [kg/m^3]	$\rho_{2,t}$ = 0.3132 [kg/m^3]	
$\rho_{avg,c}$ = 0.8202 [kg/m^3]	$\rho_{avg,t}$ = 0.3887 [kg/m^3]	
$\rho_{weighted,c}$ = 0.5791 [kg/m^3]	$\rho_{weighted,t}$ = 0.2466 [kg/m^3]	
$C_{1,c}$ = 172.9 [m/s]	$C_{1,t}$ = 162.9 [m/s]	
$C_{2,c}$ = 138.6 [m/s]	$C_{2,t}$ = 243.4 [m/s]	
$U_{1,c}$ = 199.2 [m/s]	$U_{2,t}$ = 220.7 [m/s]	
$U_{8',c}$ = 39.38 [m/s]	$U_{8',t}$ = 60.24 [m/s]	
$A_{f,c}$ = 2.447E+08 [kg/m^3s^2]	$A_{f,t}$ = 1.159E+08 [kg/m^3s^2]	
$A_{r,c}$ = 1.727E+08 [kg/m^3s^2]	$A_{r,t}$ = 7.357E+07 [kg/m^3s^2]	
$B_{f,c}$ = 35938 [Pa]	$B_{f,t}$ = 61504 [Pa]	
$B_{r,c}$ = 2117 [Pa]	$B_{r,t}$ = 6629 [Pa]	
$F_{momentum,c}$ = 52.22 [N]	$F_{momentum,t}$ = -73.5 [N]	
$Pressure_{1,c}$ = 6.629 [N]	$Pressure_{1,t}$ = 30.7 [N]	
$Pressure_{2,c}$ = 148.8 [N]	$Pressure_{2,t}$ = 260.1 [N]	
$Pressure_{3,c}$ = 1368 [N]	$Pressure_{3,t}$ = 152.6 [N]	
$Pressure_{4,c}$ = 119.7 [N]	$Pressure_{4,t}$ = 52.36 [N]	
$Pressure_{5,c}$ = -1324 [N]	$Pressure_{5,t}$ = -325.3 [N]	
$Pressure_{6,c}$ = -14.39 [N]	$Pressure_{6,t}$ = -32.82 [N]	
$Pressure_{7,c}$ = 0 [N]	$Pressure_{7,t}$ = 0 [N]	
$T_{net,c}$ = 357.2 [N]	$T_{net,t}$ = 211.1 [N]	

Table A3.1: Japikse thrust calculation solution.

$$F_{momentum,c} = \dot{m} \cdot C_{1,c} \cdot \cos(\Phi_{1,c}) - \dot{m} \cdot C_{2,c} \cdot \cos(\Phi_{2,c})$$
$$= 0.302 \cdot 172.9 \cdot \cos(0^o) - 0.302 \cdot 138.6 \cdot \cos(90^o)$$
$$= 52.22N$$

$$Pressure_{1,c} = P_{inlet,c} \cdot \pi \cdot r_{1,h,c}^2$$
$$= 43060 \cdot \pi \cdot 0.007^2$$
$$= 6.629N$$

$$Pressure_{2,c} = \frac{(P_{inlet,c} + P_{inlet,c})}{2} \cdot \pi \cdot (r_{1,t,c}^2 - r_{1,h,c}^2)$$
$$= \frac{2 \cdot 43060}{2} \cdot \pi \cdot (0.0339^2 - 0.007^2)$$
$$= 148.8N$$

$$Pressure_{3,c} = \frac{\pi}{2} \cdot A_{f,c} \cdot (r_{2,t,c}^4 - r_{1,t,c}^4)$$
$$= \frac{\pi}{2} \cdot 2.447 \times 10^8 \cdot (0.047^4 - 0.0339^4)$$
$$= 1368N$$

$$Pressure_{4,c} = \pi \cdot B_{f,c} \cdot (r_{2,t,c}^2 - r_{1,t,c}^2)$$
$$= \pi \cdot 35938 \cdot (0.047^2 - 0.0339^2)$$
$$= 119.7N$$

$$Pressure_{5,c} = -\frac{\pi}{2} A_{r,c} (r_{2,h,c}^4 - r_{8',c}^4)$$
$$= -\frac{\pi}{2} \cdot 1.727 \times 10^8 \cdot (0.047^4 - 0.0067^4)$$
$$= -1324N$$

$$Pressure_{6,c} = -\pi \cdot B_{r,c} \cdot (r_{2,h,c}^2 - r_{8',c}^2)$$
$$= -\pi \cdot 2117 \cdot (0.047^2 - 0.0067^2)$$
$$= -14.39N$$

$$Pressure_{7,c} = -P_{outlet,c} \cdot \pi \cdot (r_{2,t,c}^2 - r_{2,h,c}^2)$$
$$= -113834\pi(0.047^2 - 0.047^2)$$
$$= 0N$$

$$F_{momentum,t} = -\dot{m} \cdot C_{1,t} \cdot \cos(\Phi_{1,t}) - \dot{m} \cdot C_{2,t} \cdot \cos(\Phi_{2,t})$$
$$= -0.302 \cdot 162.9 \cdot \cos(90^\circ) - 0.302 \cdot 243.4 \cdot \cos(0^\circ)$$
$$= -73.5N$$

$$Pressure_{1,t} = P_{outlet,t} \cdot \pi \cdot r_{2,h,t}^2$$
$$= 65645 \cdot \pi \cdot 0.0122^2$$
$$= 30.7N$$

$$Pressure_{2,t} = P_{outlet,t} \cdot \pi \cdot \left(r_{2,t,t}^2 - r_{2,h,t}^2\right)$$
$$= 65645 \cdot \pi \cdot \left(0.03755^2 - 0.0122^2\right)$$
$$= 260.1N$$

$$Pressure_{3,t} = \frac{\pi}{2} \cdot A_{f,t} \cdot \left(r_{1,t,t}^4 - r_{2,t,t}^4\right)$$
$$= \frac{\pi}{2} \cdot 1.159 \times 10^8 \cdot \left(0.041^4 - 0.03755^4\right)$$
$$= 152.6N$$

$$Pressure_{4,t} = \pi \cdot B_{f,t} \cdot \left(r_{1,t,t}^2 - r_{2,t,t}^2\right)$$
$$= \pi \cdot 61504 \cdot \left(0.041^2 - 0.03755^2\right)$$
$$= 52.36N$$

$$Pressure_{5,t} = \frac{-\pi}{2} A_{r,t} \left(r_{1,h,t}^4 - r_{8',t}^4\right)$$
$$= -\frac{\pi}{2} \cdot 7.357 \times 10^7 \cdot \left(0.041^4 - 0.01025^4\right)$$
$$= -325.3N$$

$$Pressure_{6,t} = -\pi \cdot B_{r,t} \cdot \left(r_{1,h,t}^2 - r_{8',t}^2\right)$$
$$= -\pi \cdot 6629 \cdot \left(0.041^2 - 0.01025^2\right)$$
$$= -32.82N$$

$$Pressure_{7,t} = -P_{inlet,t} \cdot \pi \cdot \left(r_{1,t,t}^2 - r_{1,h,t}^2\right)$$
$$= -109195 \cdot \pi \cdot \left(0.041^2 - 0.041^2\right)$$
$$= 0N$$

$$Net_{turbo,thrust} = -F_{momentum,t} + Pressure_{1,t} + Pressure_{2,t} + Pressure_{3,t} + Pressure_{4,t} + Pressure_{5,t}$$
$$+ Pressure_{6,t} + Pressure_{7,t} - \left(F_{momentum,c} + Pressure_{1,c} + Pressure_{2,c} + Pressure_{3,c} + Pressure_{4,c} + Pressure_{5,c}\right.$$
$$\left. + Pressure_{6,c} + Pressure_{7,c}\right)$$
$$= -146.1N$$

Appendix A4: Middle rotation factor calculation

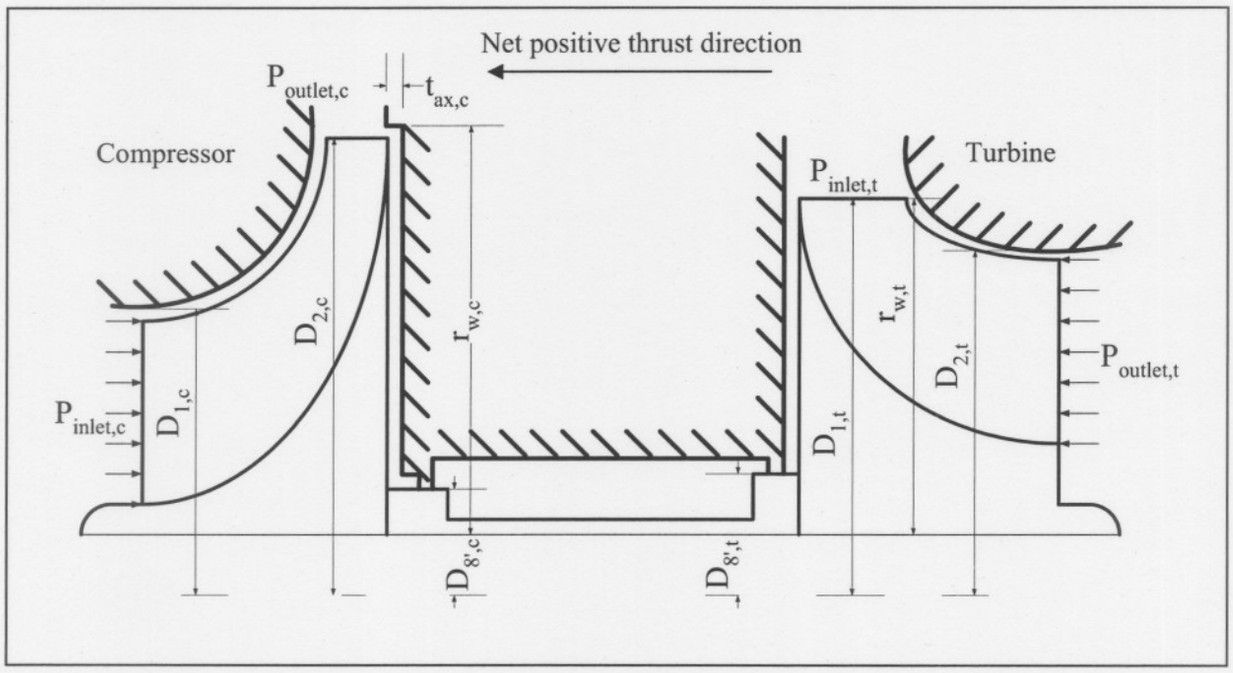


Figure A4.1: Nomenclature applied to complete turbocharger for the thrust calculation by Gülich.

Input parameters :

Compressor

$P_{outlet,c} = 113834 : [Pa]$ Compressor outlet static pressure

$T_{outlet,c} = 337.8 : [K]$ Compressor outlet static temperature

$r_{w,c} = \frac{0.0953}{2} : [m]$ Compressor outer casing radius

$r_{2,c} = \frac{0.094}{2} : [m]$ Compressor impeller outer radius

$t_{ax,c} = \frac{3.5}{1000} : [m]$ Compressor rear sidewall groove depth

$\varepsilon_{c,c} = 3.2 \times 10^{-6} : [m]$ Compressor casing surface roughness

$\varepsilon_{ic} = 1.6 \times 10^{-6} : [m]$ Compressor impeller surface roughness

Turbine

$P_{inlet,t} = 109195 : [Pa]$ Turbine inlet static pressure

$T_{inlet,t} = 792.135 : [K]$ Turbine inlet static temperature

$r_{w,t} = \frac{0.082}{2} : [m]$ Turbine impeller inlet radius

$r_{1,t} = \frac{0.082}{2} : [m]$ Turbine impeller inlet radius

$t_{ax,t} = 0 : [m]$ Turbine rear sideroom groove depth

$\varepsilon_{t,c} = 3.2 \times 10^{-6} : [m]$ Turbine casing surface roughness

$\varepsilon_{it} = 1.6 \times 10^{-6} : [m]$ Turbine impeller surface roughness

Other

$N = 56123 : [RPM]$ Rotor speed

Calculations

$$\omega = \frac{2 \cdot \pi \cdot N}{60} : [\text{rad/s}] \text{ rotor speed}$$

Compressor

$$\nu_c = \frac{\text{VISCOSITY}\left(\text{Nitrogen}, T = T_{outlet,c}, P = P_{outlet,c}\right)}{\text{DENSITY}\left(\text{Nitrogen}, T = T_{outlet,c}, P = P_{outlet,c}\right)} : [m^2/s] \text{ Compressor outlet gas kinematic viscosity}$$

$$Re_c = \frac{\omega \cdot r_{2,c}}{\nu_c} : [\text{dimensionless}] \text{ Compressor outlet Reynolds - number}$$

$$\lambda_{w,c} = \frac{0.136}{\left\{-\log\left(0.2\frac{\varepsilon_{c,c}}{r_{2,c}} + \frac{12.5}{Re_c}\right)\right\}^{2.15}} : [\text{dimensionless}] \text{ Compressor casing friction factor}$$

$$\lambda_{R,c} = \frac{0.136}{\left\{-\log\left(0.2\frac{\varepsilon_{i,c}}{r_{2,c}} + \frac{12.5}{Re_c}\right)\right\}^{2.15}} : [\text{dimensionless}] \text{ Compressor rotor friction factor}$$

$$k_{0,c} = \frac{1}{1 + \left(\frac{r_{w,c}}{r_{2,c}}\right)^2 \cdot \sqrt{\left(\frac{r_{w,c}}{r_{2,c}} + 5\frac{t_{ax,c}}{r_{2,c}}\right)\left(\frac{\lambda_{w,c}}{\lambda_{R,c}}\right)}} : [\text{dimensionless}] \text{ Compressor rotation factor without}$$

through flow in side room

Turbine

$$\nu_t = \frac{\text{VISCOSITY}\left(\text{Nitrogen}, T = T_{inlet,t}, P = P_{inlet,t}\right)}{\text{DENSITY}\left(\text{Nitrogen}, T = T_{inlet,t}, P = P_{inlet,t}\right)} : [m^2/s] \text{ Turbine inlet gas kinematic viscosity}$$

$$Re_t = \frac{\omega \cdot r_{1,t}}{\nu_t} : [\text{dimensionless}] \text{ Turbine inlet Reynolds - number}$$

$$\lambda_{w,t} = \frac{0.136}{\left\{-\log\left(0.2\frac{\varepsilon_{t,c}}{r_{1,t}} + \frac{12.5}{Re_t}\right)\right\}^{2.15}} : [\text{dimensionless}] \text{ Turbine casing friction factor}$$

$$\lambda_{R,t} = \frac{0.136}{\left\{-\log\left(0.2\frac{\varepsilon_{i,t}}{r_{1,t}} + \frac{12.5}{Re_t}\right)\right\}^{2.15}} : [\text{dimensionless}] \text{ Turbine rotor friction factor}$$

$$k_{0,t} = \frac{1}{1 + \left(\frac{r_{w,t}}{r_{1,t}}\right)^2 \cdot \sqrt{\left(\frac{r_{w,t}}{r_{1,t}} + 5\frac{t_{ax,t}}{r_{1,t}}\right)\left(\frac{\lambda_{w,t}}{\lambda_{R,t}}\right)}} : [\text{dimensionless}] \text{ Turbine rotation factor without}$$

through flow in side room

Compressor	**Turbine**	
$r_{2,c} = 0.047$ [m]	$r_{1,t} = 0.041$ [m]	N = 56123 [RPM]
$r_{w,c} = 0.04765$ [m]	$r_{w,t} = 0.0485$ [m]	$\omega = 5877$ [rad/s]
$t_{ax,c} = 0.0035$ [m]	$t_{ax,t} = 0$ [m]	
$P_{outlet,c} = 113834$ [Pa]	$P_{inlet,t} = 109195$ [Pa]	
$T_{outlet,c} = 337.8$ [K]	$T_{inlet,t} = 792.1$ [K]	
$\nu_c = 0.00001758$ [m^2/s]	$\nu_t = 0.0000757$ [m^2/s]	
$Re_c = 1.571E+07$ [dimensionless]	$Re_t = 3.183E+06$ [dimensionless]	
$\varepsilon_{c,c} = 0.0000032$ [m]	$\varepsilon_{t,c} = 0.00001$ [m]	
$\varepsilon_{i,c} = 0.0000016$ [m]	$\varepsilon_{i,t} = 0.0000016$ [m]	
$\lambda_{R,c} = 0.004063$ [m]	$\lambda_{R,t} = 0.004403$ [m]	
$\lambda_{w,c} = 0.00458$ [m]	$\lambda_{w,t} = 0.005975$ [m]	
$k_{0,c} = 0.4377$ [dimensionless]	$k_{0,t} = 0.3606$ [dimensionless]	

Table A4.1: Middle rotation factor calculation solution.

Appendix A5: Gülich thrust calculation

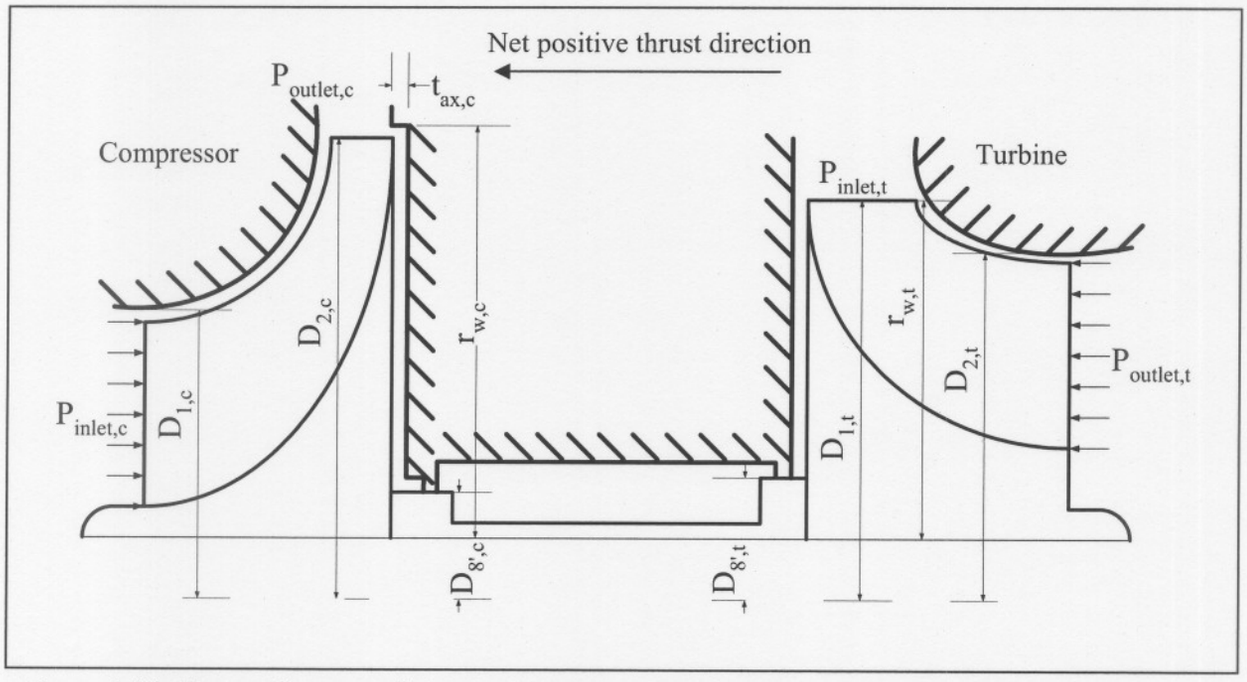


Figure A5.1: Nomenclature applied to complete turbocharger for the thrust calculation by Gülich.

Input parameters :

Compressor :

$D_{1,c} = 0.06875$: [m] Compressor casing inlet diameter

$D_{8',c} = 0.0134$: [m] Shaft diameter at the compressor side

$D_{2,c} = 0.094$: [m] Compressor outlet diameter

$P_{inlet,c} = 43060$: [Pa] Compressor inlet pressure

$T_{inlet,c} = 287.15$: [K] Compressor inlet gas temperature

$P_{outlet,c} = 113834$: [Pa] Compressor outlet pressure

$T_{outlet,c} = 337.849$: [K] Compressor outlet temperature

$\overline{k}_{Ts,c} = 0.4377$: [dimensionless] Compressor middle rotation factor

Turbine:

$D_{1,t} = 0.082$: [m] Turbine inlet diameter

$D_{2,t} = 0.075$: [m] Turbine casing outlet diameter

$D_{8',t} = 0.02$ [m] Shaft diameter on turbine side

$P_{inlet,t} = 109195$: [Pa] Turbine inlet pressure

$T_{inlet,t} = 792.135$: [K] Turbine inlet temperature

$P_{outlet,t} = 65645$: [Pa] Turbine outlet pressure

$T_{outlet,t} = 706$: [K] Turbine outlet temperature

$\overline{k}_{Ts,t} = 0.3606$: [dimensionless] Turbine middle rotation factor

Other :

$N = 56123$: [rpm] Rotational speed of rotor

Calculations

$\omega = \frac{2 \cdot \pi \cdot N}{60} : [rad/s]$ Rotor speed

Compressor

$\Delta P_c = P_{outlet,c} - P_{inlet,c} : [Pa]$ Differential pressure between compressor inlet and outlet

$\rho_{2,c} = \rho\left('Nitrogen', T = T_{outlet,c}, P = P_{outlet,c}\right) : [kg/m^3]$ Compressor outlet density

$\rho_{weighted,c} = \frac{\rho_{2,c}\left[\left(\frac{D_{8',c}}{D_{2,c}}\right)^2 + 1\right]}{2} : [kg/m^3]$ Weighted average density on rear shroud of compressor

$U_{2,c} = \omega \cdot \frac{D_{2,c}}{2} : [m/s]$ Compressor outlet peripheral velocity

$T_{net,c} = -\frac{\pi}{4} \cdot D_{2,c}^2 \cdot \left[\Delta P_c \cdot \left(1 - \frac{D_{8',c}^2}{D_{2,c}^2}\right) - \frac{\rho_{weighted,c}}{4} \cdot \bar{k}_{Ts,c}^2 \cdot U_{2,c}^2 \cdot \left(1 - \frac{D_{8',c}^2}{D_{2,c}^2}\right)^2 - \frac{\Delta P_c}{2} \cdot \left(1 - \frac{D_{1,c}^2}{D_{2,c}^2}\right)^2\right] : [N]$

Thrust developed by the compressor

Turbine

$\Delta P_t = P_{inlet,t} - P_{outlet,t} : [Pa]$ Differential pressure between turbine inlet and outlet

$\rho_{1,t} = \rho\left('Nitrogen', T = T_{inlet,t}, P = P_{inlet,t}\right) : [kg/m^3]$ Turbine inlet density

$\rho_{weighted,t} = \frac{\rho_{1,t}\left[\left(\frac{D_{8',t}}{D_{1,t}}\right)^2 + 1\right]}{2} : [kg/m^3]$ Weighted average density at the rear of turbine

$U_{1,t} = \omega \cdot \frac{D_{1,t}}{2} : [m/s]$ Turbine inlet peripheral velocity

$T_{net,t} = -\frac{\pi}{4} \cdot D_{1,t}^2 \cdot \left[\Delta P_t \cdot \left(1 - \frac{D_{8',t}^2}{D_{1,t}^2}\right) - \frac{\rho_{weighted,t}}{4} \cdot \bar{k}_{Ts,t}^2 \cdot U_{1,t}^2 \cdot \left(1 - \frac{D_{8',t}^2}{D_{1,t}^2}\right)^2 - \frac{\Delta P_t}{2} \cdot \left(1 - \frac{D_{2,t}^2}{D_{1,t}^2}\right)^2\right] : [N]$

Thrust developed by the turbine

$Net_{turbo,thrust} = T_{net,t} - T_{net,c} : [N]$ Net thrust exerted on thrust bearing

Compressor	Turbine	Other
$D_{1,c} = 0.06875$ [m]	$D_{1,t} = 0.08217$ [m]	N = 56123 [RPM]
$D_{2,c} = 0.094$ [m]	$D_{2,t} = 0.075$ [m]	$\omega = 5877$ [rad/s]
$D_{8',c} = 0.0134$ [m]	$D_{8',t} = 0.02$ [m]	$Net_{turbo,thrust} = 201.4$ [N]
$\bar{k}_{Ts,c} = 0.4377$ [dimensionless]	$\bar{k}_{Ts,t} = 0.3606$ [dimensionless]	
$P_{inlet,c} = 43060$ [Pa]	$P_{inlet,t} = 109195$ [Pa]	
$P_{outlet,c} = 113834$ [Pa]	$P_{outlet,t} = 65645$ [Pa]	
$T_{inlet,c} = 287.2$ [K]	$T_{inlet,t} = 792.1$ [K]	
$T_{outlet,c} = 337.8$ [K]	$T_{outlet,t} = 706$ [K]	
$\Delta P_c = 70774$ [Pa]	$\Delta P_t = 43550$ [Pa]	
$\rho_{2,c} = 1.135$ [kg/m^3]	$\rho_{1,t} = 0.4643$ [kg/m^3]	
$\rho_{weighted,c} = 0.5792$ [kg/m^3]	$\rho_{weighted,t} = 0.2462$ [kg/m^3]	
$T_{net,c} = -414$ [N]	$T_{net,t} = -212.6$ [N]	
$U_{2,c} = 276.2$ [m/s]	$U_{1,t} = 241.5$ [m/s]	

Table A5.1: Gülich thrust calculation solution.

$$Net_{turbo,thrust} = -\frac{\pi}{4}\cdot D_{1,t}^2\cdot\left[\Delta P_t\cdot\left(1-\frac{D_{8',t}^2}{D_{1,t}^2}\right)-\frac{\rho_{weighted,t}}{4}\cdot\bar{k}_{Ts,t}^2\cdot U_{1,t}^2\cdot\left(1-\frac{D_{8',t}^2}{D_{1,t}^2}\right)^2-\frac{\Delta P_t}{2}\cdot\left(1-\frac{D_{2,t}^2}{D_{1,t}^2}\right)^2\right]$$

$$+\frac{\pi}{4}\cdot D_{2,c}^2\cdot\left[\Delta P_c\cdot\left(1-\frac{D_{8',c}^2}{D_{2,c}^2}\right)-\frac{\rho_{weighted,c}}{4}\cdot\bar{k}_{Ts,c}^2\cdot U_{2,c}^2\cdot\left(1-\frac{D_{8',c}^2}{D_{2,c}^2}\right)^2-\frac{\Delta P_c}{2}\cdot\left(1-\frac{D_{1,c}^2}{D_{2,c}^2}\right)^2\right]$$

$$=\frac{-\pi}{4}\cdot 0.08217^2\cdot\left[43550\cdot\left(1-\frac{0.02^2}{0.08217^2}\right)-\frac{0.2462}{4}\cdot 0.3606^2\cdot 241.5^2\cdot\left(1-\frac{0.02^2}{0.08217^2}\right)^2-\frac{43550}{2}\cdot\left(1-\frac{0.075^2}{0.08217^2}\right)^2\right]$$

$$+\frac{\pi}{4}\cdot 0.094^2\cdot\left[70774\cdot\left(1-\frac{0.0134^2}{0.094^2}\right)-\frac{0.5792}{4}\cdot 0.4377^2\cdot 276.2^2\cdot\left(1-\frac{0.0134^2}{0.094^2}\right)^2-\frac{70774}{2}\cdot\left(1-\frac{0.06875^2}{0.094^2}\right)^2\right]$$

$$= 201.4\text{N}$$

Appendix A6: Liebner thrust calculation

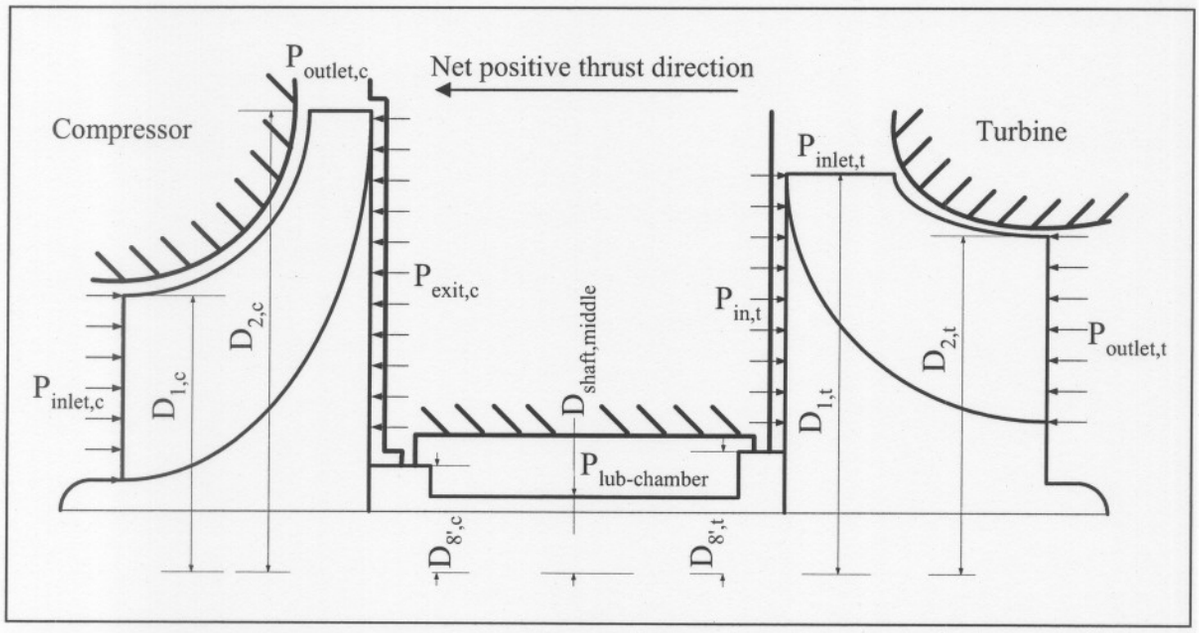


Figure A6.1: Nomenclature applied to complete turbocharger for the thrust calculation based on method by Liebner

Input parameters:

Compressor:

$D_{1,c} = 0.06875$: [m] Compressor casing inlet diameter

$D_{8',c} = 0.0134$: [m] Shaft diameter at the compressor side

$D_{2,c} = 0.094$: [m] Compressor outlet diameter

$P_{inlet,c} = 43060$: [Pa] Compressor inlet pressure

$P_{outlet,c} = 113834$: [Pa] Compressor outlet pressure

Turbine:

$D_{1,t} = 0.082$: [m] Turbine inlet diameter

$D_{2,t} = 0.075$: [m] Turbine casing outlet diameter

$D_{8',t} = 0.02$ [m] Shaft diameter on turbine side

$P_{inlet,t} = 109195$: [Pa] Turbine inlet pressure

$P_{outlet,t} = 65645$: [Pa] Turbine outlet pressure

Other:

$P_{lub\text{-}chamber} = 86500$: [Pa] Lubrication chamber pressure

$D_{shaft,middle} = 0.0127$: [m] Shaft diameter in the middle between the compressor and turbine

Calculations

$$Net_{turbo,thrust} = \frac{\pi}{4}\begin{pmatrix} -P_{inlet,c}\cdot D_{1,c}^2 + P_{outlet,c}\cdot\left(D_{2,c}^2 - D_{8',c}^2\right) + P_{lub\text{-}chamber}\cdot\left(D_{8',c}^2 - D_{shaft,middle}^2\right) \\ -P_{lub\text{-}chamber}\cdot\left(D_{8',t}^2 - D_{shaft,middle}^2\right) - P_{inlet,t}\cdot\left(D_{1,t}^2 - D_{8',t}^2\right) + P_{outlet,t}\cdot D_{2,t}^2 \end{pmatrix} : [N]$$

Net thrust exerted on turbocharger thrust bearing

Compressor	Turbine	Other
$D_{1,c} = 0.06875$ [m]	$D_{1,t} = 0.08217$ [m]	$P_{lub\text{-}chamber} = 86500$ [Pa]
$D_{2,c} = 0.094$ [m]	$D_{2,t} = 0.07624$ [m]	$D_{shaft,middle} = 0.0127$ [m]
$D_{8',c} = 0.0134$ [m]	$D_{8',t} = 0.02$ [m]	$Net_{turbo,thrust} = 351.1$ [N]
$P_{inlet,c} = 43060$ [Pa]	$P_{inlet,t} = 109195$ [Pa]	
$P_{outlet,c} = 113834$ [Pa]	$P_{outlet,t} = 65645$ [Pa]	

Table A6.1: Liebner thrust calculation solution.

$$Net_{turbo,thrust} = \frac{\pi}{4}\begin{pmatrix} -P_{inlet,c}\cdot D_{1,c}^2 + P_{outlet,c}\cdot\left(D_{2,c}^2 - D_{8',c}^2\right) + P_{lub\text{-}chamber}\cdot\left(D_{8',c}^2 - D_{shaft,middle}^2\right) \\ -P_{lub\text{-}chamber}\cdot\left(D_{8',t}^2 - D_{shaft,middle}^2\right) - P_{inlet,t}\cdot\left(D_{1,t}^2 - D_{8',t}^2\right) + P_{outlet,t}\cdot D_{2,t}^2 \end{pmatrix}$$

$$= \frac{\pi}{4}\begin{pmatrix} -43060\cdot 0.0678^2 + 113834\cdot\left(0.094^2 - 0.0134^2\right) + 86500\cdot\left(0.0134^2 - 0.0127^2\right) \\ -86500\cdot\left(0.02^2 - 0.0127^2\right) - 109195\cdot\left(0.082^2 - 0.02^2\right) + 65645\cdot 0.075^2 \end{pmatrix}$$

$$= 351.1N$$

Appendix A7: Gülich thrust calculation for a turbo diesel engine

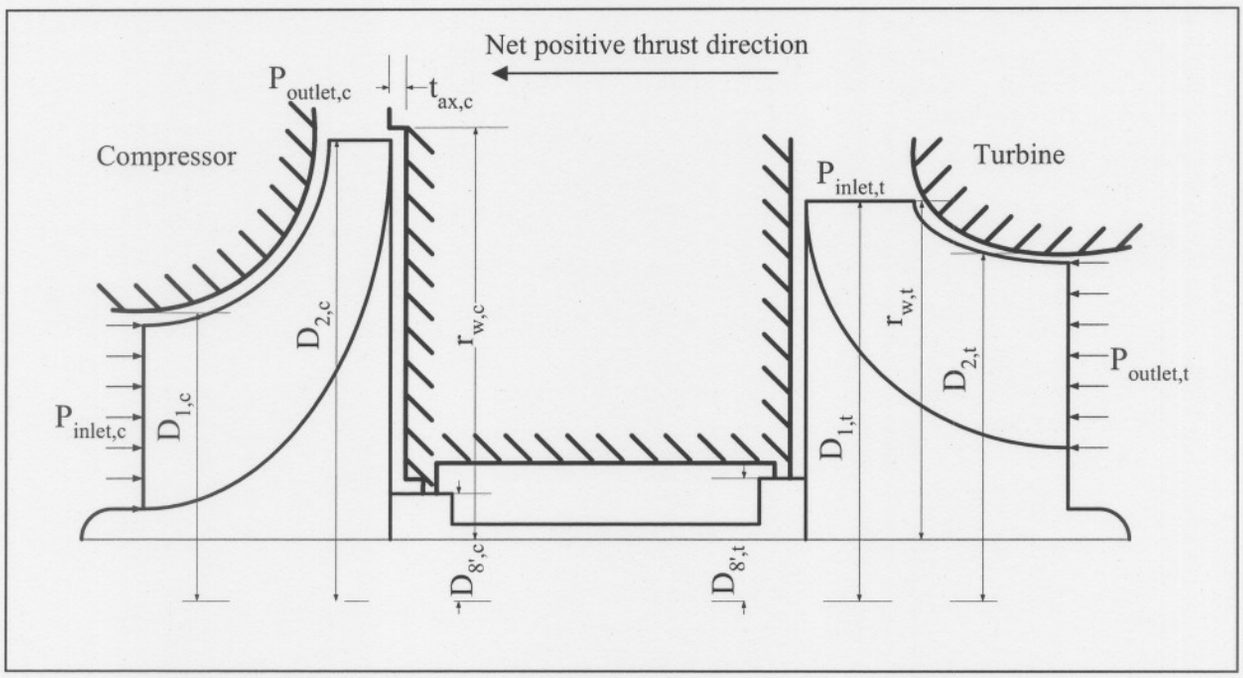


Figure A7.1: Nomenclature applied to turbocharger for the thrust calculation by Gülich.

Input parameters :

Compressor :

$\gamma_{air} = 1.4$: Ratio of specific heats for air

$PR_c = 1.8$: Compressor pressure ratio (static to static)

$D_{1,c} = 0.06875$: [m] Compressor casing inlet diameter

$D_{8',c} = 0.0134$: [m] Shaft diameter at the compressor side

$D_{2,c} = 0.094$: [m] Compressor outlet diameter

$P_{inlet,c} = 86500$: [Pa] Compressor inlet pressure

$T_{inlet,c} = 298.15$: [K] Compressor inlet gas temperature

$\overline{k}_{Ts,c} = 0.4377$: [dimensionless] Compressor middle rotation factor

Turbine:

$\gamma_{combustion} = 1.3$: Ratio of specific heats for combustion gasses

$PR_t = 1.5$: Turbine pressure ratio (static to static)

$D_{1,t} = 0.082$: [m] Turbine inlet diameter

$D_{2,t} = 0.075$: [m] Turbine casing outlet diameter

$D_{8',t} = 0.02$ [m] Shaft diameter on turbine side

$T_{inlet,t} = 773.15$: [K] Turbine inlet temperature

$\overline{k}_{Ts,t} = 0.3606$: [dimensionless] Turbine middle rotation factor

Other :

$N = 65000$: [rpm] Rotational speed of rotor

Calculations

$$\omega = \frac{2 \cdot \pi \cdot N}{60} : [\text{rad/s}] \text{ Rotor speed}$$

Compressor

$$P_{outlet,c} = P_{inlet,c} \cdot PR_c : [\text{Pa}] \text{ Compressor outlet pressure}$$

$$T_{outlet,c} = T_{inlet,c} \cdot \left[\frac{P_{outlet,c}}{P_{inlet,c}} \right]^{\frac{\gamma_{air}-1}{\gamma_{air}}} : [\text{K}] \text{ Compressor outlet temperature}$$

$$\Delta P_c = P_{outlet,c} - P_{inlet,c} : [\text{Pa}] \text{ Differential pressure between compressor inlet and outlet}$$

$$\rho_{2,c} = \rho\left('\text{Nitrogen}', T = T_{outlet,c}, P = P_{outlet,c}\right) : [\text{kg/m}^3] \text{ Compressor outlet density}$$

$$\rho_{weighted,c} = \frac{\rho_{2,c}\left[\left(\frac{D_{8',c}}{D_{2,c}}\right)^2 + 1\right]}{2} : [\text{kg/m}^3] \text{ Weighted average density on rear shroud of compressor}$$

$$U_{2,c} = \omega \cdot \frac{D_{2,c}}{2} : [\text{m/s}] \text{ Compressor outlet peripheral velocity}$$

$$T_{net,c} = -\frac{\pi}{4} \cdot D_{2,c}^2 \cdot \left[\Delta P_c \cdot \left(1 - \frac{D_{8',c}^2}{D_{2,c}^2}\right) - \frac{\rho_{weighted,c}}{4} \cdot \overline{k}_{Ts,c}^2 \cdot U_{2,c}^2 \cdot \left(1 - \frac{D_{8',c}^2}{D_{2,c}^2}\right)^2 - \frac{\Delta P_c}{2} \cdot \left(1 - \frac{D_{1,c}^2}{D_{2,c}^2}\right)^2 \right] : [\text{N}]$$

Thrust developed by the compressor

Turbine

$$P_{inlet,t} = P_{outlet,c} + 84600 : [\text{Pa}] \text{ Turbine inlet pressure}$$

$$P_{outlet,t} = \frac{P_{inlet,t}}{PR_t} : [\text{Pa}] \text{ Turbine outlet pressure}$$

$$T_{outlet,t} = T_{inlet,t} \cdot \left[\frac{P_{outlet,t}}{P_{inlet,t}} \right]^{\frac{\gamma_{combustion}-1}{\gamma_{combustion}}} : [\text{K}] \text{ Turbine outlet temperature}$$

$$\Delta P_t = P_{inlet,t} - P_{outlet,t} : [\text{Pa}] \text{ Differential pressure between turbine inlet and outlet}$$

$$\rho_{1,t} = \rho\left('\text{Nitrogen}', T = T_{inlet,t}, P = P_{inlet,t}\right) : [\text{kg/m}^3] \text{ Turbine inlet density}$$

$$\rho_{weighted,t} = \frac{\rho_{1,t}\left[\left(\frac{D_{8',t}}{D_{1,t}}\right)^2 + 1\right]}{2} : [\text{kg/m}^3] \text{ Weighted average density at the rear of turbine}$$

$$U_{1,t} = \omega \cdot \frac{D_{1,t}}{2} : [\text{m/s}] \text{ Turbine inlet peripheral velocity}$$

$$T_{net,t} = -\frac{\pi}{4} \cdot D_{1,t}^2 \cdot \left[\Delta P_t \cdot \left(1 - \frac{D_{8',t}^2}{D_{1,t}^2}\right) - \frac{\rho_{weighted,t}}{4} \cdot \overline{k}_{Ts,t}^2 \cdot U_{1,t}^2 \cdot \left(1 - \frac{D_{8',t}^2}{D_{1,t}^2}\right)^2 - \frac{\Delta P_t}{2} \cdot \left(1 - \frac{D_{2,t}^2}{D_{1,t}^2}\right)^2 \right] : [\text{N}]$$

Thrust developed by the turbine

$$Net_{turbo,thrust} = T_{net,t} - T_{net,c} : [\text{N}] \text{ Net thrust exerted on thrust bearing}$$

Compressor	Turbine	Other
$D_{1,c} = 0.06875$ [m]	$D_{1,t} = 0.08217$ [m]	N = 65000 [RPM]
$D_{2,c} = 0.094$ [m]	$D_{2,t} = 0.075$ [m]	$\omega = 6807$ [rad/s]
$D_{8',c} = 0.0134$ [m]	$D_{8',t} = 0.02$ [m]	$Net_{turbo,thrust} = 5.382$ [N]
$\bar{k}_{Ts,c} = 0.4377$ [dimensionless]	$\bar{k}_{Ts,t} = 0.3606$ [dimensionless]	
$\gamma air = 1.4$	$\gamma_{combustion} = 1.3$	
$PR_c = 1.8$	$PR_t = 1.5$	
$P_{inlet,c} = 86500$ [Pa]	$P_{inlet,t} = 240300$ [Pa]	
$P_{outlet,c} = 155700$ [Pa]	$P_{outlet,t} = 65645$ [Pa]	
$T_{inlet,c} = 298.2$ [K]	$T_{inlet,t} = 773.2$ [K]	
$T_{outlet,c} = 352.7$ [K]	$T_{outlet,t} = 704.1$ [K]	
$\Delta P_c = 69200$ [Pa]	$\Delta P_t = 80100$ [Pa]	
$\rho_{2,c} = 1.487$ [kg/m^3]	$\rho_{1,t} = 1.046$ [kg/m^3]	
$\rho_{weighted,c} = 0.7587$ [kg/m^3]	$\rho_{weighted,t} = 0.5547$ [kg/m^3]	
$T_{net,c} = -393.8$ [N]	$T_{net,t} = -388.4$ [N]	
$U_{2,c} = 319.9$ [m/s]	$U_{1,t} = 279.7$ [m/s]	

Table A7.1: Gülich thrust calculation solution for turbo diesel engine.

Appendix B1: Strain gauge installation procedure

1. Prepare thrust bearing for installation of strain gauges by abrasion with sand paper.
2. Cleaning the thrust bearing with 50-50% mixture of propane and acetone by wiping in outward radial direction only.
3. Cover the "thrust shoes" with Mylar tape to prevent damage of the thrust shoes.
4. Make radial alignment markings with a ball point pen for strain gauge positioning.
5. Clean ink by wiping in radial outward direction.
6. Position strain gauge and align with the markings.
7. Stick the strain gauge down with the Mylar tape to form a hinge (See Figure B1.1).
8. Apply a thin layer of mixed HBM EP310 high temperature epoxy to the installation area.
9. With the hinge folded back, leave the epoxy to cure at room temperature for 20 – 30 minutes.
10. Fold strain gauges down in position onto the thrust bearing.
11. Put pressure pads on strain gauges inside the oven to apply pressure for the strain gauge to stick down on the thrust bearing.
12. Load a 10kg dead weight onto each active strain gauge with a simply supported beam method. (See Figure B1.2).
13. Perform hot curing in the oven at 165°C for 90 minutes.
14. Leave the thrust bearing to cool down below 50°C inside the oven.
15. Install the soldering pads into position along with the dummy gauge with Mylar tape hinges.
16. Apply a thin layer of HBM EP310 on the installation area. Let the epoxy air dry for 20-30 minutes at ambient temperature.
17. Perform hot curing in the oven for 90 minutes at 165°C.
18. Leave the thrust bearing in the oven to cool down below 50°C.
19. Inspect the strain gauges and soldering tabs for defective curing or looseness when the thrust bearing is removed out of the oven.
20. If all is found intact, then the strain gauges are ready for wiring.

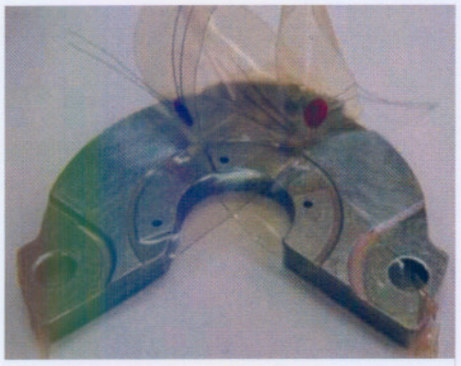


Figure B1.1: Thrust bearing with strain gauges positioned on Mylar hinges.

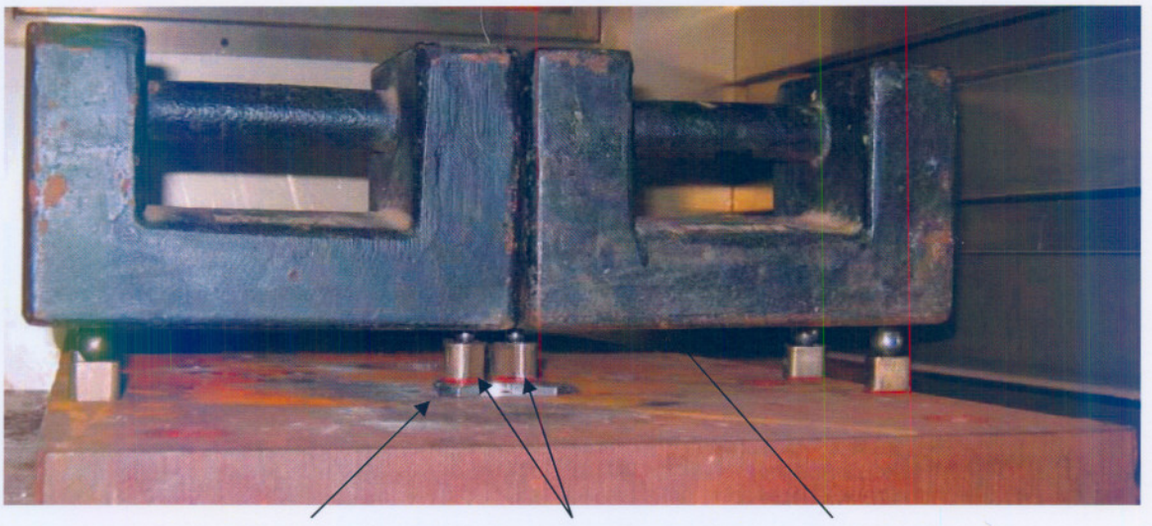


Figure B1.2: Strain gauges clamped down on thrust bearing with pressure pads.

Appendix B2: Balancing of the HBM amplifier

1. Connect the strain gauge bridge to the input port of channel 1 at the back of the amplifier.
2. Set the "Range" dial on the digital readout module to 10000.
3. Select the "Measuring point" on the digital readout module dial to channel 1 as the bridge is connected to channel 1.

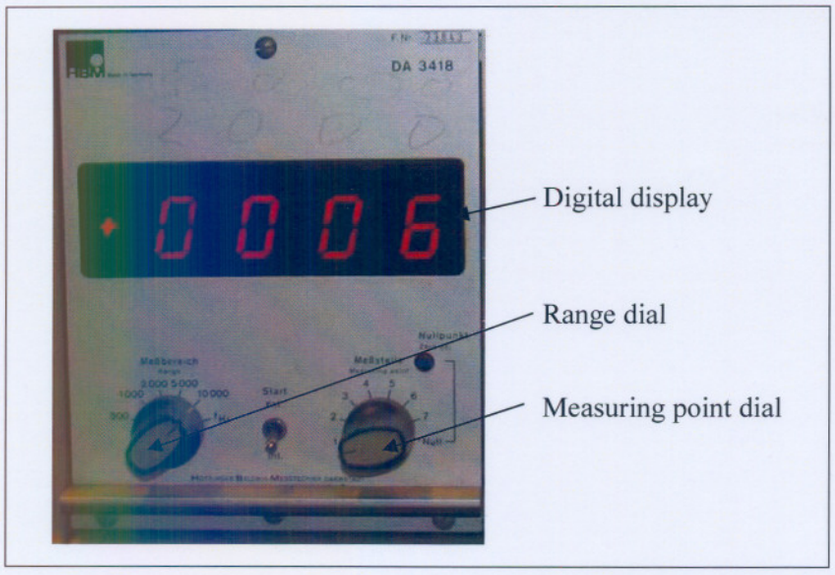


Figure B2.1: Digital readout module.

4. Set excitation voltage to 1V ("U_B" selector switch).
5. Set the "Bridge selector" switch to a full strain gauge bridge.
6. Get the digital readout as close as possible to zero by turning the "R-balance course" dial.
7. Adjust the "Range" dial to the 1mV/V setting.
8. Adjust the "C-balance" potentiometer to bring the modulation indicator at the top of channel 1 to the left as far as possible.
9. Change "Range" setting to 0.5, 0.2, 0.1, 0.05mV/V and re-adjust "C-balance" to zero again.
10. Push "Calibration" button and hold it pressed down.
11. Detune "Range fine" potentiometer to bring the reading on the readout below 2V (2000 on readout).
12. Adjust "Reference phase" while pushing the Calibration button to maximum reading possible on the readout.
13. Release the "Calibration button".
14. Recheck "C-balance" setting (push little black button below C-balance).
15. Recheck that the range is on 2V (2000 on readout) by adjusting it with the "Range fine" potentiometer when the "Calibration" button is pushed (See point 7).
16. Recheck that the "Reference phase" is set to maximum possible reading on readout (See point 8).

17. Use "R-balance fine" potentiometer to set reading to zero without pushing the "Calibration" button.
18. Press the "Calibration" button and set the "Range fine" potentiometer to re-adjust the reading to 2V (2000 on readout).

Note: The readings on the readout of 2V only holds if the excitation voltage switch is set to 1V for a full bridge.

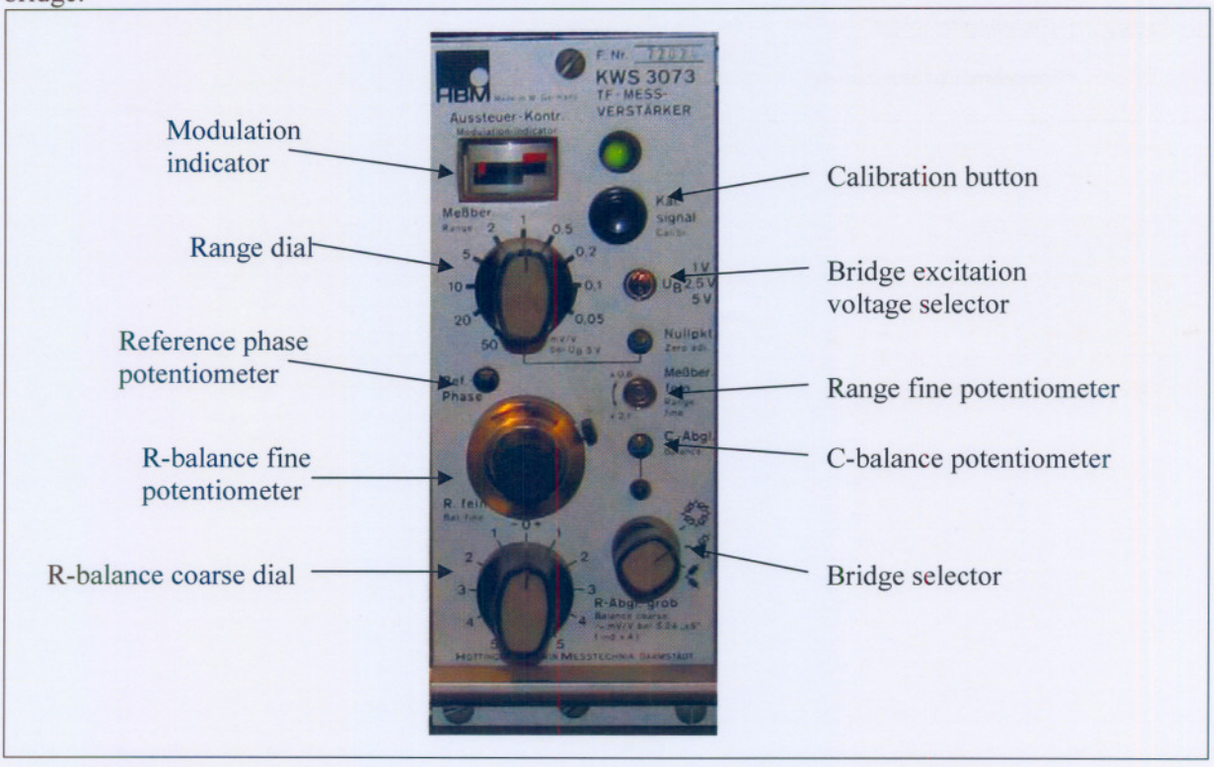


Figure B2.2: Selectors, dials and potentiometers of KWS 3073 strain gauge amplifier card.

Appendix B3: Balancing of the Vishay amplifier

1. Connect the strain gauge bridge to the input port of channel 1 at the back of the amplifier.
2. Switch on the power on the 2110 power supply module and leave the amplifier on for at least 20 minutes.
3. After 20 minutes, set the channel selector switch on the 2110 power supply module to channel 1.
4. Ensure that the "EXCIT" toggle switch on channel 1 is switched to "OFF".
5. Turn the "BRIDGE EXCIT" potentiometer so that the "Bridge voltage indicator" needle display 1V. This can also be checked more accurately by connecting a multi-meter to the positive and negative external meter connections.
6. Set the "GAIN" dial to 500. It should be noted that the gain has a factor of 2. This implicates that if the gain is set to 500, the gain is actually 1000. The gain means that the output of the strain gauge bridge is multiplied by a factor of 1000.
7. Connect the output cable at the back of Channel 1.
8. Connect the crocodile clamps of a multi-meter to the positive and negative terminals of the output cable.
9. Switch the multi-meter to display a DC millivolt reading.
10. Verify that the polarity on the multi-meter is the same as indicated by the two LED's at the top of Channel 1. If not change the crocodile clamps on the output cable around.
11. Switch the "EXCIT" toggle switch to "ON".
12. Turn the "BALANCE" dial until both LED's at the top of Channel 1 is not lit and check the reading on the multi-meter. The reading on the multi-meter should be null.
13. The amplifier is ready for measurement.

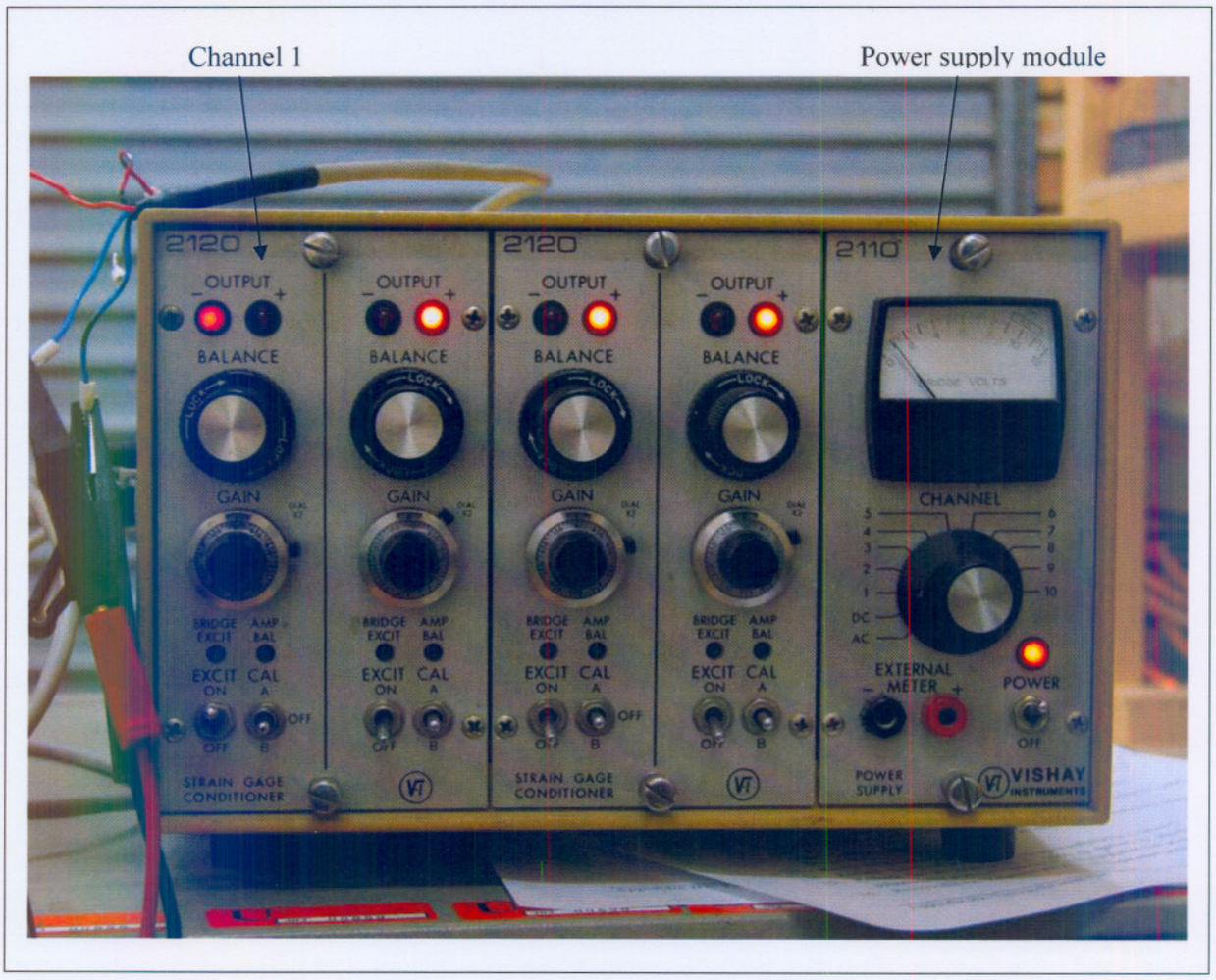


Figure B3.1: Vishay 2100 amplifier.

8. Bibliography

[1] ANON. 1986. Origin and magnitude of radial loads on centrifugal impellers. (*In* Radial loads and axial thrusts on centrifugal pumps: 1986 Seminar organized by the Fluid Machinery Committee of the Power industries division of mechanical engineers, Institution of mechanical engineers. MEP. **p 2-11.**)

[2] ANON. 1999. Experimental evaluation of axial thrust in pumps. *World pumps,*(393):34-37, **June.**

[3] Answers.com. 2005. Web results for "specific gravity". [Web:] http://www.answers.com/topic/specific-gravity. [Date of usage: 9 Nov. 2005].

[4] Baines, N.C. (ncb@conceptsnrec.com) 2006. RE: Information request. [e-mail to:] Janse van Rensburg, J. (mgijjvr@puk.ac.za) May. 3.

[5] Boresi, A.P. Schmidt, R.J. 2003. Advanced mechanics of materials. 6th ed. NY: Wiley. 681 p.

[6] Davis, J.R. 1996. Cast irons. OH: ASM International. 494 p.

[7] Duncan, A.B. 1986. A review of the pump rotor axial equilibrium problem – some case studies. (*In* Radial loads and axial thrusts on centrifugal pumps: 1986 Seminar organized by the Fluid Machinery Committee of the Power industries division of mechanical engineers, Institution of mechanical engineers. MEP. **p 39-49.**)

[8] Eder, L. 1996. Strain gauge circuitry: Wheatstone bridge. Germiston: Instruments for Engineering Measurement. 29 p.

[9] Greyvenstein, G.P. & Rousseau, P.G. 2003. Design of a physical model of the PBMR with the aid of Flownet. *Nuclear Engineering and Design,* 222:203-213.

[10] Gülich, J.F. 2003. Disk friction losses of closed turbomachine impellers. *Forschung im Ingenieurwesen,* **68:87-95**

[11] Gülich, J.F. 1999. Kreiselpumpen: Ein handbuch für Entwicklung, Anlagenplanung und Betrieb. Berlin Heidelberg: Springer-Verlag. 596 p.

[12] Han, Z. & Cizmas, G.A. 2003. A CFD method for axial thrust load prediction of centrifugal compressors. *International Journal of Turbo and Jet engines*, 20:1-16.

[13] Hottinger Baldwin Messtechnik. Operating manual: 5kHz-Carrier frequency amplifier, KWS673.D8 & KWS673.A7. Darmstad: Hottinger Baldwin Messtechnik GmbH.

[14] Hottinger Baldwin Messtechnik. 2005. [Web:] http://www.hbm.com/products/SEURLIF/ASP/SFS/CATEGORY.3/MM.3,33,-1/SFE/Listproducts.htm%20target=. [Date of usage: 4 July 2005].

[15] Hoffmann, K. 1989. An introduction to measurements using strain gages. Darmstad: Hottinger Baldwin Messtechnik GmbH. 291 p.

[16] Hoffman, K. 1974. Fundamentals of the strain gauge technique: Applying the Wheatstone bridge circuit. Darmstad: Hottinger Baldwin Messtechnik GmbH. 22 p.

[17] Japikse, D. 1996. Centrifugal compressor design and performance. Wilder, VT: Concepts ETI, Inc. 422 p.

[18] Liebner, T. (torsten.liebner@ch.abb.com) 2004. Axial force on turbocharger shafts. [e-mail to:] Venter, L.D. (MGILDV@puknet.puk.ac.za) Jul. 28.

[19] Lobanoff, V.S. & Ross, R.R. 1992. Centrifugal pumps: Design & application. 2nd ed. Houston, TX: Gulf Publishing Company. 569 p.

[20] NREC ETI, Inc. 2000. User's Guide to CCAD™ Version 7.3. White River, VT: Concepts ETI, Inc. 150 p.

[21] PBMR (Pty.) Ltd. [Web:]http://www.pbmr.co.za [Date of usage: 7 March 2005]

[22] PCB Piezotronics. 2006. [Web:] www.pcb.com/products/ [Date of usage: 4 April 2005]

[23] PU for CHE (Potchefstroom University for Christian Higher Education) 2002. Turbo Charger Design Report. PBMM 0010, revision A. July. Potchefstroom 53 p.

[24] Pulkrabek, W.W. 1997. Engineering fundamentals of the internal combustion engine. New Jersey: Prentice Hall. 411p.

[25] Roberts, J.G. (mgijgr@puk.ac.za) 2004. Beursonderhoud. [e-mail to:] Janse van Rensburg, J. (jvrensburg.cobus@columbus.co.za) Jun. 10.

[26] Shigley, J.E. Mischke, C.R. 2001. Mechanical engineering design. 6th ed. NY: McGraw-Hill. 1248p.

[27] Stepanoff, A.J. 1957. Centrifugal and axial flow pumps: theory, design and application. 2nd ed. Malabar, FL: Krieger Publishing Company. 462 p.